UNIVERSITÀ DEGLI STUDI DI MILANO

DIP. DI BIOTECNOLOGIE MEDICHE E MEDICINA TRASLAZIONALE

Ph.D. PROGRAM

EXPERIMENTAL MEDICINE AND MEDICAL BIOTECHNOLOGIES

XXXII Cohort

UNVEILING MOLECULAR PATHWAYS DISRUPTED IN SMS AND SMS-LIKE PATIENTS BY MEANS OF GENOMIC AND FUNCTIONAL APPROACHES

Tutor: Prof.ssa Palma FINELLI

Supervisor: Dott.ssa Patrizia BOSSOLASCO

PhD Thesis:

Dott.ssa Alessandra SIRONI

Matricola R11627

Academical Year 2018-2019

INDEX

ABSTRACT

Smith Magenis Syndrome (SMS, OMIM#182290) is a complex genomic disorder with incidence of 1:15000-25000, clinically characterized by neurological abnormalities with variable intellectual disability (ID), craniofacial dysmorphisms, behavioral and sleep disturbances, and speech and motor delay. SMS is caused by haploinsufficiency of *RAI1* (Retinoic Acid-Induced 1) gene to either large 17p11.2 deletion (90%) or point mutations/intragenic microdeletions (10%). *RAI1* encodes a transcription factor, working as chromatin reader in a regulatory complex, that positively regulates the expression of many neurodevelopmental and circadian rhythm genes. However, only 50% of individuals with SMS clinical suspicion is confirmed by the genetic test, suggesting that other *loci* may be involved directly or indirectly in the same pathway of *RAI1* gene, hence contributing to the SMS-like phenotype.

In order to deepen the genetic mechanisms underlying the SMS spectrum, we analyzed a cohort of 30 patients with SMS clinical diagnosis through several genetic approaches. High resolution array-CGH, performed to pinpoint rare pathogenic CNVs containing dosage sensitive genes that might be implicated in *RAI1* molecular pathways, disclosed 4 pathogenic CNVs. Further studies, namely *RAI1* NGS sequencing, MLPA, and RT-qPCR revealed in one patient multiple peculiar molecular *RAI1* defects consistent with SMS molecular diagnosis.

Considering that sleep disturbance is a main feature of SMS and the circadian genes oscillatory expression can be observed in peripheral melatonin target tissues, an additional aim of this project was the evaluation of circadian rhythm genes expression in peripheral blood cells of selected 16 SMS/SMS-like patients through RT-qPCR analysis. Among the tested genes, *CLOCK*, *BMAL2*, *PER2*, and *NR1D1* were found dysregulated in at least one patient analyzed. Thus, this study turned out to be an useful preliminary approach to evaluate any circadian dysfunctions in patients with sleep disturbance.

Another crucial aim of this thesis was the investigation of candidate genes implicated in *RAI1* molecular pathway through a functional approach. Considering that neurodevelopmental disorders (NDDs) are extraordinarily difficult to study, we used human iPSCs differentiated into neurons, in the attempt to elucidate the molecular alterations that give rise to SMS. A male patient of our cohort, bearing a rare 54 kb maternal deletion at Xq13.3 mapping 29 kb far from 5'UTR of *ZDHHC15* gene that results downregulated in blood, was selected for iPSCs reprogramming and differentiation in cortical neurons. Starting from peripheral blood mononuclear cells we successfully obtained three and two genomic stable iPSCs clones of patient and his parents, respectively. Patient's iPSCs were comparable to parents' iPSCs for morphology, pluripotency-related markers expression, and capability of embryo body formation and spontaneous differentiation into the three germ layers. The subsequent iPSCs differentiation produced cortical neurons found positive to several specific neuronal markers. Although,

we were unable to determine the amount of *ZDHHC15* mRNA on mature cortical neurons, an altered functional activity of patient's cultured iPSCs-derived neurons was disclosed. The evaluation of electrophysiological profiles of differentiated neurons revealed in the patient and his mother compared to the father the absence of a progressive increase in mEPSCs frequency and amplitude, resembling a defected excitatory synaptic development.

To sum up, the present combined approach using both genomic and functional techniques resulted an efficient strategy to deepen the molecular and genetic mechanisms underlying SMS-like phenotype, and to increase the possibility to uncover the networks of genes underlying NDDs.

INTRODUCTION

1.1 Smith Magenis Syndrome

1.1.1 Clinical overview

Smith Magenis Syndrome (SMS, OMIM#182290) is a complex neurodevelopmental disorder with an estimated birth incidence of 1:25000 [Greenberg et al., 1991] and an actual prevalence of 1:15000 [Smith et al., 2005], described for the first time by Patil and Bartley in 1984 [Patil and Bartley, 1984], and subsequently characterized by Smith and collaborators in 1986 [Smith et al., 1986]. SMS clinical features include craniofacial dysmorphisms, neurological anomalies with variable intellectual disability (ID), behavioral problems, sleep disturbances, speech and motor delay, and childhood-onset abdominal obesity [Smith et al., 2019]. Infants have also feeding difficulties, failure to thrive, hypotonia accompanied by hyporeflexia and generalized lethargy [Gropman et al., 2006; Smith and Gropman, 2010]. The facial appearance and skeletal anomalies are characterized by brachycephaly, midface hypoplasia, broad square-shaped face, prominent forehead, mildly upslanted palpebral fissures, deep-set eyes, broad nasal bridge, everted upper lip, short stature, brachydactyly, and scoliosis (**Fig.1**) [Elsea and Girirajan, 2008]. Multiple congenital defects, regarding cardiovascular and genitourinary systems, have been reported for 30-40% of the subjects [Elsea and Girirajan, 2008].

Fig.1 Facial features of Smith Magenis syndrome. On the top, a SMS male patient at 23 months, 3 years, 12 years, and 17 years. Above, a SMS female patient at 7 months, 2 years, 9 years, and 21 years. Modified from Neira-Fresneda and Potocki, 2015.

Behavioral problems, manifesting in the vast majority of SMS individuals, include hyperactivity, aggression, opposition, stereotypies, autistic traits, self-injury encompassing self-hitting, self-biting, skin picking, polyembolokoilamania (insertion of foreign bodies into body orifices), onychotillomania (pulling out nails). A suggestive SMS stereotypy is the spasmodic upper-body squeeze or "self-hug" behavior,

which might be used as an effective clinical diagnostic marker for the syndrome (**Fig.1**) [Smith et al., 2019].

Along with behavioral anomalies, sleep disturbances are a hallmark of the syndrome and have been observed in 75-100% of cases. SMS patients indeed present difficulties in falling asleep at night, early waking, frequent night-time arousals, daytime napping, and polysomnography reveals diminished REM sleep and fragmented-shortened sleep cycles [Greenberg et al., 1996; Potocki et al., 2000a; Boone et al., 2011]. The disruption of circadian rhythm, in an estimated 95% of affected individuals, is underpinned by an inverted circadian rhythm of melatonin [Boone et al., 2011]. Sleep anomalies exacerbate an already compromised behavioral phenotype and are a major issue for caregivers.

The phenotypic signature can be mild in infancy and early childhood, frequently delaying diagnosis until school age, when the characteristic facial dysmorphisms and behavioral phenotype may be more readily visible [Greenberg et al., 1991; Greenberg et al., 1996; Edelman et al., 2007; Truong et al., 2010].

1.1.2 Molecular and genetic basis - SMS Etiopathogenesis

At molecular level the most common genetic cause, accounting for about 90% of SMS cases, is the interstitial deletion at 17p11.2, whose extension might range between 1.5 to 9 Mb [Girirajan et al., 2006]. A common deletion spanning approximately 3.7 Mb is observed in about 70–80% of all the deleted patients, and is due to Non Allelic Homologous Recombination (NAHR) using flanking low copy repeats as substrate [Potocki et al., 2003; Vlangos et al., 2003]. Microdeletions, indeed, are promoted by the presence of specific DNA blocks (10-400 kb) with a >95% sequence identity known as Low-Copy Repeats (LCR) or Segmental Duplications (SD), making the region particularly unstable. 17p11.2 is one highly rearrangement-prone cytogenetic band due to the presence of four small LCR elements (LCR17pA, LCR17pB, LCR17pC e LCR17pD), and three larger LCRs (SMS-REPs), that based on their position along the chromosome, are called SMS-REPP (proximal), SMS-REPM (middle) and SMS-REPD (distal) (**Fig.2**) [Shaw et al., 2002; Elsea and Williams, 2011].

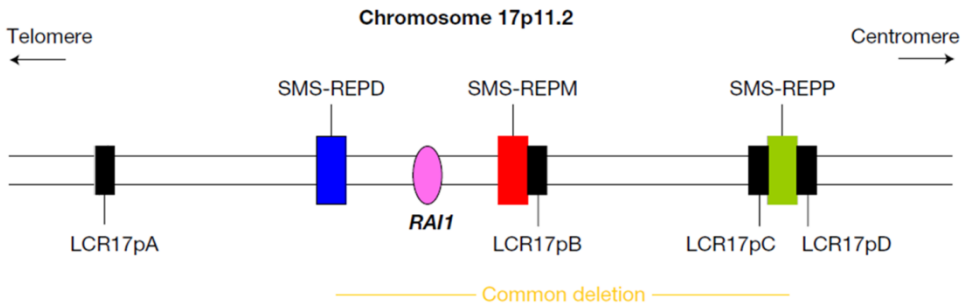

Fig.2 Genomic structure of 17p11.2 region. The three large LCRs are shown in blue (SMS-REPD), red (SMS-REPM) and green (SMS-REPP); the smaller one in black. Modified from Elsea and Williams, 2011.

The genomic instability of 17p11.2 results also from the presence of repetitive elements such as *Alu* elements and AT-rich repeats, that through NAHR and Non Homologous End Joining (NHEJ) mechanisms

are causative of the remaining 20-25% of SMS cases that display atypical deletions [Shaw et al., 2004; Shaw and Lupski, 2005]. Moreover, this genomic region is subject to rearrangements associated with other diseases in addition to SMS: Potocki-Lupski Syndrome (PTLS, OMIM#610883), Charcot-Marie-Tooth disease (CMT1A, OMIM#118220), and the hereditary neuropathy with liability to pressure palsies (HNPP, OMIM#162500) [Elsea and Girirajan, 2008]. This genomic architectural landscape corroborates the idea of 17p12p11.2 as a complex-rearrangement keen genomic region.

Approximately 80 known genes are included in 17p11.2 region and for long time SMS has been considered a contiguous gene syndrome [Greenberg et al., 1991]. Scanning the different-sized SMS deletions a common critical region of 1.5 Mb, involving 13 genes, was identified [Slager et al., 2003; Vilboux et al., 2011]. Subsequently, sequence analyses of these 13 genes in three patients with SMS phenotype, lacking the common deletion, disclosed frame-shift mutations on *RAI1* (*Retinoic Acid-Induced 1*), identifying it as the SMS causing gene [Slager et al., 2003]. Further studies revealed missense, non- sense and in-frame mutations mostly located on exon 3 (**Fig.3**) [Slager et al., 2003; Bi et al., 2004; Girirajan et al., 2005; Bi et al., 2006; Elsea and Girirajan 2008; Truong et al., 2010; Vieira et al., 2012]. All the identified pathogenic mutations, interfering with the protein structure and/or function, result in *RAI1* haploinsufficiency responsible for SMS phenotype.

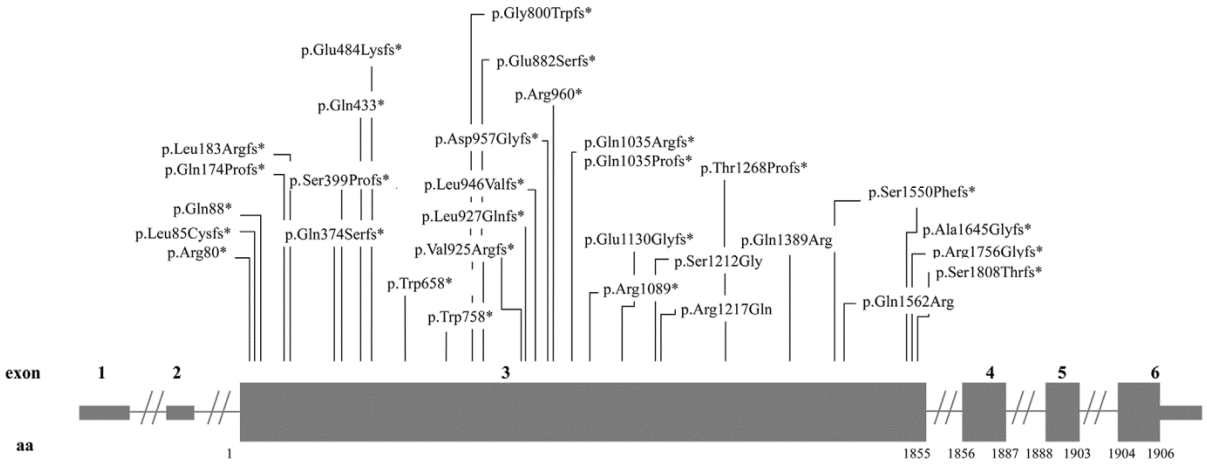

Fig.3 Schematic representation of *RAI1* genomic structure. The six exons are indicated by dark grey boxes, the introns by thin inreconnecting lines. All the reported mutations stored in HGMD cluster to exon 3 . Modified from Acquaviva et al., 2016.

Up to now, about 50 mutations associated with SMS have been detected (http://www.hgmd.cf.ac.uk/ac/all.php HGMD Professional, version 2018.3), and disclosed in 10% of patients with classical SMS clinical features but lacking the 17p11.2 deletion [Elsea and Girirajan, 2008; Williams et al., 2012]. A high phenotypic overlap is observed among patients harboring the 17p11.2 classical deletion and *RAI1* mutated patients. Nevertheless, cardiac and renal anomalies, motor delay, short stature, and hearing loss are associated with 17p11.2 deletions rather than *RAI1* mutations [Girirajan et al., 2006; Edelman et al., 2007; Yan et al., 2007; Ricard et al., 2010].

SMS is inherited in an autosomal dominant manner and is typically caused by *de novo* deletions or pathogenic variants in *RAI1* at 17p11.2, although some familial cases have been observed [Zori et al., 1993; Yang et al., 1997; Campbell et al., 2014]. Zori and collaborators identified a maternal mosaicism for 17p11.2 deletion [Zori et al., 1993]; other SMS cases of parental mosaicism are known, including one family with three affected sibs due to maternal mosaicism [Campbell et al., 2014]. Even complex chromosome rearrangements leading to 17p11.2 deletion are rare but have been reported [Yang et al., 1997; Park et al., 1998; Goh et al., 2014]. Moreover, Acquaviva and collaborators in 2017 reported for the first time an SMS patient, harboring a *RAI1* frameshift mutation, having offspring with the same alterations [Acquaviva et al., 2017].

1.1.3 RAI1 gene: a chromatin reader

RAI1 (OMIM*607642, NM_030665), the SMS causing gene, is composed of six exons, four of which are protein coding, and is widely expressed particularly in the brain. The 8.5 kb transcript encodes a 1,906 amino acids protein with a molecular mass of 203 kDa [Slager et al., 2003; Toulouse et al., 2003]. RAI1, highly conserved in different species, contains different functional domains: starting with N-terminal a polyglutamine rich tract (Poly-Q), a polyserine rich domain (Poly-S), a bipartite Nuclear Localization Signal (NLS), a second Poly-S tract, a nucleosome-binding domain (NBD), and a C-terminal "plant homeo-domain" (PHD) are present (**Fig.4**) [Carmona-Mora and Walz, 2010; Carmona-Mora et al., 2010; Darvekar et al., 2012; Darvekar et al., 2013; Huang et al., 2016]. The RAI1 PHD domain, which contains a His-Cys5-His-Cys2-His motif, is extremely conserved in nuclear proteins implicated in chromatin remodeling and in transcriptional regulation [Milne et al., 2002; Nakamura et al., 2002; Bi et al., 2004].

Fig.4 RAI1 protein organization. Key functional domains include Glutamine-rich stretches in green, Polyserine-rich regions in orange, two NLS in black, NBD in light blue, and PHD in blue.

RAI1 is a transcription factor that regulates the expression of many neurodevelopmental genes in the mammalian brain and is involved in the maintenance of circadian rhythmicity [Williams et al., 2012; Garay et al., 2016; Huang et al., 2016]. Indeed, haploinsufficiency of *RAI1* in patients' fibroblasts induces a transcriptional dysregulation of the circadian clock causing an altered expression of many circadian genes [Williams et al., 2012]. A similar transcriptional alteration was observed in the hypothalamus of *Rai1*$^{+/-}$ mice, which share the same human RAI1 protein structure with 82% of sequence homology [Williams et al., 2012]. Moreover, RNASeq data from cortex and striatum neurons of *Rai1* conditional knockout mice showed that RAI1 regulates BDNF (Brain Derived Neurotrophic Factor) [Garay et al., 2016] and genes involved in cell adhesion, axon guidance and neuronal morphogenesis, such as *CDH7*,

CDH8, *CDH9*, *EPHA7*, *PCDH20*, and *SEMA3A* [Huang et al, 2016]. Recent data showed also that murine Rai1 preferentially occupies active promoters and enhancer regions of genes mainly related in circuit assembly and neuronal communication (**Fig.5**) [Huang et al., 2016].

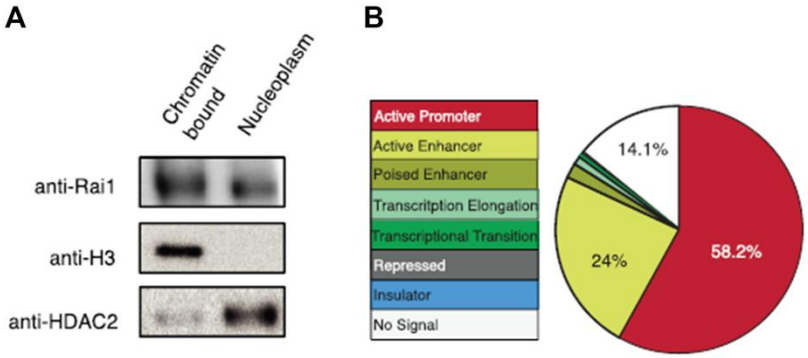

Fig.5 Mouse Rai1 occupies promoter regions of active chromatin *in vivo*. A) Cellular fractionation assay on mouse cortex cells reveals that Rai1 is present in both nucleoplasmic (HDAC2) and chromatin-binding (histone H3) fractions. **B)** Recording of Rai1 binding sites detected by ChIP-seq experiments shows that that Rai1 binds active promoter and enhancer regions. Modified from Huang et al., 2016.

Additionally, recent studies demonstrated that RAI1 works as chromatin reader acting in a complex, named "RAI1 complex", including iBRAF (HMG20B), PHF14 and TCF20, that binds unmethylated H3K4 and recruits MLL1 (KMT2A) to tri-methylate H3K4, thereby promoting gene transcription (**Fig.6**) [Eberl et al., 2013; Garay et al., 2016].

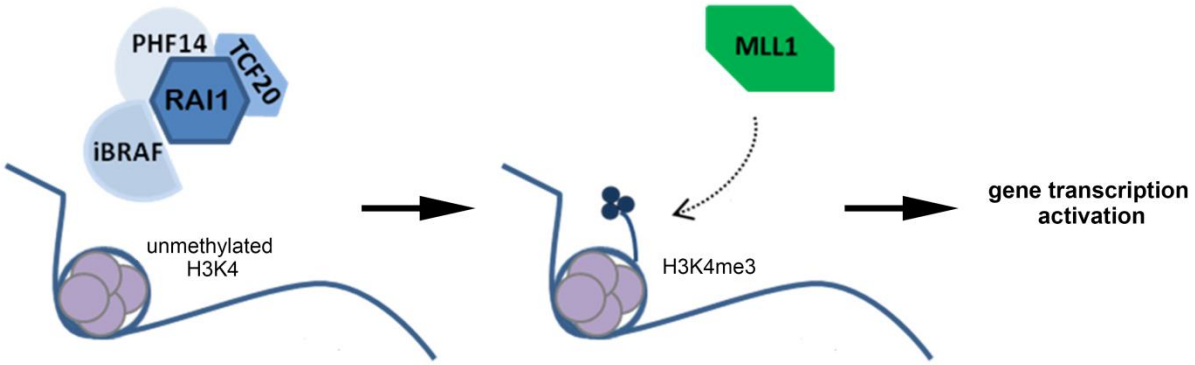

Fig.6 Model of RAI1 complex activity on histone H3K4 methylation, promoting genes transcription activation. Modified from Garay et al., 2016.

Notably, *TCF20* (OMIM*603107) is associated to a developmental disorder [Vetrini et al., 2019] and *MLL1*, encoding an H3K4me writer is the causative gene of Wiedemann-Steiner syndrome (OMIM#605130) [Jones et al., 2012]. Moreover, *RAI1* shows >50% sequence similarity with *TCF20* gene, that encodes an SPRE-binding transcription factor, strongly expressed in pre-migratory neural crest cells [Darvekar et al., 2013]. Structural commonalities between RAI1 and TCF20 protein are illustrated in **Figure 7** [Vetrini et al., 2019].

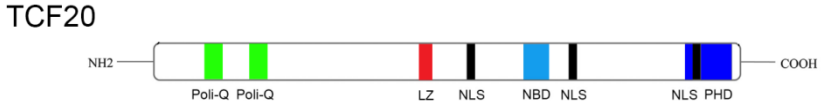

Fig.7 TCF20 protein organization. Key functional domains of TCF20, shared with RAI1, include Glutamine-rich stretches in green, NLS in black, NBD in light blue, and PHD in blue. A further unique domain present in TCF20 is a Leucine zip (LZ) domain in red.

Recent studies suggested that the high sequence homology and conservation of specific protein domains might be attributed to an ancestral gene duplication event during early vertebrate evolution [Darvekar et al., 2013].

The "RAI1 complex" seems to counterbalance the activity of the SD1-CoREST repressor complex, that negatively regulates the expression of neuron-specific genes, removing histone modifications [Garay et al., 2016]. Overall both complexes, regarded as two chromatin modifying machineries, show a gene expression regulation essential for learning, memory and neuronal plasticity [Loebrich and Nedivi, 2009; Ebert and Greenberg et al., 2013].

1.1.4 Potocki-Lupski Syndrome: the SMS reciprocal syndrome

Potocki-Lupski Syndrome (PTLS, OMIM#610883), also known as trisomy 17p11.2, is the SMS reciprocal syndrome affecting 1 in 20,000 live births (**Fig.8**) [Shuib et al., 2017]. By dissecting the duplications identified in different PTLS patients, a minimum common region extending for 125 kb and containing only *RAI1* gene has been observed [Zhang F et al., 2010]. Experiments on mouse models have established that alterations in *Rai1*, which is a dosage-sensitive gene, are responsible for the SMS and PTLS phenotypes [Walz et al., 2006; Carmona-Mora and Walz, 2010; Shuib et al., 2017].

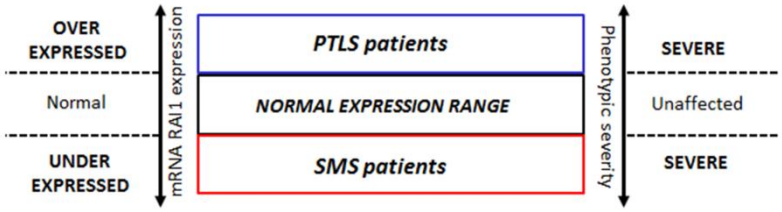

Fig.8 *RAI1* is a dosage-sensitive gene. When chromosomal region 17p1121 is altered due to genomic imbalance, manifestation of either SMS or PTLS results. *RAI1* mRNA expression studies provide the evidence for the impact of a genomic abnormality on this dosage-sensitive gene. *RAI1* duplication typically affects mRNA expression, leading to increased levels ranging from 1.50- to 1.80-fold over normal levels, while *RAI1* deletion typically reduces mRNA expression to ~ 0.5-fold of normal.

PTLS is characterized by speech and language impairment, ID, behavioral problems (attention deficit, hyperactivity, anxiety, autistic features), infantile hypotonia, failure to thrive, congenital cardiovascular anomalies, and sleep difficulties characterized by moderate to severe sleep latency and sleep maintenance [Neira-Fresneda and Potocki, 2015; Mullegama et al., 2017; Praticò et al., 2018]. The molecular characterization of sleep features in PTLS has not been performed, but recent studies have shown an altered circadian rhythm associated to *RAI1* overexpression [Mullegama et al., 2017]. Most of PTLS individuals show facial features which would not be considered as proper dysmorphic, nevertheless shared traits, such as triangular face, broad forehead, smooth philtrum, micrognathia, long nasal tip, and downslanting palpebral fissures are observed (**Fig.9**) [Neira-Fresneda and Potocki, 2015].

Fig.9 Facial features of Potocki-Lupski syndrome. On the top, a PTLS male patient at 6 months, 6 years, 10 years, and 19 years. Above, a SMS female patient at 8 months, 3 years, 10 years, and 28 years. Modified from Neira-Fresneda and Potocki, 2015.

PTLS phenotypic features are reportedly less comprehensibly characterized and much milder than those observed in SMS. Indeed, less than 50 individuals with PTLS have been reported [Praticò et al., 2018], supporting the fact that genomic duplications are generally better tolerated than the corresponding deletions. In addition, the presence of a poorly characterized phenotype, that exhibits mild clinical signs shared with SMS, makes PTLS diagnosis tricky. A representative example is the study conducted by Alaimo and collaborators in 2015: the proband, initially clinically diagnosed as SMS due to the presence of a maternal deletion at 17p11.2 upstream of *RAI1*, showed an increase of *RAI1* transcript levels, that led to the clinical re-evaluation of the proband and to a PTLS diagnosis [Alaimo et al., 2015].

1.1.5 SMS Overlapping syndromes

Despite the existence of peculiar phenotypic characteristics, SMS clinical diagnosis is often wrong and/or underestimated due to delayed onset of evident craniofacial dysmorphisms and due to the phenotype partially shared by other syndromes. Indeed, SMS might enter in differential diagnosis with syndromes displaying distinctive *facies*, brachydactyly, developmental delay, infantile hypotonia, ID, sleep disturbance and behavioral problems, such as 2q23.1 deletion (OMIM#156200), Brachydactly Mental Retardation (BDMR, OMIM#600430), and Kleefstra syndrome (KS, OMIM#610253), [Kleefstra et al.,2006; Williams et al., 2010a; Williams et al., 2010b; Morris et al., 2012; Mullegama et al., 2015a; Larizza and Finelli, 2018] as shown in Venn diagram (**Fig.10**).

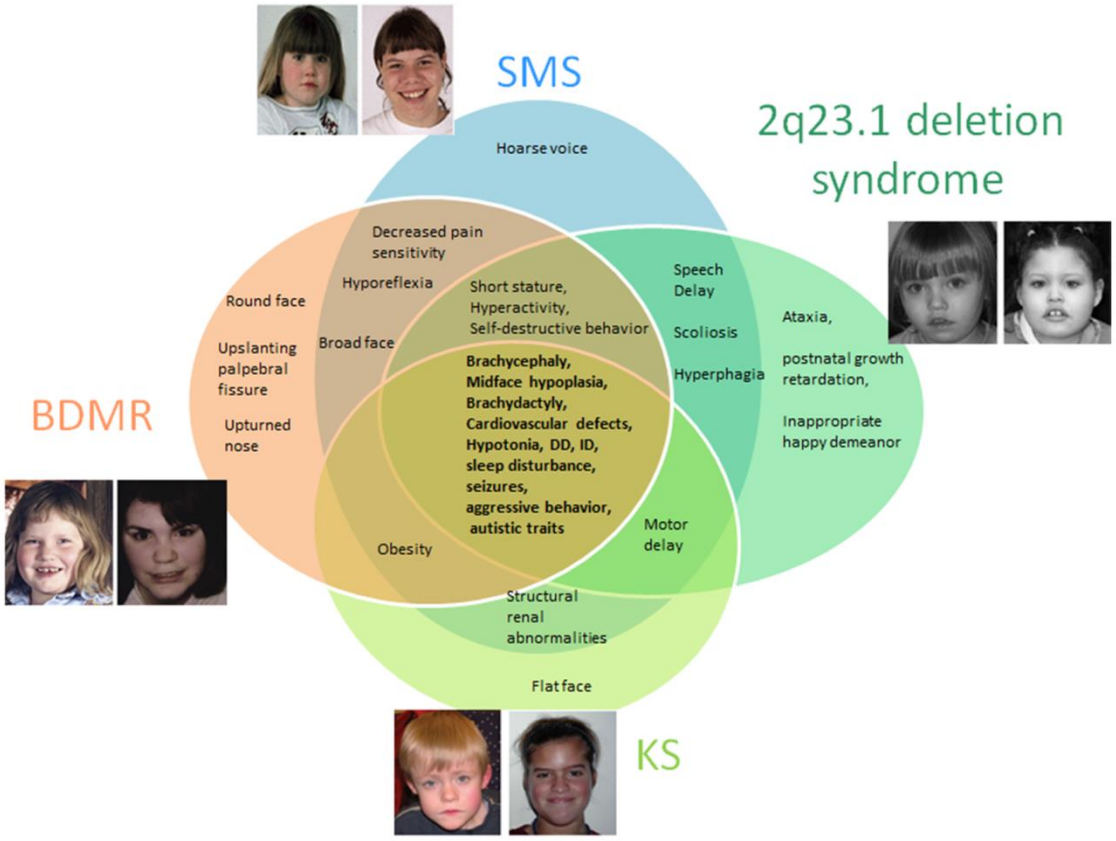

Fig.10 Venn diagram showing common and specific clinical features of SMS-overlapping disorders (2q23.1 deletion, BDMR and Kleefstra syndromes). The main clinical signs shared by patients are depicted in black-bolded characters. Patients pictures from Kleefstra et al., 2006; Williams et al 2010 a –b; Smith et al., 2019. Modified from Larizza and Finelli, 2018.

The phenotypic overlap of 2q23.1 deletion, BDMR and Kleefstra syndrome with SMS is likely resulting from the direct or indirect connection between their causative genes and *RAI1*.

- 2q23.1 deletion syndrome is caused by haploinsufficiency of *MBD5* gene, encoding a member of the methyl-CpG-binding domain (MBD) family involved in DNA methylation and chromatin remodeling [Mullegama and Elsea, 2016]. In addition to MBD domain, MBD5 contains a tryptophan-rich domain (PWWP), known as a recognition motive for histone marks predominantly associated with actively transcribed chromatin [Walz and Young, 2014], suggesting a possible role of MBD5 in transcriptional regulation [Mullegama et al., 2015a]. *MBD5* disruption might be mediated by either deletion in the chromosomal region 2q23.1 [Jaillard et al., 2009; Williams et al., 2010a] or loss of function mutations, leading to an overlapping phenotype [Talkowski et al., 2011; Kleefstra et al., 2012; Carvill et al., 2013]. Nearly all cases of 2q23.1 deletions reported in literature have arisen *de novo*; however, there are also reported familiar cases of inherited 2q23.1 microdeletion [van Bon et al., 2010; Hodge et al., 2014; Tadros et al., 2017; Woodbury-Smith at al., 2017], where the healthy transmitting parents might present the rearrangement in a mosaic form [Tadros et al., 2017]. The fact that *MBD5* might positively control *RAI1* transcription has been sustained by *RAI1* downregulation in lymphoblastoid cell lines (LCLs) of patients with 2q23.1 deletion [Mullegama et al., 2015a]. Further expression studies on patients' LCLs

and on siRNA knockdown cells relate *MBD5* haploinsufficiency to downregulation of circadian rhythm pathway genes, thus accounting for sleep disturbance in both SMS and 2q23.1 deleted patients [Mullegama et al., 2015b].

- BDMR, also described in literature as 2p37 deletion syndrome, is associated with haploinsufficiency of *HDAC4* gene, which encodes the histone deacetylase 4, a chromatin eraser essential for normal bone, muscle and neurological development [Falk and Casas, 2007; William et al., 2010b; Leroy at al., 2013]. *HDAC4* has a negative role in transcriptional regulation of several genes encoding constituents of central synapses, thereby affecting synaptic architecture and transmission [Sando et al., 2012]. As in the case of *MBD5*, it might be assumed that *HDAC4* plays a role in *RAI1* transcriptional regulation, since BDMR patients show *RAI1* downregulation [Williams et al., 2010b; Le et al., 2019]. The fact that *HDAC4* is the primary causative gene for BDMR is supported by identified small 2q37.3 microdeletions including only *HDAC4*, as well as *HDAC4* mutations [Williams et al., 2010b;]. BDMR presents broad and heterogeneous clinical features, i.e. developmental delay is the most highly penetrant sign, while ID shows a variable severity and can be absent in the patients [Jean-Marcais at al., 2015; Wheeler et al., 2014].

- Microdeletions or point mutations in *EHMT1* gene are responsible for KS, also known as 9q34.3 deletion syndrome [Kleefstra et al., 2006]. The *EHMT1* gene encodes a histone methyltransferase, considered as a histone writer involved in chromatin remodeling during neurodevelopment and synaptic plasticity, that mono- and di-methylates H3K9 (histone 3 lysine 9) [Benevento et al., 2016]. Moreover, the H3K9me2/3 increase correlates with altered expression of protocadherins, principal regulators of cell-cell adhesion and neuronal connectivity associated with ASD etiology [Iacono et al., 2018]. Though a direct molecular link with *RAI1* remains to be assessed for *EHMT1*, a connection between KS and SMS is likely mediated by *MBD5*. Indeed, pathogenic *de novo* variants in *MBD5* and in other epigenetic regulators such as *SMARCB1*, *NR1I3*, and *KMT2C* were reported in individuals with clinical diagnosis of Kleefstra syndrome [Kleefstra et al., 2012; Koemans et al., 2017].

1.1.6 High throughput genome-wide analyses in SMS

Only 50% of individuals with SMS clinical suspicion are confirmed by the genetic test, suggesting that other *loci* may be involved directly or indirectly in the same pathway of *RAI1* gene, hence contributing to the SMS-like phenotype. The best approach to understand and discover the molecular basis of a complex disorder is genome-wide investigation, such as array-CGH and Next Generation Sequencing (NGS). Array-CGH screening in SMS-like patients, displaying most of SMS clinical features but lacking either the classical SMS deletion or *RAI1* mutation, disclosed *HDAC4* and *MBD5* alterations [Williams et al., 2010a; Williams et al., 2010b]. However, the great majority of patients analyzed by array approaches turned out to be negative for any rare variant involving genes possibly related to *RAI1*: for this purpose, the application of NGS might be a valuable complementary tool to discover the molecular defects of the

pathology. Up to now, whole exome sequencing (WES) analysis has been performed only in 21 individuals with a clinical suspicion of SMS but without a molecular diagnosis, evidencing potentially deleterious variants in different genes including *KMTD2*, *MECP2, KDM5C, IQSEC2* and *DEAF1* [Loviglio et al., 2016; Berger et al., 2017]. Vetrini et al, recently analyzed by a combined approach using WES and array-CGH 31 unrelated families with clinical characteristics resembling those observed in SMS. Notably, they reported pathogenic variants in *TCF20* (25 inactivating single nucleotide variants/indels and 4 deletions), supporting the commonalities in gene structure and function between *TCF20* and *RAI1* thus explaining the shared core clinical features and molecular effects [Vetrini et al., 2019].

1.2 Circadian Clocks & Circadian Rhythms in SMS and related disorders

Sleep disturbance is one of the most incisive and clinically troublesome features of SMS, and is a consequence of an inverted melatonin secretion observed in the majority of SMS cases (**Fig.11**) [Boone et al., 2011].

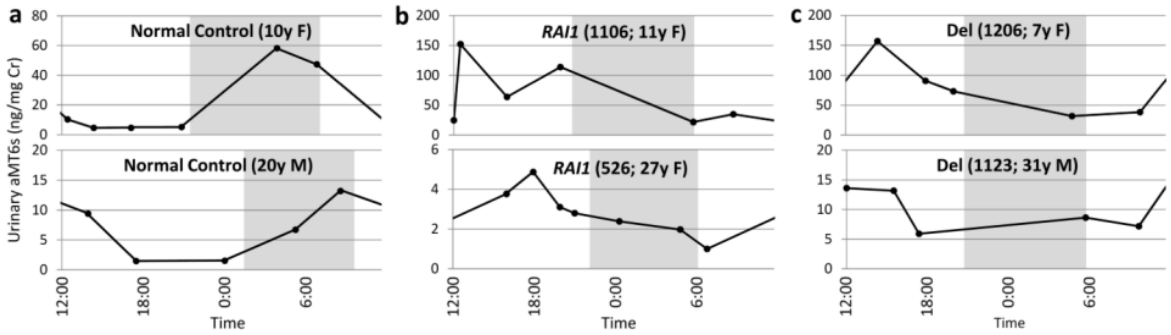

Fig.11 Impairment of melatonin rhythmicity in SMS patients. Levels of urinary6-sulfatoxymelatonin (aMT6s), a surrogate for serum melatonin concentration, detected in healthy individuals (a), RAI1 mutated patients (b), and individuals with the SMS common deletion (c). The rhythmicity is inverted in SMS patients compared to controls. Shaded areas show the period of darkness. Modified from Boone et al.,2011.

In healthy controls the highest level of urinary 6-sulfatoxymelatonin (aMT6s), a surrogate for serum melatonin, is observed in the first morning sample, reflecting the normal rise of serum melatonin during the night; in SMS patients the aMT6s concentration peak is found instead during the day (**Fig.11**) [Boone et al., 2011]. Combined treatments with β_1-adrenergic antagonists (acebutolol) during the day to block the abnormal melatonin release, and an evening melatonin administration was found to improve the overall sleep disorder of SMS patients [Carpizio et al., 2006; De Leersnyder, 2013].

The PTLS sleep phenotype has not been extensively elucidated: however recent studies demonstrated that PTLS patients exhibit an intrinsic sleep dyssomnia [Mullegama et al., 2017].

In both disorders sleep problems may be due to defect in circadian rhythms mediated by the abnormal functioning of *RAI1* gene.

The circadian rhythm consists of a biological cycle of about 24 hours, aimed at controlling several physiological and behavioral functions according to the environmental context. The exposure of retina

to light impacts on transcription of specific genes and initiates a molecular loop based on transcriptional and post-transcriptional mechanisms. In mammals, circadian rhythm is controlled by a master clock located in the suprachiasmatic nucleus of the hypothalamus, and is responsible for the transcriptional regulation of many genes, allowing the organism to anticipate and adapt to environmental changes during the day. This occurs thanks to secondary clocks located in peripheral organs, acting independently from each other but continuously reclocked to the master clock by means of melatonin, whose synthesis takes place in the epiphysis and is positively regulated by the master clock and negatively by light exposure. Several studies on animal models demonstrated that melatonin regulates the expression of different genes including *CLOCK*, *BMAL1*, *PER1*, *PER2*, *CRY1*, both in the central nervous system and in the periphery [Charrier et al., 2017].

The core of transcriptional mechanism involves the trigger protein CLOCK (Clock Circadian regulator) and BMAL1 (Brain and Muscle ARNT-Like protein1), two transcriptional factors able to heterodimerize in the cytoplasm, then migrating into the nucleus where they drive the transcription activation of many target genes, by binding E-box elements (**Fig.12**) [Gekakis et al., 1998]. The proteins encoded by some of these target genes are themselves components of the circadian clock, such as PER (Period) and CRY (Cryptochrome) proteins. The genes, regulated by circadian clock and whose products transmit the rhythm information to the rest of the body, are called clock-controlled genes (CCGs). PER and CRY proteins are unstable and need to be stabilized by other proteins. These stabilizer proteins are produced and accumulated during the day, allowing PER and CRY to heterodimerize and finally migrate to the nucleus, where they inhibit the CLOCK-BMAL1 activity and consequently their own transcription and transcription of other CLOCK-dependent genes (**Fig.12**). The PER-CRY heterodimer activity reaches the maximum level at the beginning of the night and then decreases. At the same time, the CLOCK-BMAL1 heterodimer returns to normal asset progressively during the night. Therefore, this molecular regulation mechanism consists of a feedback cycle including a positive regulator (CLOCK-BMAL1) and a negative one (PER-CRY) (**Fig.12**). A further regulatory system concerns the nuclear receptors of *REV-ERB* (*NR1D*) and *ROR* families, whose transcription is switched on by the CLOCK-BMAL1 heterodimer. These nuclear receptors activate (ROR) or inhibit (REV-ERB) the transcription of *BMAL1* [Preitner et al., 2002; Sato et al., 2004; Cho et al., 2012] and *CLOCK* [Crumbley and Burris, 2011], thus modulating their own activators (**Fig.12**). This secondary feedback is called "stabilizing loop". A post-transcriptional mechanism is responsible for the degradation of PER and CRY, necessary for the starting of a new cycle. PER and CRY have many phosphorylation sites that regulate the ubiquitination and degradation of the two proteins, e.g. CKIε (protein Casein Kinase 1 Epsilon) phosphorylates PER, making it less stable and unable to move into the nucleus [Charrier et al., 2017].

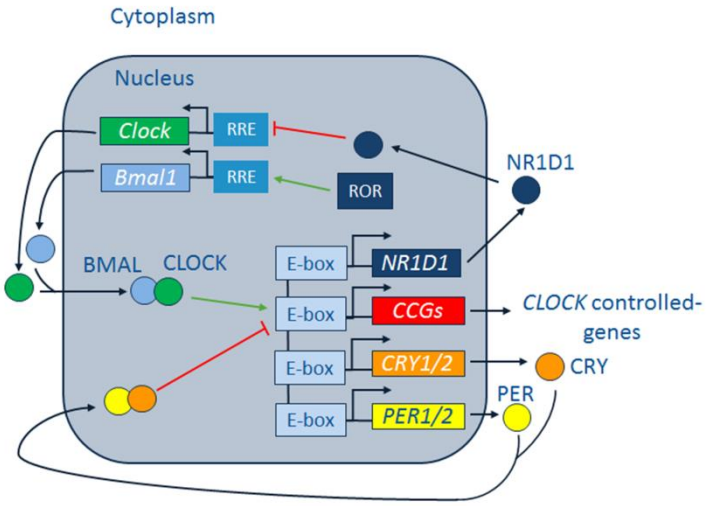

Fig.12 Molecular machinery and molecular feedback loops of the circadian clock.

Expression studies, carried out on both SMS, PTLS patients and *in vitro*, confirmed the involvement of *RAI1* in the regulation of circadian clock, since circadian rhythm genes show a significant deregulation compared to controls (**Fig.13**) [Williams et al., 2012; Mullegama et al., 2017]. Moreover, Williams and collaborators identified a region of 51 bp mapping in IVS1 of *CLOCK* that interacts with *RAI1* [Williams et al., 2012]. In addition, the correlation between *RAI1* haploinsufficiency and expression alterations of genes involved in the circadian rhythm was confirmed by RT-qPCR on RNA extracted from SMS patients' fibroblasts (**Fig.13 A**)[Williams et al., 2012]. In the same study, the authors demonstrated that a reduction in *RAI1* expression mediated by siRNA knockdown in HEK293T cells results in decreased expression of many circadian clock genes including *CLOCK, RORC, RORA, PER3, CRY1, CRY2, NR1D1,* and *NRD1D2* (**Fig.13 B**)[Williams et al., 2012].

In PTLS patients the expression of circadian clock genes was tested in lymphoblastoid cell lines (LCLs) [Mullegama et al., 2017]. The transcription levels of *PER* genes were significantly reduced, while no differences were observed compared to controls for CRY genes (**Fig.13 C**) [Mullegama et al., 2017]. Since *CLOCK* and *BMAL1* genes are poorly expressed in LCLs, RAI1 overexpression was induced in HEK293T cells, where the transcription levels of *CLOCK* and *BMAL1* result comparable to those of controls, and a deregulation has been pointed out for both *PER* and *CRY* genes (**Fig.13 D**) [Mullegama et al., 2017]. These findings suggest that increased *RAI1* expression might not impair the master regulators (*CLOCK* and *BMAL1*), though affecting the circadian clock. Furthermore, the different mRNA levels of *CRY* genes in LCLs and HEK293T cells suggest a tissue-specific regulation [Mullegama et al., 2017].

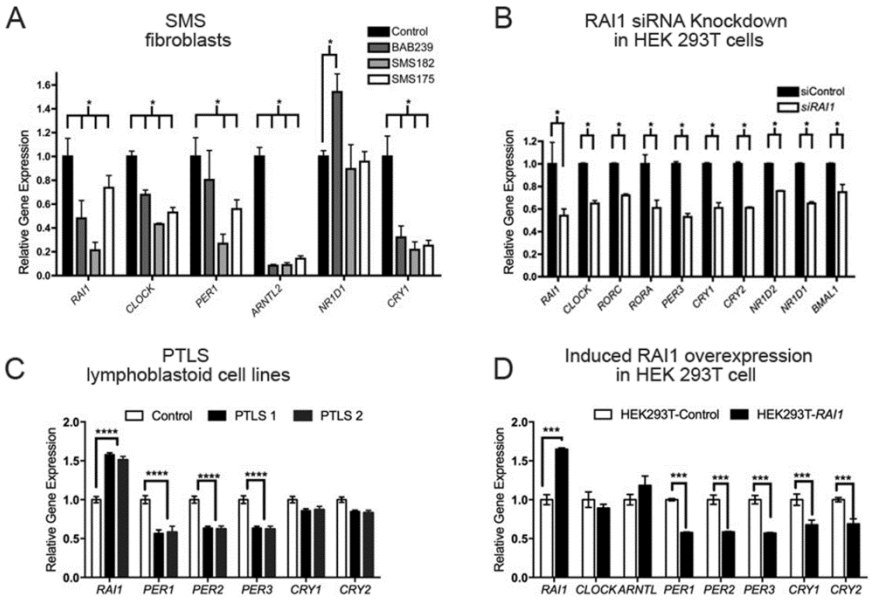

Fig.13 Circadian-gene expression analysis in SMS, PTLS patients and *in vitro.* A) Altered expression of core genes in SMS fibroblasts assessed 24 hr after cell synchronization by cell passage. BAB239 represents a SMS patient with the common 3.4 Mb deletion, SMS182 a patient with a small unusual 17p11.2 deletion, and SMS175 is a patient harboring a RAI1 pathogenic missense mutation. B) Circadian-gene expression in HEK 293T cells treated for knockdown of RAI1 by siRNA. C) Expression study of downstream target genes of CLOCK in PTLS patient's lymphoblastoid cell lines. D) Circadian-gene expression in HEK 293T cells overexpressing RAI1. Significant differences in gene expression are indicated by asterisks. Modified from Williams et al.,2012 and from Mullegama et al., 2017.

1.3 Human iPSCs model of neurodevelopmental disorders

Neurodevelopmental disorders (NDDs) refer to a very broad group of disabilities, involving disruption of the physiological CNS development. By definition neural networks and activity are affected, resulting in a wide spectrum of emotional, cognitive and motor deficits, such as ID, ASD, communication disturbances, specific learning and motor disorders [Ardhanareeswaran et al., 2017]. NDDs can be found in non-syndromic and syndromic forms, in which other clinical and behavioral signs are present, and typically have onset in childhood, before puberty.

The NDDs pathogenesis is extremely challenging to study, due to the complexity of human brain, the lack of a suitable model, and the inability to isolate populations of neurons from living subjects. Up to now, scientists have studied human brain development through the analysis of postmortem tissue, but this kind of samples provides only a single endpoint reading and offer little insight into the early pathogenic processes that give rise to the observed disorders [Ardhanareeswaran et al., 2017]. Indeed, even if patients manifest symptoms postnatally, all genetic NDDs are likely to involve prenatal structural and/or functional brain alterations [Johnson et al., 2009]. A poor understanding of pathogenesis of NDDs has been also provided by rodent models as they lack the human brain complexity, especially concerning the cortex. Mice and rats, in fact, have fewer neurons and lower neuronal density than humans [Herculano-Houzel, 2009]. Moreover, human brain development is also much slower than that of the rodent brain, resulting in an increased outgrowth of prefrontal and temporal cortices [Rakic,

1995]. These areas are usually associated to high cognitive functions, such as language and emotions, and are most relevant to NDDs. Moreover, the identification of few CNS-targeted drugs for NDDs *via* rodent models, suggests their limitations for NDDs study [Ghosh et al., 2013].

A new approach is provided by the recent technological advances in the generation and the following neural differentiation of human induced pluripotent stem cells (hiPSCs). HiPSC model can resume the progression of brain development and the consequences of its dysfunctions "in a dish", recapitulating the alterations responsible for NDDs. Moreover, this technique enables to maintain the genetic background of patients, which is very useful to assess if the defect might affect the physiological neuronal growth and function, allowing to study the contribution of genetic and non-genetic factors underlying both normal and diseased neuronal circuitry [Russo et al., 2019].

HiPSCs are undifferentiated cells with self-renewal capability, equivalent to embryonic stem cells (ESCs) since they are able to differentiate into most cell types of the body; these features are a consequence of their unique epigenetic status characterized mainly by open chromatin structure, resulting in active transcription. However, unlike ESCs, hiPSCs can be derived from any somatic cell [Ardhanareeswaran et al., 2017]. Up to now, different cell types have been tested to enhance reprogramming procedure and efficiency, and to reduce the invasiveness of obtaining patient samples. The first cell type used to obtain hiPSCs were fibroblasts derived from dermal punch biopsies [Takahashi et al., 2007; Yu et al., 2007]. Nonetheless, obtaining fibroblast cell lines is somewhat invasive. In 2008, Aasen and collaborators tried to generate hiPSCs from keratinocytes, that are easily obtainable from patients by plucking hairs, but the reprogramming was challenging to reproduce early on [Aasen et al., 2008]. The gold standard for hiPSCs generation are the peripheral blood mononuclear cells (PBMCs): they are both easily obtained from patients and easily reprogrammed [Staerk et al., 2010]. Recent studies demonstrated the ability to reprogram also renal epithelial cell from urine [Xue et al., 2013] and dental pulp stem cells from deciduous teeth [Yan et al., 2010].

Great improvements have been made in neural differentiation protocols during the years: the early protocols utilized embryoid body (EB) intermediates, emulating the process of gastrulation in order to direct some tissue down the ectodermal lineage [Johnson et al., 2007], while more recent procedures require dual SMAD inhibition using Noggin to restrict the cells differentiation to ectodermal tissues [Germain et al., 2013]. Nowadays, hiPSCs can be differentiated into specific populations of neuronal subtypes, such as cortical neurons, dopaminergic neurons, excitatory and inhibitory neurons, astrocytes, oligodendrocytes, and microglia; it is also possible to generate 3D organoids in which several brain cell types and tissue layers develop from precursor cells [Ardhanareeswaran et al., 2017].

In view of this, researchers started to use hiPSCs as *in vitro* model to study human genetic disorders, and shed light on the molecular mechanisms underlying the diseases (**Fig.14**). HiPSC-derived neurons have

been reported to recapitulate the cellular pathological phenotypes, including altered morphology and neurite degeneration. In particular neurodegenerative disorders such as amyotrophic lateral sclerosis (ASL) [Chen et al., 2014; Sances et al., 2016], Huntington disease [Zhang N et al., 2010; Juopperi et al., 2012], Parkinson's disease [Nguyen et al., 2011; Jiang et al., 2012; Sanchez-Danes et al., 2012], and Alzheimer disease [Yagi et al., 2011; Israel et al., 2012; Kondo et al., 2013] have been largely studied. Recently, hiPSCs have been successfully generated also for modeling NDDs: namely Rett [Marchetto et al., 2010; Cheung et al., 2011; Farra et al., 2012], Fragile X [Urbach et al., 2010; Sheridan et al., 2011; Doers et al., 2014], Prader-Willi [Chamberlain et al.,2010; Yang et al., 2010; Martins-Taylor et al., 2014], Angelman [Chamberlain et al.,2010], Phelan McDermid [Shcheglovitov et al., 2013] and Rubinstein-Taybi syndromes [Alari et al., 2018]. Even in this case, the derived neurons showed altered cellular morphological and electrophysiological phenotypes.

Besides neurological disorders, up to now several pathological conditions affecting other tissues or organs have been studied by means of hiPSCs, including immunological disorders, cardiac disease, juvenile diabetes, cystic fibrosis, and cancer [Park et al., 2008].

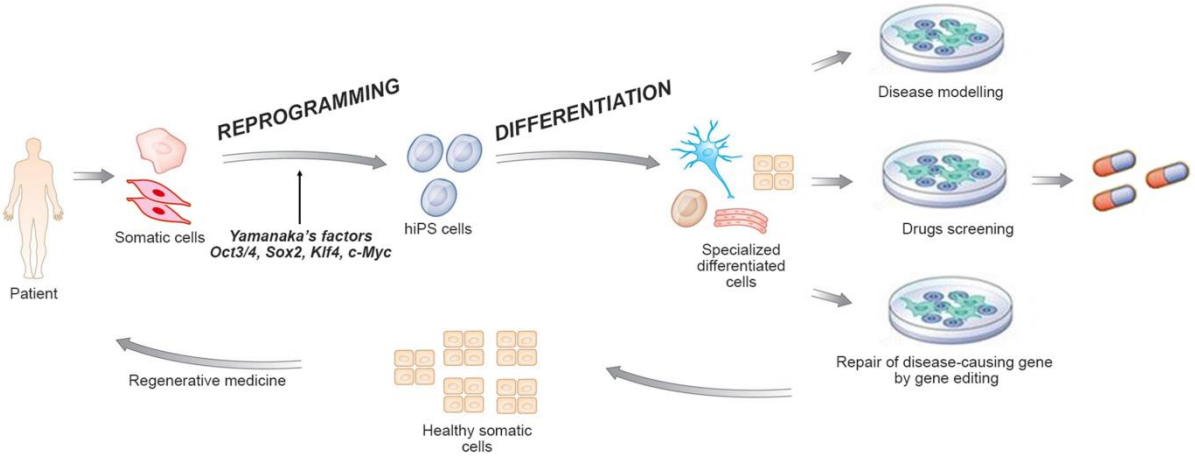

Fig.14 Potential applications of hiPSCs. Somatic cells from the patient are used for the generation of hiPSCs, by addition of the four Yamanaka factors, Oct, Sox2, Klf4, and c-Myc, which can further differentiate into desired types of cells. The obtained cells can be used as disease model to highlight the pathomechanism, to discover and screen new drugs, and might be repaired by in vitro Gene Editing and the generated healthy somatic cells transplanted back to the patient.

HiPSCs can be also used in translational applications, as they could be differentiated and implanted into individuals to cure injury or disease (autologous stem cells transplants) (**Fig.14**) [Chamberlain, 2016].

Finally, the iPSCs technology enables to test a myriad of drugs in a safe environment with human relevance and background (**Fig.14**) [Russo et al., 2019].

AIM

SMS patients are characterized by peculiar craniofacial dysmorphisms, neurological alterations with variable ID, speech and motor delay, behavioral problems, and sleep disorders. Only 50% of individuals with SMS clinical suspicion presents the classical microdeletion at 17p11.2 encompassing *RAI1* and/or mutation in this gene, suggesting that other *loci* may be involved directly or indirectly in the same molecular pathway, hence contributing to the SMS-like phenotype. The difficulty of an appropriate clinical diagnosis is also emphasized by a mild phenotypic signature in infancy and early childhood becoming more readily visible during school age.

In order to unveil the *RAI1* interconnected pathway underlying the SMS spectrum and to deepen the genetic mechanisms responsible for SMS-like phenotype, we analyzed by several approaches a cohort of 30 patients with ascertained clinical diagnosis but without the known genetic defects.

- High resolution array-CGH was applied searching for rare possibly pathogenic CNVs. This genome-wide approach has proven very useful to pinpoint rare CNVs containing dosage sensitive genes that might be implicated in *RAI1* molecular pathways leading to SMS-like phenotype.
- As sleep disturbance is a main feature of SMS and few data are available about the molecular alterations of this condition, an additional aim was to evaluate circadian rhythm genes expression level in peripheral blood cells of selected SMS/SMS-like patients through RT-qPCR analysis.
- Another crucial goal was to investigate using a functional approach candidate genes implicated in *RAI1* molecular pathway, resulting in SMS-like clinical manifestation. Considering that NDDs are extraordinarily difficult to study by only applying patients deep phenotyping and genomic tests on their accessible tissues, we modeled their disease by iPSC-derived neurons in the attempt to elucidate the pathway alterations that give rise to SMS/SMS-like phenotype. IPSCs, indeed, can be generated from patient's blood cells retaining the donor unique genetic signature, and can be differentiated into neurons, thus enabling us to reconstruct the genetic defects with a major role in the outcome of alterations in brain development. To address this point, a male patient (SMS8) of the cohort was selected for iPSCs reprogramming and differentiation into cortical neurons, to investigate the morpho-functional alterations of his cortical neurons as compared to control neurons.

Preliminary studies

Upon array-CGH analysis we selected the SMS8 patient, a male with SMS-like phenotype carrying a rare 54 kb deletion at Xq13.3 inherited form his healthy mother. The identified deletion does not involve any gene but a highly conserved insulator sequence and maps 29 kb far from the 5'UTR of *ZDHHC15* (Zinc Finger DHHC domain-containing protein 15) gene. RT-qPCR analysis performed on patient's peripheral blood cells revealed downregulation of *ZDHHC15* transcript, demonstrating that the gene expression alteration is likely mediated by the deletion through a position effect. Interestingly, *ZDHHC15,* encoding for a palmitoyl-transferase highly expressed in the brain and involved in neuronal differentiation and in synaptic plasticity [Shah et al., 2019], has been previously associated to a nonsyndromic X-linked intellectual disability [Mansouri et al., 2005]. Moreover another evidence of a relationship between palmitoylation and Central Nervous System (CNS) is the finding that alterations in zDHHC genes lead to neurological disorders such as Alzheimer's and Huntington's diseases, schizophrenia, ID, and major depressive disorder [Zareba-Kozioł at al., 2018].

Protein palmitoylation, catalyzed by a family of enzymes that transfer the fatty acid palmitate on the cysteine residue of its target, is the most common reversible post-translational lipid modification in the brain (**Fig.15 A**) [Shah et al., 2019]. In mammals 23 multi-pass transmembrane proteins are known and contain a conserved aspartate-histidine-histidine-cysteine (DHHC) motif, located within a cysteine-rich zinc finger-like domain, required for its enzymatic activity (**Fig.15 B**) [Globa and Bamji, 2017].

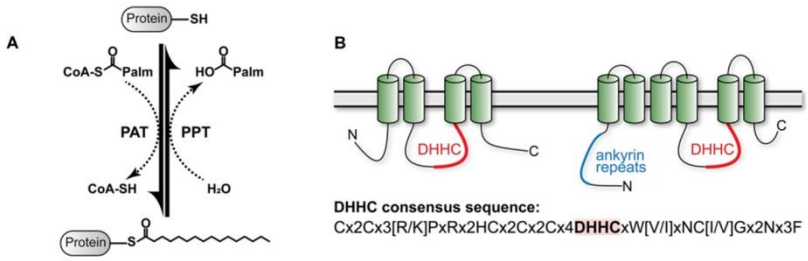

Fig.15 Protein Palmitoylation. A) Palmitoyl transferase (PAT) catalyses the transfer of a palmitate (Palm) on cysteine residue of its target protein, by thioester bond. The reverse hydrolytic cleavage is catalysed by selective palmityol protein-thioesterases (PPT). **B)** Membrane topology of ZDHHC proteins. ZDHHCs have four (left) or six (right) transmembrane domains (in red) with N- and C-termini in the cytoplasm. The ankyrin repeats are indicated in blue. At the bottom the consensus sequence of the DHHC domain. Modified from Matt et al., 2019.

Palmitoylation seems to be important for structure, stability and function of proteins, as well as trafficking, localization, interaction patterns, and cellular signaling regulation [Fukata and Fukata, 2010]. The protein palmitoylation status is controlled by the reverse process of depalmitoylation, catalysed by palmitoyl-protein thioesterases (PPTs) contain a/b-hydrolase domains (**Fig.15**) [Lin and Conibear, 2015].

In order to unveil the putative interconnection between RAI1 and ZDHHC15, we checked whether RAI1 would have any palmitoylation sites, thus becoming a putative substrate for reversible post-translational modification mediated by ZDHHC15. According to predictions, RAI1 is supposed to have up to 7 palmitoylation sites, mostly located on the C-terminal domain which is crucial for its intracellular localization. Taking into account the RAI1 involvement in circadian gene control and the presence of

sleep disturbance in SMS/SMS-like patients, in silico prediction of palmitoylation sites was extended to the main circadian gene proteins, and most of them resulted palmitoylated. To test *in vitro* whether a transient knock down of RAI1 and ZDHHC15 would lead to change in the expression of genes associated to the regulation of circadian rhythms, silencing experiments on human BE(2)-M17 neuroblastoma cell line were performed. Both RAI1 and ZDHHC15 silenced cells displayed significant deregulation of expression in up to half of the circadian genes, corroborating our working hypothesis.

MATERIALS AND METHODS

2.1 GENOMIC APPROACHES

2.1.1 Patients

The cohort recruited for this study includes 30 patients (16 females and 14 males) referred to our laboratory for SMS clinical suspicion raised by clinical geneticists or pediatricians. The main clinical features of Smith-Magenis syndrome have been evaluated and are reported in **Table 1**.

Clinical data was collected for all patients by clinicians at different hospitals who participated in this study, using the same clinical datasheet. Due to the lack of a minimum universally agreed clinical diagnostic criteria for SMS, patients were included in the study based on the clinical assessment by experienced clinicians of a cluster of features suggestive of SMS such as gestalt, unusual sleep function, and behavioral and developmental abnormalities. The absence of sleep disturbances, which are important components of 'classic' SMS, did not exclude study participation, especially because many individuals were enrolled in the early years of life. The phenotypic heterogeneity that characterizes SMS is well apparent also in our cohort, since not all patients present the totality of the SMS peculiar clinical signs, but some of them show a mild (SMS-like) phenotype.

Tab.1 Clinical features of analysed SMS patients. ID: Intellectual Disabilty; DD: Developmental Delay; NA: Not Available

	SMS1	SMS2	SMS3	SMS4	SMS5	SMS6	SMS7	SMS8	SMS9	SMS10
Gender	M	F	M	F	F	F	M	M	M	M
Age	15 y	19 y	NA	19 y	16 y	14 y	24 y	9 y	11 y	16 y
Dysmorphic facial features	Brachycephaly Midface hypoplasia	Midface hypoplasia Frontal bossing Broad forehead	Midface hypoplasia Broad and square face Broad teeth Large ears	NA	Midface hyploplasia Round face High nasal root Smooth philtrum Prognathism	Midface hyploplasia Broad face Upslanting palpebral fissures Broad nasal bridge Small bulbous nose Ear abnormalities	Brachycephaly Midface hyploplasia Square face Thick eyebrows and synophrys Hypertelorism with downslanting palpebral fissures Mild prognathism	Brachycephaly Broad and round face Thick eyebrows Broad nasal bridge Dental anomalies Cupped and low-set ears	Brachycephaly Midface hyploplasia Round face Micrognathia Small bulbous nose	Broad and round face Broad forehead Prominent large simple ears
Skeletal abnormalites	Short stature	Short stature Scoliosis	Brachydactyly	Scoliosis	No	No	Short stature Brachydactyly	Brachydactyly of hands and feet	Short stature	No
Neurological findings	DD Infantile hypotonia Seizures	DD ID Infantile hypotonia	DD Severe ID Infantile hypotonia	DD	DD ID Infantile hypotonia	DD ID	DD ID	DD, ID Infantile hypotonia Decreased pain sensitivity Hyporeflexia	DD ID Infantile hypotonia	DD ID
Sleep disturbance	No	NA	Severe	NA	Yes (in the first years of life treated with Nopron)	Yes	Yes	Yes	Yes	No
Behavioral problems	Hyperactivity Aggressive behavior Stereotypies Hyperphagia	NA	Self hugging Hand biting Self injurious behavior	NA	Aggressive and oppositional behavior	NA	Aggressive behavior Anxiety Stereotypies	Hyperactivity Aggressive and self-destructive behavior Wrist-biting Head-banging Limited social interactions Short attention span	Aggressive and self-destructive behavior Short attention span	Aggressive behavior Stereotypies
Other signs	No	Congenital heart defect	Deep voice tone Hearing loss Myopia and strabismu	Obesity, Hypermetropia	Obesity	Astigmatism	Nasal voice	Congenital heart defect Feeding difficulties in infancy; Eczema Lymphopenia treated with Cotrimoxazole	No	Obesity Esotropia and astigmatism

	SMS11	SMS12	SMS13	SMS14	SMS15	SMS16	SMS17	SMS18	SMS19	SMS20
Gender	F	M	F	F	M	F	M	F	M	M
Age	14 y	15 y	13 y	20 y	9 y	10 y	9 y	13 y	16 y	8 y
Dysmorphic facial features	Brachycephaly Broad and round face Arched and thick eyebrows Upslanting palpebral fissures Small ears with large lobules Thin upper lip Dental anomalies	Midface hypoplasia Thick eyebrows Upslanting palpebral fissures Thin upper lip	Round face Broad forehead Arched eyebrows Upslanting palpebral fissures Broad nasal bridge Thin upper lip	Midface hypoplasia Round face Thick eyebrows Upslanting palpebral fissures Broad nasal bridge Large and prominent nose	Brachycephaly Midface hypoplasia Broad and round face Micrognathia Arched eyebrows Upslanting palpebral fissures Broad nasal bridge Small bulbous nose Thin upper lip	Midface hypoplasia Broad and round face Frontal bossing Broad forehead Micrognathia Arched eyebrows	Arched eyebrows	Midface hypoplasia Broad and round face Upslanting palpebral fissures Large simple ears Thin upper lip	Brachycephaly, Midface hypoplasia	Brachycephaly Midface hypoplasia Broad face Broad forehead Small ears with large lobules Broad nasal bridge Broad upturned nose
Skeletal abnormalites	No	No	No	No	Brachydactyly	No	Brachydactyly	Brachydactyly	Brachydactyly	Brachydactyly
Neurological findings	DD Mild ID Infantile hypotonia Epilepsy	DD ID Seizures	DD ID	DD ID Infantile hypotonia Seizures	DD ID	DD ID	DD ID	DD ID	DD ID	Speech delay ID
Sleep disturbance	Yes	No	No	Yes	No	No	No	No	No	Yes
Behavioral problems	Hyperactivity Aggressive and self-destructive behavior Wrist-biting Stereotypies Autistic traits Limited social interactions Short attention span Hyperphagia	Aggressive and self-destructive behavior	Aggressive and self-destructive behavior Autistic traits	Aggressive behavior	Hyperactivity Aggressive and self-destructive behavior Limited social interactions Short attention span Hyperphagia	Autistic traits	NA	Hyperactivity Aggressive behavior	Hyperactivity Aggressive and self-destructive behavior	Short attention span
Other features	Obesity Esotropia	No	Obesity	Feeding difficulties in infancy Astigmatism	Obesity Ears infections Gynecomastia	Congenital heart defect	No	Obesity	Obesity Myopia	No

	SMS21	SMS22	SMS23	SMS24	SMS25	SMS26	SMS27	SMS28	SMS29	SMS30
Gender	F	M	F	F	F	M	F	F	M	F
Age	18 y	10 y	9 y	8 y	19 y	9 y	17 y	8 y	49 y	32 y
Dysmorphic facial features	Brachycephaly Midface hypoplasia Broad and round face Thick eyebrows Upslanting palpebral fissures Large simple ears	Brachycephaly Midface hypoplasia Broad and round face Small prominent ears with large lobules Upslanting palpebral fissures Broad nasal bridge Large prominent nose	Brachycephaly Prominent and low-set ears	Midface hypoplasia Broad face Upslanting palpebral fissures Broad nasal bridge Large prominent and bulbous nose	Brachycephaly Midface hypoplasia Broad face Thick eyebrows	Broad forehead Prominent large and simple ears Broad nasal bridge	Brachycephaly Broad and round face Thick eyebrows Broad nasal bridge Broad upturned and prominent nose	Midface hypoplasia Round face Thin upper lip	Midface hypoplasia Thick helix Thick eyebrows Prognathism Macroglossia	Brachycephaly Midface hypoplasia Broad and round face Thick eyebrows Simple ears with large lobules Small bulbous nose Thin upper lip
Skeletal abnormalites	No	No	No	Short stature	Brachydactyly	No	Yes	Short stature Brachydactyly	Brachydactyly Scoliosis	Short stature Brachydactyly
Neurological findings	DD, ID Febrile seizures in infancy	DD, ID	DD, ID Infantile hypotonia	DD, ID Infantile hypotonia Seizures	DD, ID Infantile hypotonia	DD, ID	DD, ID	Speech delay	DD, Severe ID Hypotonia Seizures	DD, ID
Sleep disturbance	Yes	Yes	Yes	Yes	Yes	Yes	Yes	Yes	Yes	No (in the first years of life treated with Nopron)
Behavioral problems	Self-destructive behavior Stereotypies Limited social interactions Hyperphagia	Aggressive behavior Limited social interactions Short attention span	Hyperactivity Aggressive and self-destructive behavior Self-hugging Wrist-biting Head-banging Onychotillomania Limited social interactions	NA	Hyperactivity Aggressive and self-destructive behavior Self-hugging Polyembolokoilamania Stereotypies Limited social interactions Short attention spanHyperphagia	Hyperactivity Aggressive behavior Short attention span	Hyperactivity Aggressive behavior Limited social interactions Short attention span	Stereotypies Autistic traits Limited social interactions Short attention span	Hyperactivity Aggressive and self-destructive behavior Self-hugging Stereotypies Short attention span Short tempers Anxiety	Aggressive and self-destructive behavior Limited social interaction Hyperphagia
Other signs	Obesity Astigmatism	Feeding difficulties in infancy	Congenital heart defect Feeding difficulties in infancy	Congenital heart defect Eye abnormalities	Obesity Hoarse voice	Feeding difficulties in infancy	No	No	Hearing loss Diabetes Myopia	Obesity Congenital heart defect Myopia Astigmatism

In order to disclose the molecular alterations underlying the patients' phenotype, combined genomic approaches were carried out as shown in the flowchart (**Fig.16**). First of all, high resolution array-CGH analyses were conducted to identify the classical 17p11.2 deletion or rearrangements in genes causing overlapping syndromes. In case of positive result the patient received a molecular or differential diagnosis after a clinical re-evaluation. Otherwise, a Next Generation Sequencing (NGS) custom gene panel and Multiplex Ligation-dependent Probe Amplification (MLPA) analyses were carried out to identify mutations or micro-deletions/duplications in *RAI1* gene. For negative patients additional studies were conducted: high resolution array-CGH analyses were assessed beyond the targeted 17p11.2 region in order to pinpoint rare CNVs involving dosage sensitive genes that may lead to an SMS-like phenotype, and quantitative expression analyses through RT-qPCR were performed to evaluate a potential *RAI1* haploinsufficiency caused by disruption in new genes involved in *RAI1* pathway or by deletion affecting *RAI1* regulatory regions not investigated by NGS approach.

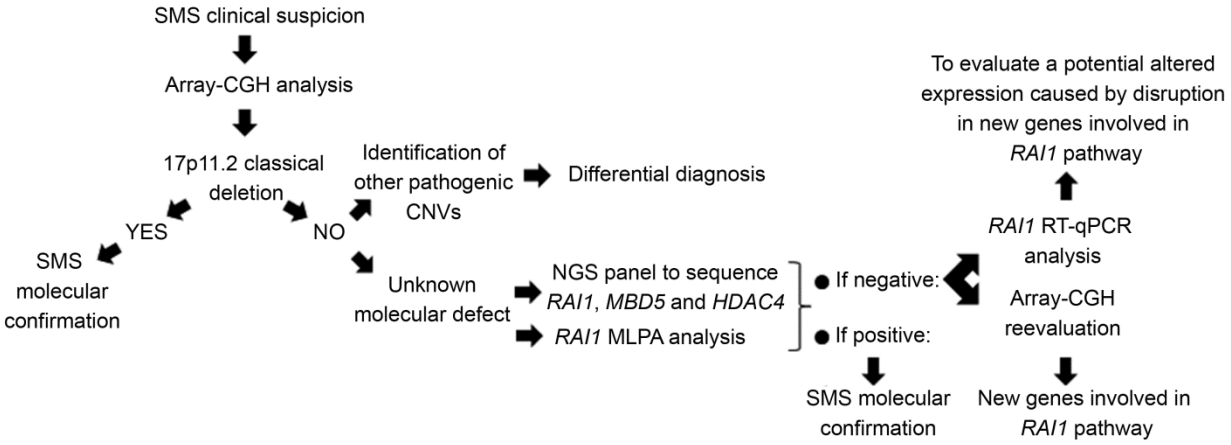

Fig.16 Flowchart of molecular analyses for patients with SMS clinical suspicion

2.1.2 Genomic DNA (gDNA) extraction from peripheral blood

For gDNA extraction peripheral blood was collected in EDTA tubes, and the GenElute Blood Genomic DNA Kit (Sigma-Aldrich) was used following the manufacturer's protocol. The DNAs were then quantified by NanoDrop ONE UV-Vis Spectrophotometer and the quality determined by agarose 0.8% gel electrophoresis.

2.1.3 Array-CGH analysis

High-resolution array-based Comparative Genomic Hybridization (array-CGH) analysis was performed on gDNA of patients, using the Human Genome CGH Microarray 244K (4 patients) and the SurePrint G3 Human CGH Microarray 2x400K (27 patients) in accordance with the manufacturer's instructions (Agilent Technologies), in order to identify a 17p11.2 rearrangement or to disclose rare CNVs involving dosage sensitive genes that may lead to an SMS-like phenotype. Copy Number Variants (CNVs) were analyzed using Agilent CytoGenomics 3.0 and mapped using the Human Genome assembly

GRCh37/hg19. CNVs classification was performed according to the Database of Genomic Variants (DGV) (http://projects.tcag.ca/variation/, release March 2016) to exclude common polymorphic CNVs with a frequency >1% in healthy controls. We proceeded with the gene content analysis of rare CNVs investigating public databases *ad hoc*, helpful to the assessment of possible pathogenic significance of the imbalances identified. In detail:

- the UCSC Genome Browser (http://genome.ucsc.edu/cgi-bin/hgGateway), NCBI Entrez Gene (http://www.ncbi.nlm.nih.gov/gene), and GeneCards (http://www.genecards.org/) which are useful to collect information about the genes involved in CNVs (i.e. gene function, molecular structure, presence of different isoforms, expression in different tissues, pathways in which they are involved, etc.);
- the Decipher database (http://decipher.sanger.ac.uk/) which allows to compare rare CNVs detected in our SMS-like patients to pathogenetic CNVs reported to date;
- the OMIM database (Online Mendelian Inheritance in Man) (http://www.ncbi.nlm.nih.gov/omim) which provides information about all Mendelian disorders, paying particular attention to genotype-phenotype correlation;
- PubMed (http://www.ncbi.nlm.nih.gov/pubmed) which is useful to examine the international medical literature.

Array-CGH analysis was extended to the parents, when available, to determine whether the rearrangements identified are de novo or inherited.

Thus, the establishment of CNV pathogenicity was made considering gene content, inheritance, and the guidelines suggested by Miller et al. in 2010 [Miller et al., 2010] and by Kearney et al. in 2011 [Kearney et al., 2011] with minor modifications.

2.1.4 Next Generation Sequencing

A next generation diagnostic panel, including *RAI1* (NM_030665) and other genes known for their association with SMS, such as *MBD5* (NM_018328) and *HDAC4* (NM_006037), was performed. The clinical effect of variants was assessed using the InterVar classify system tool (http://wintervar.wglab.org), based on the official published ACMG guidelines [Richards et al., 2015], and focusing on the inheritance.

2.1.5 MLPA-technique (Multiplex Ligation-dependent Probe Amplification)

In order to detect deletions or duplications in 17p11.2 region, a commercially available MLPA kit, SALSA MLPA probe mix P369-A2 (MRC-Holland), was used according to the kit instructions. Briefly, samples and controls DNAs were pre-heated to 98°C to denature samples, then probe mix were added to the DNAs for hybridization for 16-20 hours at 60°C. After the ligation step (15 min at 54°C and 5 min at 98°C), probes are amplified simultaneously using the same PCR primer pair. PCR products were separated on an ABI PRISM 3500 Genetic Analyzer (Applied Biosystems) and data analysis was carried on

by the Coffalyzer DB software (Software version: v131211) providing data related to copy number variants. The P369-A2 MLPA kit contains 8 MLPA probes specific for *RAI1* gene, 15 probes mapping in other genes at 17p11.2, and two probes targeting the 2q37.3 region, among which one probe for *HDAC4* gene. In addition, these kit contains ten reference probes expected to have a normal copy number that we used for intra-sample normalization, and nine internal quality control fragments generating an amplification product smaller than 120 nucleotides.

2.1.6 RNA extraction from peripheral blood

RNA from peripheral blood of patient, parents, and 10 healthy controls was collected in Tempus Blood RNA Tubes (Thermo Fisher Scientific) and isolated according to Tempus Spin RNA isolation Reagent Kit (Thermo Fisher Scientific). Briefly, blood was drawn directly into Tempus Blood RNA Tube containing a stabilizing reagent which lyses blood cells and stabilizes RNA, and shaken vigorously at least for 10 sec. Then stabilized blood was transferred to 50-mL tube, diluted with 1X PBS, and vortex for at least 30 sec, ensuring that the lysate travels to the top of the tube. Samples were centrifuged at 4°C at 3000 × g, the supernatant carefully discarded and RNA pellet resuspended. Finally, the resuspended RNA was purified using a purification filter and eluted using a microcentrifuge. The RNA was then quantified by NanoDrop ONE UV-Vis Spectrophotometer and stored at -80°C until used.

2.1.7 Quantitative RAI1 mRNA expression analysis by RT-qPCR

For quantitative gene expression analysis, 500 ng of total RNA samples were reverse-transcribed using the High-Capacity cDNA Reverse Transcription kit (Thermo Fisher Scientific). RT-qPCR was performed using a QuantStudio 12K Flex Real-Time PCR System (Thermo Fisher Scientific). The amounts of mRNA were calculated using the $2^{-\Delta\Delta Ct}$ method, normalized against housekeeping genes *GAPDH* (glyceraldehyde 3-phosphate dehydrogenase) and *TBP* (TATA box binding protein). RT-qPCR reactions were carried out using the TaqMan method (TaqMan ID# Hs01554690_m1 *RAI1* NM_030665 ex 3-4, Hs99999905_m1 *GAPDH*; Hs00427620_m1 *TBP*), and data were analyzed using the QuantStudio 12K Flex Software v1.2.3 (Thermo Fisher Scientific). We established the proper range of gene expression in healthy controls calculating the mean value ±2 standard deviations (SD). If the expression level in the sample was out of the control range, a dysregulation of the index gene could be inferred.

2.1.8 Molecular characterization of RAI1 gene in patient SMS25

Amplification of the deletion junction fragment

To localize the deletion breakpoints, Long-Range PCR was performed on genomic DNA using TaKaRa LA Taq™ kit (TaKaRa) and on cDNA using the KAPA2G Robust PCR Kit (KAPA BIOSYSTEMS). Primer pairs and amplification conditions used to amplify the deletion breakpoints are shown in **Table 2**.

Tab.2 List of Long-Range PCR primers used.

Oligo Name	Primer Sequence (5'->3')	Ta (°C)
LR-PCR on gDNA	Fw: TAGCAACTGTTTAGTGGTGGGACTTGTA Rev: CAAAGGCCCGGTTGGGGCTCTGTT	TD:69.1→ 62.1
LR-PCR on cDNA	Fw: AAAGGATGCCTCCACACCTACCACTAC Rev: CAAAGGCCCGGTTGGGGCTCTGTT	66.6

Subsequently, amplicons were sequenced using the Big Dye® Terminator v.3.1 Cycle Sequencing kit (Thermo Fisher Scientific). Deletion junction sequences were aligned to the human reference genome sequence (human genome assembly GRCh37/hg19), and electropherograms analyzed with the ChromasPro 1.5 software (Technelysium Pty Ltd).

Gene expression analysis

RT-qPCR reactions were carried out on patient's and her parents' peripheral blood cells using the TaqMan method as described above in 2.1.7 section (TaqMan ID# Hs00430773_m1 *RAI1* NM_030665 ex 2-3). To assess an eventual different allelic expression, RT-qPCR experiments, based on SYBR® Green methodology (Thermo Fisher Scientific), were performed with specific primers able to detect only the not deleted allele (**Tab.3**).

Tab.3 Primers used for assessment of an eventual different allelic expression.

Gene	Primer Sequence (5'->3')	Amplicon Length
RAI1 exons 4-5	Fw: ACCTACCACTACCCGTGTGC Rev: TGTTTGGGACATTTCAAAGAA	77 bp
GAPDH Housekeeping gene	Fw: GGGAAGCTTGTCATCAATGGA Rev: CGCCCCACTTGATTTTGG	73 bp
TBP Housekeeping gene	Fw: GTTCTGGGAAAATGGTGTGC Rev: GCTGGAAAACCCAACTTCTG	100 bp

Sequencing of *RAI1* regulatory regions

Promoter and regulatory regions, selected based on the presence of predicted elements using the UCSC browser (Tracks: Integrated Regulation from ENCODE → Layered H3K27Ac; ENCODE Histone Modification → Broad ChromHMM), were amplified using the AmpliTaq Gold DNA Polymerase Kit (Thermo Fisher Scientific) or, in case of CG-rich regions, the KAPA2G Robust PCR Kit. Primer pairs and amplification conditions are shown in **Tables 4-8**.

Tab.4 List of primers used for Sanger sequencing of region chr17:17584419-17587127, hg19.

Oligo Name	Primer Sequence (5'->3')	Tm (°C)	Ta (°C)	Amplicon Length
REG1_*RAI1*_1	Fw:ACAGGTGAGGGCTAATGGTG	56.3	60.3	464 bp
	Rev:ACTCGCTCTCCCACTCGTCT	58.3		
REG1_*RAI1*_2	Fw:GCTCGTCCGCTCTTCCTG	57.7	TD:63→56	539 bp
	Rev:CACACCACACAAAGCAAGGA	54.2		
REG1_*RAI1*_3	Fw:ATCCTAGGCCGGGTGATG	55.4	58.4	384 bp
	Rev:GTCACGCATGGGGAAGTC	55.4		
REG1_*RAI1*_4	Fw:GAGTGTGGCAAGGGATCTG	55.9	60	327 bp
	Rev:GCTACAGAGCTCCCCAGGT	58		
REG1_*RAI1*_5	Fw:CTCTCTGCGGTGTCCCTACC	60.4	TD:61.2→54.2	453 bp
	Rev:CAAGAGCCCCAAGAAAGAAA	52.2		

REG1_*RAI1*_6	Fw:GAGGGGAAGCGAAACACC	55.4	TD:60.8→53.8	448 bp
	Rev:TGCCCTTGAATTCTCAACAC	52.2		
REG1_*RAI1*_7	Fw:ACGGTTCCTCCCACCAATAC	56.3	59.3	333 bp
	Rev:TGAGCAGAGCGAGGACTGTA	56.3		
REG1_*RAI1*_8	Fw:TGGGTTAGGCTAGCTCTGATG	56.6	58.4	491 bp
	Rev:TCCTATTTTGCCCACTCCAC	54.2		

Tab.5 List of primers used for Sanger sequencing of region chr17:17596278-17599551, hg19.

Oligo Name	Primer Sequence (5'->3')	Tm (°C)	Ta (°C)	Amplicon Length
REG2_*RAI1*_1	Fw:GAGAAGGTGGTGTGGAATGC	56.3	58.3	417 bp
	Rev:TCTCCCCTCTCCTTTTGTGA	54.2		
REG2_*RAI1*_2	Fw:TCATTCCTCCACCTCCTCTG	56.3	TD:61.3→54.3	470 bp
	Rev:ACAAAGCCCTGTTTGTTTGC	52.2		
REG2_*RAI1*_3	Fw:CGGCAGGTAGCTGAGAAAGA	56.3	59.3	413 bp
	Rev:CAATGACGGGACAAGGGTAG	56.3		
REG2_*RAI1*_4	Fw:ACGTAGGACTCGCTGGCTTA	56.3	59.3	365 bp
	Rev:CGTCTTCCTGGCTATGTTCC	56.3		
REG2_*RAI1*_5	Fw:AGGCCTGAGGAACCAAACTG	56.3	60.3	229 bp
	Rev:GGCCTGACAGCTCCTACCTA	58.3		
REG2_*RAI1*_6	Fw:ACCTGGCCCACCTCTCAG	57.7	59.6	476 bp
	Rev:CAACGCTGGGACTGGAAG	55.4		
REG2_*RAI1*_7	Fw:GGTCTTTTTCCGGGAACG	53.2	57.3	379 bp
	Rev:CCCTTCTTTCTCCTGCCC	55.4		
REG2_*RAI1*_8	Fw:GCCTCTCAGCTGCAGTCTCT	58.3	60.3	355 bp
	Rev:AGGCGGCTGTGGAGTAGTAA	56.3		

Tab.6 List of primers used for Sanger sequencing of region chr17:17612671-17618254, hg19.

Oligo Name	Primer Sequence (5'->3')	Tm (°C)	Ta (°C)	Amplicon Length
REG3_*RAI1*_1	Fw:CCACACAACTGCCCTCTGGA	58.3	61.5	415 bp
	Rev:GGGGTGTGAGTGTAAGAGTGC	58.6		
REG3_*RAI1*_2	Fw:CTAAACGCACAGCCAAGACC	56.3	59.5	465 bp
	Rev:GCGCCCTCAGTAGCCATTATT	56.6		
REG3_*RAI1*_3	Fw CATCGCGCTTACCGAGTGGA	58.3	61.5	402 bp
	Rev:CCCGCCGAAAACACAAAGCTC	58.6		
REG3_*RAI1*_4	Fw:CTCACATTTGTTTCTCCCAAGG	55.1	57.7	520 bp
	Rev:CTTCCGCCAATACCACATTC	54.2		
REG3_*RAI1*_5	Fw:CTCCCCTTTCCTCCACAAAG	56.3	59.5	417 bp
	Rev:TCCAGGGGAAGTGTTTGAAGC	56.6		
REG3_*RAI1*_6	Fw GATGGGAAACTTCCCGAGAG	56.3	59.5	552 bp
	Rev:CTGAAGTCACCAGCCAATCAC	56.6		

Tab.7 List of primers used for Sanger sequencing of region chr17:17626371-17628581, hg19.

Oligo Name	Primer Sequence (5'->3')	Tm (°C)	Ta (°C)	Amplicon Length
REG4_*RAI1*_1	Fw:ACTCCTACCCCGACTCTCTT	56.3	59.3	460 bp
	Rev:CCTCCTGGGTGCTCATTCA	56.3		
REG4_*RAI1*_2	Fw:GTGCAGCTTCCAGAATCTT	54.2	68.3	426 bp
	Rev:CCGCTGGGTTCTGATTCTCT	56.3		
REG4_*RAI1*_3	Fw:CACATACACTTGGCACCAGG	56.3	60.3	436 bp
	Rev:GGGAGTCCTAGTCTTGGTGG	58.3		
REG4_*RAI1*_4	Fw:GTGAGTCAGAGGCTGCCA	55.4	59.9	412 bp
	Rev:CAGGAGAGCTCTGGAGTACG	58.3		
REG4_*RAI1*_5	Fw:TCTGTAGGTGGGGACCTTTG	56.3	59.3	473 bp
	Rev:AGGGCCTGTGTGTTTCTGTC	56.3		
REG4_*RAI1*_6	Fw:GCCTGAGAGGCTGGTGATAG	58.3	61.3	419 bp
	Rev:GTCCATCCCGTGTACACCTC	58.3		
REG4_*RAI1*_7	Fw:GCTTGCCATTCAGTCCTTTC	54.2	57.2	425 bp
	Rev:TGAATGCTTTGTCCCTCCTC	54.2		
REG4_*RAI1*_8	Fw:CAACGAGAGCAAAACTCCATC	54.7	57.2	455 bp
	Rev:AGGCATGCAAGCAGAACAG	53.7		

Tab.8 List of primers used for Sanger sequencing of region chr17:17653916-17656865, hg19.

Oligo Name	Primer Sequence (5'->3')	Tm (°C)	Ta (°C)	Amplicon Length
REG5_*RAI1*_1	Fw:TGCACCATTGTACTCCGTCT	54.2	57.2	328 bp
	Rev:GAAGGCGGAAGGAAACAGAT	54.2		
REG5_*RAI1*_2	Fw:TCTGGTTTTGTGCTTGTCCA	52.2	56.2	346 bp
	Rev:TTGATGAGGCTCCACTTCCT	54.2		
REG5_*RAI1*_3	Fw:TTGACAAGTGCTGGCATGTT	52.2	56.2	414 bp
	Rev:TACGGACAAGGGGAAAACAC	54.2		
REG5_*RAI1*_4	Fw:CTTGCCCAGAACAGTGACCT	56.3	60.3	439 bp
	Rev:GGGAACGGGTACTAGGTTCG	58.3		
REG5_*RAI1*_5	Fw:CTCTTCCTGGAGAGCCACAG	58.3	61.3	413 bp
	Rev:GGGCCTCCACTTCCTAGTCT	58.3		
REG5_*RAI1*_6	Fw:GATCTCAAGCACCCGAACAT	54.2	TD:63.1→56.1	419 bp
	Rev:CGCGCCAGTACAAGACCAG	58		
REG5_*RAI1*_7	Fw:TTTCCTGCCTTTTGTGTTCG	52.2	TD:61.3→54.3	500 bp
	Rev:GAGTGTCCAGGAATGACGTG	56.3		
REG5_*RAI*_8	Fw:GGGCCGACCACCTTACTT	55.4	58.9	494 bp
	Rev:GGTGAATGGCCTACTGTGCT	56.3		
REG5_*RAI*_9	Fw:GACTTGGGAGGAAGGGAGAC	58.3	60.3	385 bp
	Rev:GGGTAAGGGGTGTGGAGATT	56.3		

Evaluation of potentially cryptic microdeletions

In order to assess the number of copies of some regulatory elements upstream of *RAI1* gene that cannot be evaluated using array-CGH, qPCR experiments using the SYBR® Green method were performed. Primers were selected within regions of unique non-repetitive sequence using Primer3 software (http://bioinfo.ut.ee/primer3-0.4.0/) (**Tab.9**) and following the subsequent conditions (qPCR primers need different features compared to the primers normally used in a standard PCR reaction):

Product Size Ranges (n. of bases) →60-100;

Primer size (n. of bases) →Min 18; Opt 20; Max 22;

Primer Tm (°C) →Min 59; Opt 60; Max 63;

Product Tm (°C) →Min 65; Opt 80; Max 90;

Max Self Complementarity →4.

A control amplicon was selected with the same parameters in *PCNT* gene at 11q14.1.

Tab.9 Primers used for assessment of eventual cryptic microdeletions upstream of *RAI1* gene

Nucleotide Position#	qPCR Probes	Primer Sequence (5'->3')	Amplicon Length
chr21:47864661-47864728	*PCNT*	Fw:TCCAGAACATTCCTTGACAGAG	68 bp
		Rev:GTACCCCTCCCAATCTTTGC	
chr17:17579657-17579725	*RAI1*_1	Fw:CCAGGCAGGAAACATGATCT	69 bp
		Rev:CATCTGTGTGGCCTTGAACTT	
chr17:17579279-17579351	*RAI1*_2	Fw:CCAGGCAGGAAACATGATCT	73 bp
		Rev:CATCTGTGTGGCCTTGAACTT	
chr17:17573245-17573318	*RAI1*_3	Fw:CCCATCTGCTCCTGGTCTC	74 bp
		Rev:CTCAATCGGGCACTGGAG	
chr17:17569730-17569811	*RAI1*_4	Fw:AGCTCTGGATGGACATGAGG	82 bp
		Rev:AGCAACAGGGAACGAACACT	
chr17:17566340-17566424	*RAI1*_5	Fw:GCTGCTGGTACAGGATCACA	85 bp
		Rev:TTCCCCCTCAATAAGCACAG	
chr17:17566932-17567011	*RAI1*_6	Fw:CCAGTGCCAACCTCTTATGG	80 bp
		Rev:CCCTCCTGTGGGTAATGCTA	
chr17:17565321-17565402	*RAI1*_7	Fw:GTGGTCAGGTCAGCCTTTTC	82 bp
		Rev:CGGGAGTGACAAAATGATAGG	

chr17:17545230-17545307	*RAI1*_8	Fw:TGGTATCTCCCCAGTTCACC Rev:GCACTGTTTGCCTGGTGTT	78 bp

[#]Physical position of the identified rare CNVs based on the UCSC Genome Browser, hg19, released February 2009.

The experiment is analyzed by calculating the "threshold cycle" (Ct) of each reaction using the QuantStudio 12K Flex Software v1.2.3 (Thermo Fisher Scientific), as described before in 2.1.7 section.

2.2 EXPRESSION ANALYSIS OF CIRCADIAN RHYTHM GENES ON PERIPHERAL BLOOD OF SELECTED SMS/SMS-LIKE PATIENTS

Fifteen patients, showing sleep disturbance and carrying different genomic alterations, and 3 patients without sleep alterations but harboring others SMS clinical signs were selected to:

- study the expression levels of the main circadian rhythm genes in peripheral blood cells,
- address a correlation between the presence of sleep disorders and impaired expression of these genes.

The expression of genes of interest was first verified on a control blood RNA as well as on commercial RNAs of human brain (Clontech Laboratories), by means of PCR using specific pairs of primers (**Tab.10**). Then, cDNA was obtained from peripheral blood RNA collected in the morning (10:00-12:00 am) of both controls and patients, and subsequently RT-qPCR was performed using SYBR Green methodology.

Tab.10 List of primers used for the PCR reaction on cDNA.

Gene	Primer Forward	Primer Reverse	Amplicon Length
CLOCK	TGCACTGTTGAAGAACCCAAT	GGTGGTGCCCTGTGATCTA	86 bp
BMAL2	TGGATGCTTACCCAACTCAA	GGAGGCCAGCTTCTCAAGTA	84 bp
CRY1	CAGGTTGTAGCAGCAGTGGA	TGTCGCCATGAGCATAGTGT	66 bp
PER1	TCTGCCGTATCAGAGGAGGT	TCTGCCGTATCAGAGGAGGT	87 bp
PER2	CATGTGCAGTGGAGCAGATT	TTCATTCTCGTGGCTTTTCC	94 bp
NR1D1	ACAACACAGGTGGCGTCAT	TAGAGGGATTCAGGGCTGGT	76 bp
MTNR1A	CAACCTCCTGGTCATCCTGT	CAGGTCTGCCACCGCTAAG	91 bp
MTNR1B	CTCAGGAACCGCAAGCTC	GGATTAGCGGGTAGGGGTAG	97 bp
ACTB *Housekeeping gene*	CTGGCACCCAGCACAATG	GCCGATCCACACGGAGTACT	69 bp

2.3 FUNCTIONAL APPROACH: HUMAN INDUCED PLURIPOTENT STEM CELLS (iPSCs)

2.3.1 Separation of peripheral blood mononuclear cells (PBMCs)

Reprogramming to iPSCs was performed from SMS8 patient's and parents' peripheral blood mononuclear cells (PBMCs). For the isolation of the PBMCs 6-8 mL blood in Lithium-Heparin were collected and mixed with an equal volume of balanced salt solution (PBS or physiological saline). The diluted blood sample was layered on top of 4 mL of Ficoll-Paque media solution (GE Healthcare) and centrifuged at 1500 rpm for 30 min at room temperature without brake. After the 30-min spin, PBMCs

retained at the interface between the Ficoll gradient and the upper plasma were washed with PBS (Gibco) and 10% FBS (Fetal Bovine Sierum, Sigma-Aldrich) and centrifuged at 1500 rpm for 10 min.

2.3.2 Generation and culture of iPSCs

iPSCs were generated from 5×10^5 PBMCs seeded in a 24-well plate in StemPro™-34 medium (Thermo Fisher Scientific) supplemented with SCF (100 ng/mL), FLT-3 (100 ng/mL), IL-3 (20 ng/mL) and IL-6 (20 ng/ml) cytokines (Peprotech). Half medium was daily changed and fresh cytokines added. After four days, reprogramming was performed using the integration-free CytoTune-iPS 2.0 Sendai Reprogramming Kit (Thermo Fisher Scientific) consisting of the four Yamanaka factors, Oct, Sox2, Klf4, and c-Myc, following manufacturer's instructions (KOS (Klf4–Oct3/4–Sox2) MOI=5, hcMyc MOI=5 and hKlf4 MOI=3). After three days, transduced cells were grown on Mouse Embryonic Fibroblasts (MEF) feeder layer in StemPro™-34 medium without the cytokines for four days. Thereafter cultures were carried on in Essential 8 medium (Thermo Fisher Scientific). Three weeks post-transduction, colonies ready for transfer were individually manually picked and seeded onto Matrigel (Thermo Fisher Scientific) coated dishes. Colonies, passaged using an EDTA 0.5 µM solution, were expanded in Essential 8 medium for at least six passages before being characterized and differentiated.

2.3.3 Karyotyping and a-CGH of iPSC clones / Genotyping of patient-derived iPSCs

The conventional cytogenetic analysis was performed on at least 30 QFQ-banded metaphases obtained from peripheral blood lymphocytes and iPSC clones using standard procedures.

Genomic blood and iPSCs DNAs were extracted by the means of GenElute Blood Genomic DNA kit (Sigma-Aldrich). High-resolution array comparative genomic hybridization (array-CGH) was performed using the SurePrint G3 Human CGH Microarray Kit 2x400K and 4x180K in accordance with the manufacturer's instructions (Agilent Technologies). Probe positions are referred to human genome assembly GRCh37/hg19.

2.3.4 Characterization and in vitro spontaneous differentiation of iPSCs

Total RNA of each iPSCs clone was isolated using the TRIzol reagent (Invitrogen) and the Direct-zol™ RNA MiniPrep Plus kit (Zymo Research) following manufacturer's instructions and 500-800 ng were reverse transcribed into cDNA using the High-Capacity cDNA Reverse Transcription kit (Thermo Fisher Scientific). Briefly, the reaction was primed with Random Primers and incubated at 25°C for 10 min, then at 37°C for 120 min and finally 5 min at 85°C. cDNAs were amplified using AmpliTaq Gold (Thermo Fisher Scientific). Reverse transcription-PCR (RT-PCR) was performed to monitor the endogenous expression of stem cell factors Sox2, Oct3/4 and Nanog with specific primers designed to amplify only cDNAs (**Tab.11**) [Takahashi et al., 2007].

Tab.11 Primer sequences for pluripotency detection.

Gene	Forward primer	Reverse primer	Amplicon Length
SOX2	TTGCGTGAGTGTGGATGGGATTGGTG	GGGAAATGGGAGGGGTGCAAAA GAGG	151 bp
OCT3/4	GACAGGGGGAGGGGAGGAGCTAGG	CTTCCCTCCAACCAGTTGCCCCAAAC	144 bp
NANOG	CAGCCCTGATTCTTCCACCAGTCC	GTTCTGGAACCAGGTCTTCACCTG	244 bp

The expression of others pluripotency markers (Alkaline Phosphatase (PA), SSEA-4, and TRA-1-60) was monitored by immunofluorescence staining.

In addition, pluripotency of established iPSCs was tested *in vitro* through embryoid bodies (EBs) formation and subsequent spontaneous differentiation into the three germ layers, whose expression was evaluated by immunofluorescence using specific markers (βIII tubulin for ectoderm, desmin for mesoderm and alpha-fetoprotein (AFP) for endoderm). EBs formation was performed by gently resuspending iPSCs colonies in non-tissue culture-treated plates in HuES medium (DMEM/F12, 20% knock-out serum replacement, 2mM L-glutamine, 10 U/ml penicillin, 10 μg/ml streptomycin, 0.1mM MEM NEAA, 110 μM β-mercaptoethanol) (all reagents from Thermo Fisher Scientific). Medium was changed daily and after 7 days, EBs were collected and plated on Matrigel-coated plates in Essential 8 medium.

2.3.5 Characterization of ZDHHC15 defects in iPSC cell lines

Clones which bypassed the check for genome stability and trilineage differentiation potential were analyzed by RT-qPCR based on the TaqMan methodology to examine *ZDHHC15* transcript levels. RT-qPCR reactions were carried out on RNA extracted by each iPSCs clone using the protocol described above in 2.1.7 section (TaqMan ID# Hs00327516_m1 ZDHHC15 NM_001146256 ex 3-4).

2.3.6 In vitro differentiation of iPSCs into cortical neurons

Selected iPSCs clones, found to have maintained full genomic stability and expressing stemness markers, were differentiated into cortical neurons according to the monolayer protocol in N2B27 medium (Neurobasal medium, 2% B27, 1% N2, 1% Insulin Transferrin Selenium, 2mM L-glutamine, P/S) (all reagents from Thermo Fisher Scientific) supplemented with 500 ng/ml Noggin (R&D Systems) [Germain et al., 2014]. Neural rosettes, usually formed after 14-16 days, were manually passaged on poly lysine-laminin (Sigma-Aldrich) coated dishes and maintained in the same medium for further two weeks. At day 28 the N2B27 medium was changed to Neural Differentiation Medium (Neurobasal medium, 2% B27, 1% NEAA, 2mM L-glutamine) (all reagents from Thermo Fisher Scientific), plus 10 ng/ml BDNF, 10 ng/ml GDNF (both from Peprotech), 1 μM Ascorbic Acid and 200 μM cAMP (both from Sigma-Aldrich). After one week, neural progenitor cells (NPCs) were plated at low density (1×10^5–1.5×10^5 cells) for terminal differentiation and not passaged any more. Neurons were maintained in culture by half media changes twice a week until 70-100 days.

2.3.7 Characterization of cortical neurons markers

RT-PCR was performed on RNA extracted from post-mitotic neurons and retro-transcribed as described above to identify the expression of specific neuronal markers, such as CUX1, GAD67, MAP2, and TBR1. The sequences of the primers are reported in **Table 12**.

Tab.12 Primer sequences to evaluate the presence of specific neuronal markers.

Gene	Forward primer	Reverse primer	Amplicon Length
CUX1	CACAGATGTCCACCACCTCA	TTTCCAGGGCTGTTTGTAGG	72 bp
GAD67	GGCGCACAGAGACTGACTTC	GGAGTATGTCCACCACTTCCA	108 bp
MAP2	GAGAATGGGATCAACGGAGA	TCCTTGCAGACACCTCCTCT	67 bp
TBR1	CGAACAACAAAGGAGCTTCA	TTCACTTCCACCACATGCAG	94 bp

Moreover, the expression of other markers specific for cortical neurons (βIII tubulin, MAP2, SMI312, and VGLUT1) was checked by IF.

2.3.8 Electrophysiological in vitro recordings of differentiated neurons

Whole-cell voltage clamp, patch-clamp recordings were obtained from differentiating neurons (in particular at 50, 55, 62 and 72 days of differentiation) using the Axopatch 200B amplifier and the pClamp-10 software (Axon Instruments). Recordings were performed in Krebs'-Ringer's-HEPES (KRH) external solution (NaCl 125 mM, KCl 5 mM, MgSO4 1.2 mM, KH2PO4 1.2 mM, CaCl2 2 mM, glucose 6 mM, HEPES-NaOH pH 7.4 25 mM). Recording pipettes were fabricated from glass capillary (World Precision Instrument) using a two-stage puller (Narishige); they were filled with the intracellular solution potassium-gluconate (KGluc 130 mM, KCl 10 mM, EGTA 1 mM, HEPES 10 mM, MgCl2 2 mM, MgATP 4 mM, GTP 0.3 mM) and the tip resistance was 3-5 MΩ. In order to identify excitatory miniature events, differentiating cells were held at -70 mV. The recorded traces have been analyzed using Clapfit-pClamp 10 software, after choosing an appropriate threshold.

2.3.9 Immunofluorescence staining

For immunofluorescence neurons grown on a 12 mm coverslip (Thermo Fisher Scientific) were washed with PBS and fixed by addition of 4% paraformaldehyde solution and incubated for 20 min at room temperature. The fixed cells were washed twice with PBS and thereafter with 10% NGS in PBS. Permeabilization was performed using 0.3% Triton X-100 and ice-cold 100% methanol for nuclear staining for 5 minute. Then cells were incubated for 20 min in a blocking solution (10% NGS in PBS), in order to avoid nonspecific binding of antibodies. Subsequently, primary antibodies, diluted in blocking solution, were added for 90 min at 37°C. To remove the primary antibody cells were washed two times with 10% NGS in PBS and stained with Alexa fluor 488 (Polyclonal anti-rabbit) or Alexa fluor 555 (Monoclonal anti-mouse) conjugated secondary antibodies for 45 min at room temperature. For nuclei staining, 4',6-Diamidino-2-Phenylindole, Dihydrochloride (DAPI) 2 µg/ml was finally added for 7 min at room temperature after further washing steps with 10% NGS in PBS. Coverslips were rinsed with PBS

and mounted with FluorSave (Merck). Confocal images were acquired with Nikon Eclipse Ti microscope. Primary and secondary antibodies used are listed in **Table 13**.

Tab.13 Immunocytochemistry primary and secondary antibodies used.

Primary antibody	**Supplier**	**Secondary antibody**
Tra-1-60 (Podocalyxin) (TRA-1-60)	Invitrogen	Alexa 555
SSEA4 (eBioMC-813-70 (MC-813-70)	Invitrogen	Alexa 555
Alkaline Phosphatase (AP)	Abcam	Alexa 488
Alpha-fetoprotein (AFP)	Invitrogen	Alexa 555
βIII tubulin (EP1569Y)	Abcam	Alexa 488
Desmin (D33)	DAKO	Alexa 488
Nestin	Chemicon	Alexa 555
PAX6	Abcam	Alexa 488
CUX1	Proteintech	Alexa 555
VGLUT1	Proteintech	Alexa 488
SMI312	Covance	Alexa 555
MAP2	Abcam	Alexa 488 – Alexa 555

RESULTS

3.1 GENOMIC APPROACHES

3.1.1 Identification and classification of CNVs identified by array-CGH

The cohort consists of 28 patients with SMS clinical suspicion but without classical microdeletion at 17p11.2, and 2 patients carrying a typical deletion previously disclosed by FISH (Fluorescence *in situ* hybridization), analyzed by high resolution array-CGH to identify CNVs possibly implicated in the pathogenesis of disorders in the SMS spectrum, and to map finely the deletion breakpoints, respectively. Out of 30, 25 patients (detection rate 83%) were found to bear rare CNVs (one or more) not yet reported or identified at a very low frequency (<<1%) in healthy subjects according to the DGV database .

Overall 60 rare CNVs were disclosed, ranging from 10 kb to 3.46 Mb, including 25 gains (42%) and 35 losses (58%). Among them, 2 duplications out of 25 were homozygous CNVs. In order to establish whether the identified rearrangements were *de novo* or inherited, the analysis was extended to parents, when available. The inheritance for 8 CNVs (13%) was unknown, 3 were *de novo* (6%), and 49 inherited (79%), 24 from the mother (49%) and 25 from the father (51%), 1 of which present in a mosaic state.

A detailed list of the identified rare CNVs is provided in **Table 14**.

According to the guidelines reported by Miller et al. [Miller et al., 2010], and Kearney [Kearney et al., 2011], 4 rare detected CNVs were classified as pathogenic. Indeed, we identified 2 patients harboring the classical 17p11.2 deletion (SMS molecular diagnosis confirmed); 1 patient with a 2q23.1 deletion involving *MBD5* gene responsible for a syndrome that shares some SMS clinical features (2q23.1 deletion syndrome differential diagnosis, MIM #156200); and 1 patient carrying a *de novo* deletion of SHANK3 gene responsible for Phelan-McDermid syndrome (MIM #606232).

Based on gene content and inheritance, 13 rare CNVs of the remaining 56 were classified as VOUS (variants of unknown significance), and 45 as likely benign.

Tab.14 List of rare CNVs identified in the SMS/SMS-like cohort by means of array-CGH analysis

Patient ID	Gender	Array-CGH resolution	Chromosomal band	Gain/ Loss	Size	N° of genes	Gene(s)	Nucleotide position [#]	Inheritance	Clinical relevance
SMS1	M	244K	/	/	/	/	/	/	/	/
SMS2	F	244K	/	/	/	/	/	/	/	/
SMS3	M	244K	/	/	/	/	/	/	/	/
SMS4	F	244K	/	/	/	/	/	/	/	/
SMS5	F	400K	2q23.1	Loss	29 kb	2	*ORC4,* ***MBD5***	chr2:148751165-148780140	**Paternal mosaicism**	**Pathogenic**
SMS6	F	400K	4q35.2	Gain	185 kb	3	*F11-AS1, MNTR1A, FAT1*	chr4:187333416-187518766	Maternal	VOUS
SMS7	M	400K	20p11.1	Loss	22 kb	1	*ZNF331-AS1*	chr20:25628270-25650194	Maternal	Likely benign
SMS8	M	400K	Xq13.3	Loss	54 kb	/	(***ZDHHC15***)	chrX:74772380-74826319	Maternal	VOUS
SMS9	M	400K	11p12	Loss	55 kb	/	/	chr11:39827458-39882585	Paternal	Likely benign
			18q22.1	Loss	189 kb	/	/	chr18:66020789-66210263	Paternal	Likely benign
			19p13.2	Loss	39 kb	1	*ZNF788*	chr19:12191936-12230890	Paternal	Likely benign
SMS10	M	400K	4p11	Loss	21 kb	1	*FRYL*	chr4:48744210-48765091	Paternal	Likely benign
			19p12	Loss	429 kb	2	*ZNF675, ZNF681*	chr19:23624728-24054225	Maternal	Likely benign
			Xq21.31	Loss	26 kb	/	/	chrX:90705611-90731236	Maternal	Likely benign
			Yq11.23	Gain	199 kb	/	/	chrY:28460973-28660436	Paternal	Likely benign
SMS11	F	400K	/	/	/	/	/	/	/	/
SMS12	M	400K	4q26	Loss	66 kb	/	/	chr4:117335666-117401207	Paternal	Likely benign
			9q21.13	Gain	325 k	4	*PCSK5, RFK, RPSAP9, GCNT1*	chr9:78831267-79155816	Paternal	VOUS
			9q21.13	Gain	507 kb	/	(*PSAT1*)	chr9:81165084-81671888	Paternal	VOUS
			10p15.2	Gain	42 kb	1	*DIP2C*	chr10:599481-641403	Maternal	Likely benign
SMS13	F	400K	Xq13.1	Gain	97 kb	1	*TAF1*	chrX:70572853-70669480	NA	VOUS
			Xq26.3	Gain	52 kb	1	*CXorf48*	chrX:134293036-134345039	NA	Likely benign
SMS14	F	400K	16p13.3	Gain	25 kb	1	*LUC7L*	chr16:258392-283058	Maternal	VOUS
			16q22.1	Gain	173 kb	5	*EXOSC6, AARS, DDX19B, DDX19A, ST3GAL2*	chr16:70280883-70454161	Paternal	Likely benign
SMS15	M	400K	/	/	/	/	/	/	/	/
SMS16	F	400K	6p25.1	Loss	304 kb	2	*LYRM4, FARS2*	chr6:5191773-5495425	Maternal	VOUS
			8p23.1	Loss	166 kb	2	*MCPH1, AGPAT5*	chr8:6477768-6644251	Maternal	VOUS
SMS17	M	400K	4q34.3	Loss	162 kb	/	(*AGA*)	chr4:178641589-178803218	Maternal	VOUS
			9q34.2-34.3	Gain	118 kb	/	/	chr9:137341142-137458716	Maternal	Likely benign
SMS18	F	400K	1p33	Loss	116 kb	1	*AGBL4*	chr1:49713684-49829386	Paternal	Likely benign
SMS19	M	400K	20q13.33	Loss	23 kb	1	*CDH4*	chr20:60257826-60280961	Paternal	Likely benign

Tab.14 Continued

SMS20	M	400K	6p25.1	Loss	141 kb	2	*LYRM4, FARS2*	chr6:5249765-5390787	Maternal	VOUS
			7q32.2	Loss	14 kb	1	*TMEM209*	chr7:129811316-129825166	Paternal	Likely benign
			11p15.4	Gain*	120 kb	5	*TRPC2, ART5, ART1, CHRNA10, NUP98*	chr11:3628792-3748627	Paternal*	Likely benign
			19p13.3	Gain	44 kb	1	*ZFR2*	chr19:3802646-3846650	Maternal	Likely benign
SMS21	F	400K	3q22.1	Gain	16 kb	1	*TMEM108*	chr3:132746242-132762002	Paternal	Likely benign
			7q36.3	Gain	29 kb	1	*DNAJB6*	chr7:157191382-157220103	Maternal	VOUS
			20q13.33	Loss	15 kb	1	*CHRNA4*	chr20:62007557-62022735	Paternal	Likely benign
SMS22	M	400K	11q14.1	Loss	37 kb	3	*NDUFC2-KCTD14, THRSP, NDUFC2,*	chr11:77769872-77806844	Maternal	Likely benign
			13q33.1	Loss	10 kb	/	/	chr13:103357376-103367294	Paternal	Likely benign
			20q11.23	Gain	70 kb	1	*SOGA1*	chr20:35434174-35504355	Maternal	Likely benign
SMS23	F	400K	4q34.2	Loss	9 kb	1	*GPM6A*	chr4:176714343-176723172	Maternal	Likely benign
			13q14.11	Gain*	55 kb	1	*VWA8*	chr13:42207879-42263242	Maternal[a]	Likely benign
SMS24	F	400K	13q14.3	Gain	240 kb	/	/	chr13:54892875-55133333	NA	Likely benign
			Xq21.33	Loss	63 kb	/	/	chrX:94326259-94388781	NA	Likely benign
SMS25	F	400K	4q22.2	Loss	38 kb	1	*GRID2*	chr4:93901670-93939526	Maternal	Likely benign
			5q22.2	Loss	12 kb	1	*EPB41L4A*	chr5:111678466-111690525	Paternal	Likely benign
			14q23.3	Loss	11 kb	/	/	chr14:65353202-65363795	Paternal	Likely benign
SMS26	M	400K	4p15.31	Loss	14 kb	1	*LCORL*	chr4:17932120-17945717	Paternal	Likely benign
			6q22.31	Loss	10 kb	1	*C6orf170*	chr6:121595512-121605035	Paternal	Likely benign
			Xp21.2	Gain	502 kb	3	*Xorf21, GK, TAB3*	chrX:30357433-30859152	Maternal	Likely benign
			Xp11.4	Gain	216 kb	/	/	chrX:42067557-42283728	Maternal	Likely benign
SMS27	F	400K	5q13.3	Loss	82 kb	2	*IQGAP2, F2RL2*	chr5:75830107-75911828	Maternal	Likely benign
			7q21.11	Gain	83 kb	1	*MAGI2*	chr7:78849054-78932019	Paternal	Likely benign
			19p13.3	Gain	66 kb	4	*CCDC94, SHD, TMIGD2, FSD1*	chr19:4248456-4314206	Paternal	Likely benign
			22q13.33	**Loss**	101 kb	4	***SHANK3***, *ACR, RPL23AP82, RABL2B*	chr22:51123491-51224252	***de novo***	**Pathogenic**
SMS28	F	400K	3p22.2	Gain	190 kb	3	*GOLGA4, C3orf35, ITGA9*	chr3:37343646-37533531	Paternal	Likely benign
			13q21.2	Gain	830 kb	2	*DIAPH3, TDRD3*	chr13:60623429-61453435	Paternal	Likely benign
			16p13.3	Loss	99 kb	5	*POLR3K, SNRNP25, RHBDF1, MPG, NPRL3*	chr16:93628-192304	Maternal	VOUS
			8q12.2	Loss	17 kb	1	*KIAA1328*	chr18:34552240-34569102	Maternal	Likely benign
SMS29	M	400K	3p26.1	Gain	49 kb	1	*LMCD1-AS1*	chr3:8380358-8429654	NA	Likely benign
			4p16.1	Gain	96 kb	4	*S100P, MRFAP1L1, BLOC154, KIAA0232*	chr4:6692803-6789162	NA	Likely benign

Tab.14 Continued

			17p11.2	**Loss**	3.46 Mb	68	*TNFRSF13B, MPRIP, PLD6, FLCN, COPS3, NT5M, MED9, RASD1, PEMT, SMCR2,* ***RAI1****, RAI1-AS1, SMCR5, SREBF1, TOM1L2, DRC3, ATPAF2, GID4, DRG2, MYO15A, ALKBH5, LLGL1, FLII, MIEF2, TOP3A, SMCR8, SHMT1, EVPLL, LINC02076, KRT17P5, KRT16P1, LGALS9C, USP32P2, FAM106A, CCDC144B, TBC1D28, ZNF286B, FOXO3B, TRIM16L, FBXW10, TVP23B, PRPSAP2, SLC5A10, FAM83G, GRAP, SNORD3B-1, SNORD3B-2, SNORD3D, GRAPL, LOC79999, SNORD3A, SNORD3C, LOC388436, EPN2, EPN2-IT1, EPN2-AS1, B9D1, MAPK7, MFAP4, RNF112, SLC47A1, SNORA59B, ALDH3A2, SLC47A2, ALDH3A1, ULK2, AKAP10, SPECC1*	chr17:16757564-20219464	***de novo***	**Pathogenic**
SMS30	F	400K	6q26	Loss	76 kb	1	*AGPAT4*	chr6:161568015-161643744	NA	Likely benign
			17p11.2	**Loss**	3.46 Mb	72	*TNFRSF13B, MPRIP, PLD6, FLCN, COPS3, NT5M, MED9, RASD1, PEMT, SMCR2,* ***RAI1****, RAI1-AS1, SMCR5, SREBF1, MIR6777, MIR33B, TOM1L2, DRC3, ATPAF2, GID4, DRG2, MYO15A, ALKBH5, LLGL1, FLII, MIEF2, TOP3A, SMCR8, SHMT1, MIR6778, EVPLL, LINC02076, KRT17P5, KRT16P1, LGALS9C, USP32P2, FAM106A, CCDC144B, TBC1D28, ZNF286B, FOXO3B, TRIM16L, FBXW10, TVP23B, PRPSAP2, SLC5A10, FAM83G, GRAP, SNORD3B-1, SNORD3B-2, SNORD3D, GRAPL, LOC79999, SNORD3A, SNORD3C, LOC388436, EPN2, EPN2-IT1, EPN2-AS1, B9D1, MIR1180, MAPK7, MFAP4, RNF112, SLC47A1, SNORA59B, ALDH3A2, SLC47A2, ALDH3A1, ULK2, AKAP10, SPECC1*	chr17:16757564-20219464	***de novo***	**Pathogenic**
			Xp22.31	Loss	163 kb	/	(*STS*)	chrX:7329149-7491949	NA	Likely benign

[#] Physical position of the identified rare CNVs according to GRCh37/hg19 genome assembly, released February 2009. * Rare CNVs identified in homozygous condition. () Genes potentially perturbed by rare CNVs through a position effect. NA: not available.

3.1.2 RAI1 Next Generation Sequencing

Subsequently patients, with the exception of the 2 patients harboring the 3.46 Mb classical deletion at 17p11.2, were subjected to a NGS diagnostic panel, in order to unveil mutations in *RAI1* or in other genes known for their association with SMS, such as *MBD5* and *HDAC4*. The sequencing analysis identified 5 rare variants (unreported or reported with MAF <0.01 in population database, i.e. 1000 Genomes Project and gnomAD exomes) as shown in detail in **Table 15**. All the variants, 3 identified in *RAI1* and 2 in *MBD5,* were inherited and nonsynonimous. The clinical effect, assessed using the InterVar tool and the inheritance information, classified all identified variants as of "uncertain significance".

Tab.15 List of rare sequence variants identified in the SMS/SMS-like cohort by means of NGS panel

Patient ID	Gene	Variation type	Protein change	Inheritance	Already reported in literature	Effect
SMS9	*MBD5*	Missense c.2569G>A rs769330358	p.A857T	Maternal	Wagenstaller et al., 2007	Uncertain Significance
SMS14	*RAI1*	Missense c.4657T>C rs145585334	p.C1553R	Paternal	/	Uncertain Significance
SMS23	*RAI1*	Missense c.4228G>A rs774984414	p.G1410S	Paternal	/	Uncertain Significance
SMS25	*RAI1*	Missense c.3272C>A	p.A1091D	Maternal	/	Uncertain Significance
SMS27	*MBD5*	Missense c.3143C>T rs145475623	p.T1048I	Maternal	Wagenstaller et al., 2007	Uncertain Significance

3.1.3 RAI1 MLPA analysis

MLPA analysis, carried out to unveil microdeletion or microduplication affecting *RAI1* gene, did not identify any alterations in the patients tested, except for patient SMS25 in which a *de novo* heterozygous deletion encompassing *RAI1* exon 5, that encodes for the PHD functional domain, was disclosed (**Fig.17**).

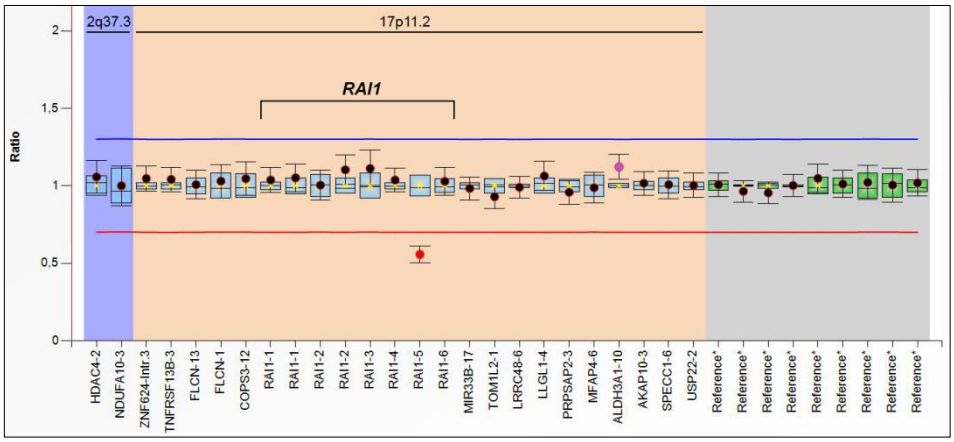

Fig.17 MLPA profile of 2q37.3 and 17p11.2 *loci* in proband SMS25 revealed a heterozygous deletion of *RAI1* exon 5. Each black dot displays the final probe ratio for each locus analyzed, and refers to the interval of values obtained by reference samples (light blue rectangles). The red and blue lines indicate the arbitrary borders for loss and gain, respectively. Standard deviations were set up according to the Coffalyzer DB software v131211.

3.1.4 RAI1 mRNA expression study

In order to evaluate a potential *RAI1* haploinsufficiency, RT-qPCR studies were carried out using TaqMan assay on *RAI1* exon junctions 3-4, on available patient's peripheral blood (24 patients out of 30). As shown in **Fig.18**, the RT-qPCR analysis detected normal levels of *RAI1* transcripts in all patients analysed, except, as expected, for patients SMS29 and SMS30 (red squares in scatter plot), both harboring the 17p11.2 classical deletion, and for patient SMS25 who unexpectedly showed a significant increase in *RAI1* transcript levels (blue square at the top of scatter plot). Moreover, we observed in patient SMS5 (green square), who carries a deletion involving *MBD5* gene, a normal *RAI1* expression, in contrast with literature data that showed a reduced *RAI1* expression in lymphoblastoid cell lines of patient affected by 2q23.1 deletion syndrome [Mullegama et al., 2015b].

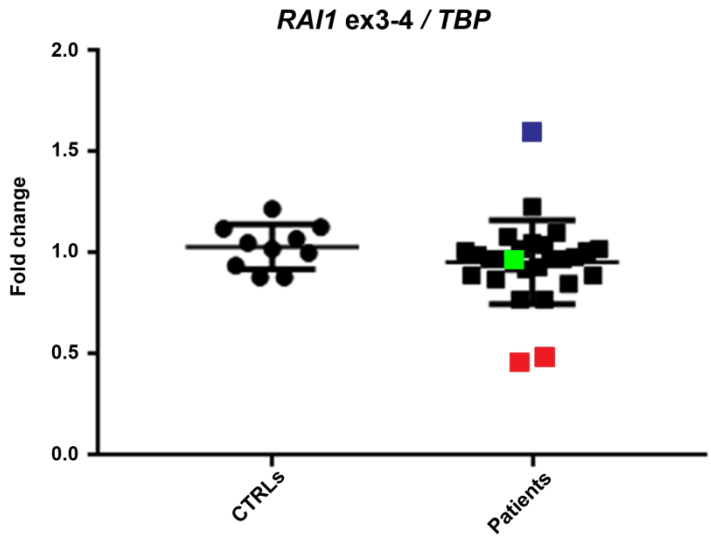

Fig.18 *RAI1* RT-qPCR results. Scatter plots, obtained using TaqMan probes, showing *RAI1* gene relative expression in 10 normal controls (circles), and in the 24 patients analyzed (squares). In patients SMS29 and SMS30 (red squares) we observed a decrease in *RAI1* transcripts, in SMS25 (blue square) an increase in *RAI1* expression, and in SMS5 (green square) *RAI1* transcript levels similar to those of controls. The horizontal black bars indicate the range between mean ±2 standard deviation values. Data were normalized against *TBP* (TATA box binding protein) as housekeeping gene.

3.1.5 Molecular characterization of RAI1 gene in patient SMS25

Patient SMS25 is a 17 years old girl with a classical SMS phenotype. She is the only child of healthy unrelated parents, with negative family history for ID or any other relevant genetic conditions. Preliminary analysis excluded the typical recurrent 17p11.2 deletion, but identified in *RAI1* gene the yet unreported heterozygous variant p.A1091D mapping in exon 3 and inherited from the healthy mother, and a *de novo* heterozygous deletion encompassing *RAI1* exon 5, consistent with the initial clinical suspicion (see paragraph 3.1.2 and 3.1.3).

To finely characterize the deletion breakpoints at nucleotide level, Long-Range PCR experiments were carried out on patient`s genomic DNA, using primers designed within IVS4 (upstream the deletion) and in 3' UTR within exon 6 (downstream the non deleted region according to MLPA studies). The subsequent Sanger sequencing allowed to establish that in addition to exon 5 the deletion partially involves also exon 6. The deletion of 3.4 kb starts, indeed, within IVS4 (2633 bp before exon 5) and ends within exon 6 (144 bp after the stop codon) (**Fig.19**). An overlapping region

of 5 bp (GTGGA) between intron 4 and exon 6 was found. Considering the overlapping sequence as part of intron 4 the deletion was refined at chr17:17,710,071 -17,713,440 (hg19).

To confirm the partial loss of exon 6, PCR experiments were performed on the patient's cDNA: the sequencing of the obtained amplicon pointed out the lack of a larger portion of exon 6 compared to that identified on genomic DNA sequencing. Indeed, since the canonical acceptor site was deleted, the new alternative splicing between exon 4 and exon 6 recognized a new splicing AG acceptor site downstream the genomic breakpoint (**Fig.19**). At transcript level the deletion causes the loss of the canonical stop codon which is replaced by a new one 946 bp downstream. In the predicted protein, the deletion causes the loss of the 20 amino acids, encoding for the PHD functional domain, and induces the insertion of 64 new amino acids.

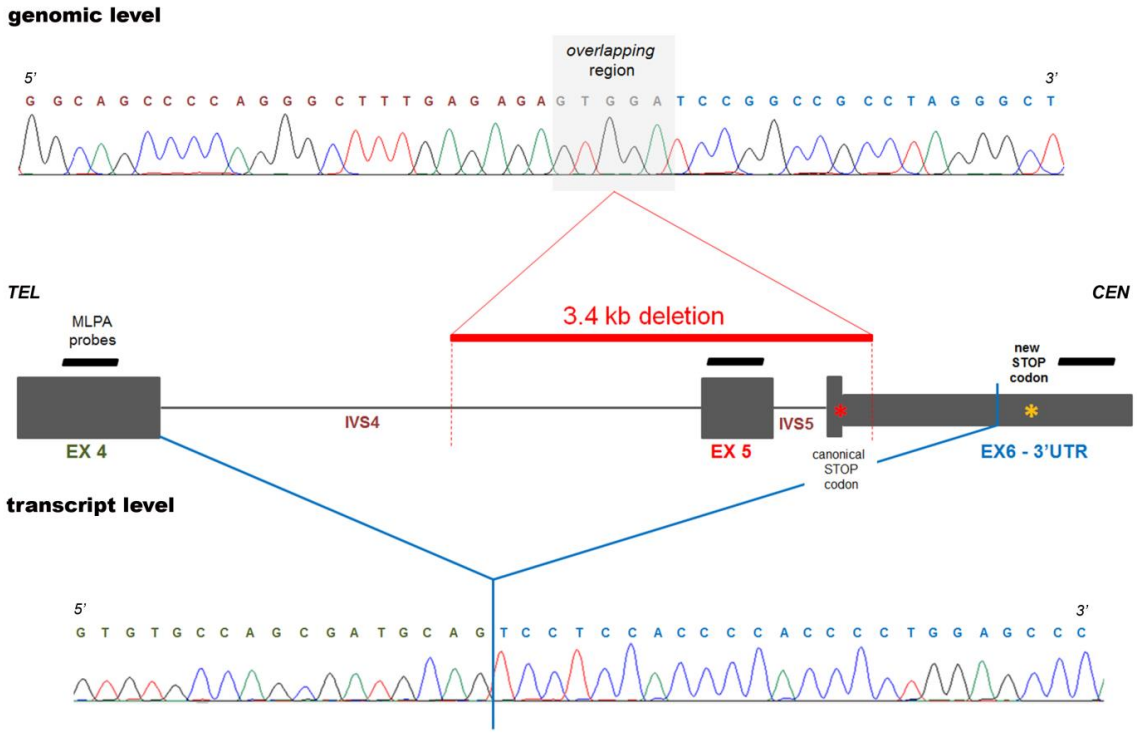

Fig.19 Schematic view of *RAI1* intragenic deletion identified in patient SMS25.

Moreover, as mentioned before in paragraph 3.1.4, RT-qPCR studies showed an unexpected significant increase in blood *RAI1* transcript levels of patient compared to those of 10 controls (**Fig.18**). To clarify this finding in the context of a SMS phenotype, further expression analysis were carried out using another TaqMan probe on *RAI1* exons junction 2-3 and extending the study to parents' samples, revealing an increase in transcript levels of both patient's and mother's peripheral blood cells compared to those of father and 10 healthy controls (**Fig.20 A**). It is well known that *RAI1* overexpression is associated to PTLS, the SMS reciprocal syndrome caused by duplication at 17p11.2. To evaluate whether the increased transcript levels identified in the SMS25 patient and her mother concerns both alleles or is specific for only one of them, we carried out further expression studies. Using primers designed to amplify the exons junction 4-5 (the non deleted allele in SMS25),

expression levels of both alleles has been evaluated in the mother with an outcome comparable to the previous experiments, whereas in the patient, harboring the heterozygous deletion of *RAI1* exon 5, only the transcript levels of wt allele was determined. To this purpose RT-qPCR experiments, based on SYBR Green methodology, were performed and showed that SMS25 presents a halved expression compared to controls and one-third compared to that identified in her mother (**Fig.20 B**). By comparing this data with the results of previous RT-qPCR, that identifies both alleles and shows triple levels transcript in the proband and in her mother, we can conclude that the overexpression is monoallelic both in patient and mother, and concerns the patient's deleted allele which is hence inherited from the mother (**Fig.20 C**). This approach, repeated using another housekeeping gene (TBP), confirmed the result.

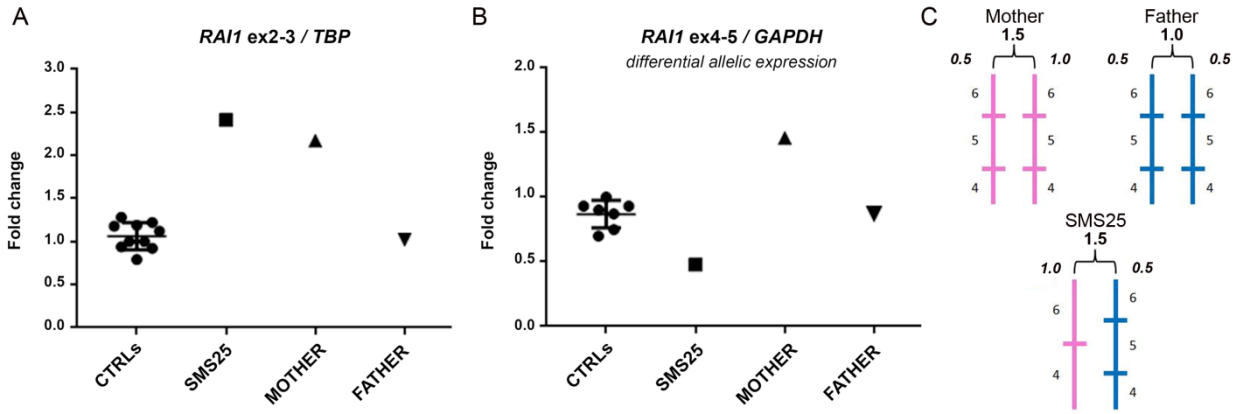

Fig.20 *RAI1* expression analysis and assessment of a differential allelic expression in SMS25 peripheral blood. **A)** Scatter plots obtained using TaqMan probe on exons junction 2-3, showing *RAI1* gene relative expression in 10 normal controls (circles), in the patient SMS25 (square), in the transmitting mother (triangle pointing upward) and in the father (triangle pointing downward). In both patients SMS25 and mother we observed an increase in *RAI1* expression, while in the father *RAI1* shows transcript levels similar to those of controls. The horizontal black bars indicate the range between mean ±2 standard deviation values. Data were normalized against *TBP* as housekeeping gene. **B)** Scatter plot showing expression of non deleted *RAI1* transcript. In patient (square) and in the mother (triangle pointing upward), respectively, a decrease and an increase of expression levels compared to those observed in the father (triangle pointing downward) and in the controls (circles) were found. Data were normalized against *GAPDH* (glyceraldehyde-3-phosphate dehydrogenase). **C)** Schematic drawing of *RAI1* alleles in patients and in her parents. SMS25 presents a wt allele of paternal origin (depicted in blue) and a deleted allele, missing exon 5 and part of exon 6, overexpressed and of maternal origin (depicted in pink).

In order to identify potential *cis* rare variants that could be related with *RAI1* overexpression observed in the patient and in her mother's peripheral blood, *RAI1* promoter and several regulatory regions were sequenced. These regions were selected based on the presence of predicted elements using the UCSC site, in particular active promoters and acetylation of H3K27 often found near active regulatory elements (**Fig.21**).

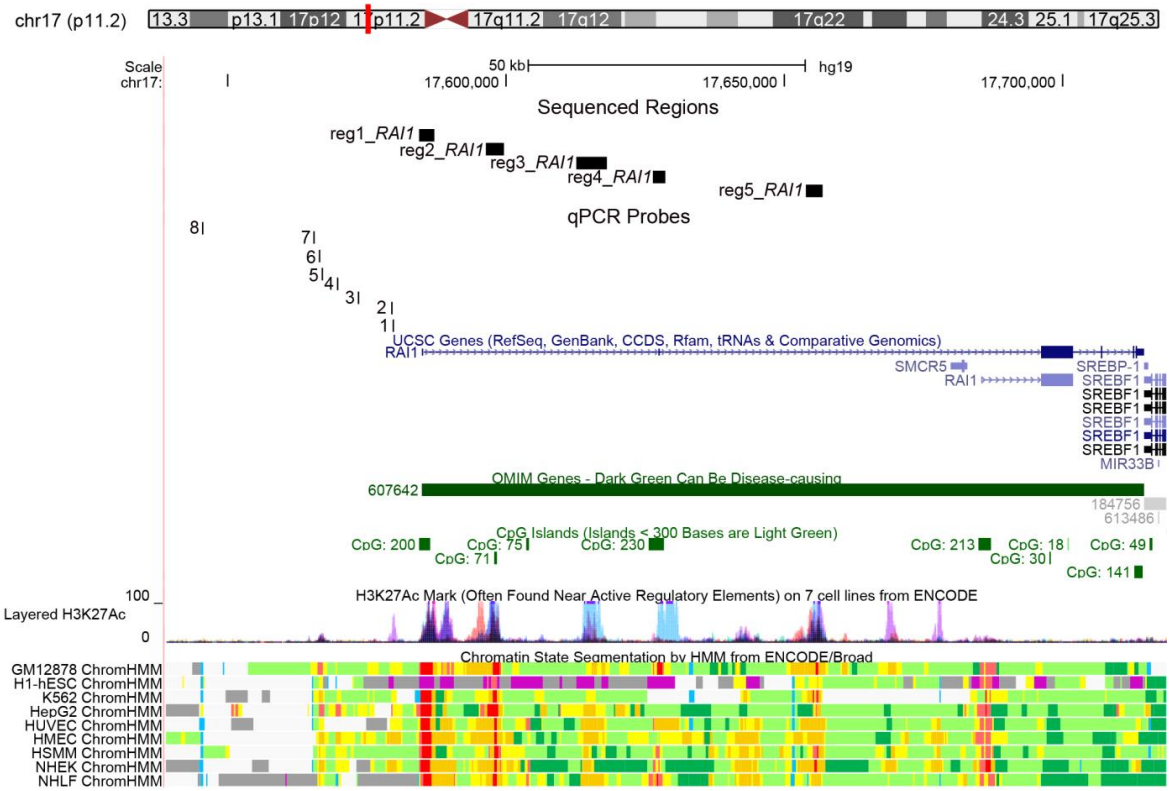

Fig.21 UCSC genome browser view of the 17p11.2 region where *RAI1* maps (chr17:17538839-17718702, hg19). UCSC genes are shown in blue, and OMIM gens in green. Regulatory elements prediction based on ENCODE chromatin state segmentation in nine human cell lines is shown: red, promoter; yellow, weak enhancer; orange, strong enhancer; dark green, transcriptional elongation; light green, weak transcribed; light blue, insulator; dark grey, polycomb-repressed; light grey, heterochromatin. Violet/light-blue spikes represent acetylation of H3K27 sites. At the top, black bars depict regulatory regions Sanger sequenced, and the 8 probes used in qPCR experiments

This analysis disclosed 12 common variants and 3 rare variants with MAF < 0.01 inherited from the father who presents normal *RAI1* expression levels (**Table 16**). Therefore, no alteration shared with the mother, that could be responsible for *RAI1* overexpression, was found.

Tab.16 List of sequence variants identified in SMS25 in putative regulatory regions.

Identified Variant	Nucleotide position[#]	Patient SMS25 Genotype	MAF	Origin
rs117908897	17:17585146	T/C	(C) 0.40	n.a.
rs12449524	17:17596461	C/A	(A) 0.21	n.a.
rs4925102	17:17596751	G/C	(C) 0.40	n.a.
rs2882552	17:17612910	G/T	(T) 0.42	n.a.
rs2350961	17:17613070	T/C	(C) 0.27	n.a.
rs12603857	17:17613073	G/C	(C) 0.27	n.a.
rs35272447	17:17626654	-/CC	(CC) 0.32	n.a.
rs546306892	17:17627667	T/-	(-) **<0.01**	**Pat**
rs540928629	17:17627668	T/A	(A) **<0.01**	**Pat**
rs9907986	17:17628141	C/T	(T) 0.42	n.a.
rs9906532	17:17628241	C/T	(T) 0.37	n.a.
rs11656775	17:17654319	A/G	(G) 0.22	n.a.
rs941448	17:17654542	C/G	(GG) 0.42	n.a.
rs574589747	17:17654804	G/A	(A) **<0.01**	**Pat**
rs9910075	17:17655073	C/T	(T) 0.08	n.a.

Moreover, qPCR experiments carried out to find out eventual cryptic microdeletions upstream the *RAI1* promoter (**Fig.21**) excluded losses and/or acquisitions in the number of copies in the genome of

SMS25 patient (data not shown). The presence of microdeletions that might have mediated the overexpression identified in patient and her mother was thus ruled out. The genetic determinant of *RAI1* overexpression peculiar of this patient is currently unknown.

3.2 EXPRESSION ANALYSIS OF CIRCADIAN RHYTHM GENES IN PERIPHERAL BLOOD OF SELECTED SMS/SMS-LIKE PATIENTS

Sleep disturbance is a main feature of SMS phenotype and few data are available about the molecular dysregulation of this condition. Another aim of this study was to evaluate quantitatively the expression levels of principal circadian rhythm genes in peripheral blood cells of 16 SMS/SMS-like patients belonging to the analysed cohort and sharing sleep disorders. Among the selected patients we considered 2 patients (SMS29-SMS30) with the classical 17p11.2 deletion, one patient with a *RAI1* intragenic microdeletion (SMS25) and her mother characterized by a *RAI1* overexpression (M-SMS25), one patient carrying an inherited *RAI1* missense variation (SMS14), one affected by 2q23.1 deletion syndrome (SMS5), one with a *SHANK3 de novo* deletion (SMS27), and other 9 patients showing sleep disturbance but without pathogenic rare CNVs (SMS6-SMS7-SMS8-SMS9-SMS16-SMS20-SMS21-SMS22-SMS26-SMS28). Moreover, we analyzed also 3 patients of the cohort without sleep alterations but showing others SMS clinical signs (SMS12-SMS15-SMS17), for a total of 20 subjects tested. The inclusion of the last three patients was done to corroborate a possible correlation between the presence of sleep disturbance and an impaired expression of circadian rhythm genes.

The circadian rhythm genes analyzed are shown in **Table 17**.

Tab.17 List of circadian rhythm genes analyzed by RT-qPCR

Gene	Chromosomal band	Gene Function
CLOCK	4q12	They encode transcription factors that heterodimerize and induce the transcription activation of several proteins of the circadian clock, including PER and CRY [Gekakis et al., 1998].
BMAL2	12p11.23	
CRY1	12q23.3	They encode the components of the circadian core oscillator, which negatively regulates the heterodimers CLOCK-BMAL [Charrier et al., 2017].
PER1	17p13.1	
PER2	2q37.3	
MTNR1A	4q35.2	These genes encode the two high affinity forms of receptors for melatonin, mediating its circadian action.
MTNR1B	11q14.3	
NR1D1	17q21.1	It encodes a transcriptional repressor, in particular acts on the transcriptional inhibition of *BMAL.*

First of all, the actual expression of genes of interest on peripheral blood and, simultaneously, on commercial human brain was verified by means of PCR. As shown in **Fig.22**, *MTNR1A* and *MTNR1B* genes were found to be specifically expressed in the central nervous system, so it could not be possible to test their expression on blood.

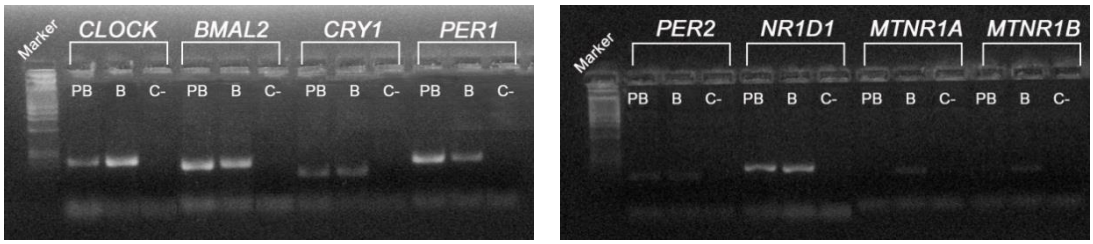

Fig.22 Circadian rhythm genes expression on peripheral blood and on commercial human brain by means of RT-PCR. All genes tested are expressed both on blood and on brain, except for *MTNR1A* and *MTNR1B*, whose expression is restricted to brain tissue (PB=Peripheral Blood; B=Brain; C-=Negative control).

RT-qPCR analyses enabled us to establish for each gene tested the average variability of mRNA controls, which has been used to compare the expression levels of patients. As illustrated in **Fig.23**, among the circadian rhythm genes examined, a dysregulation of *CLOCK*, *BMAL2*, *PER2*, and *NR1D1* emerged.

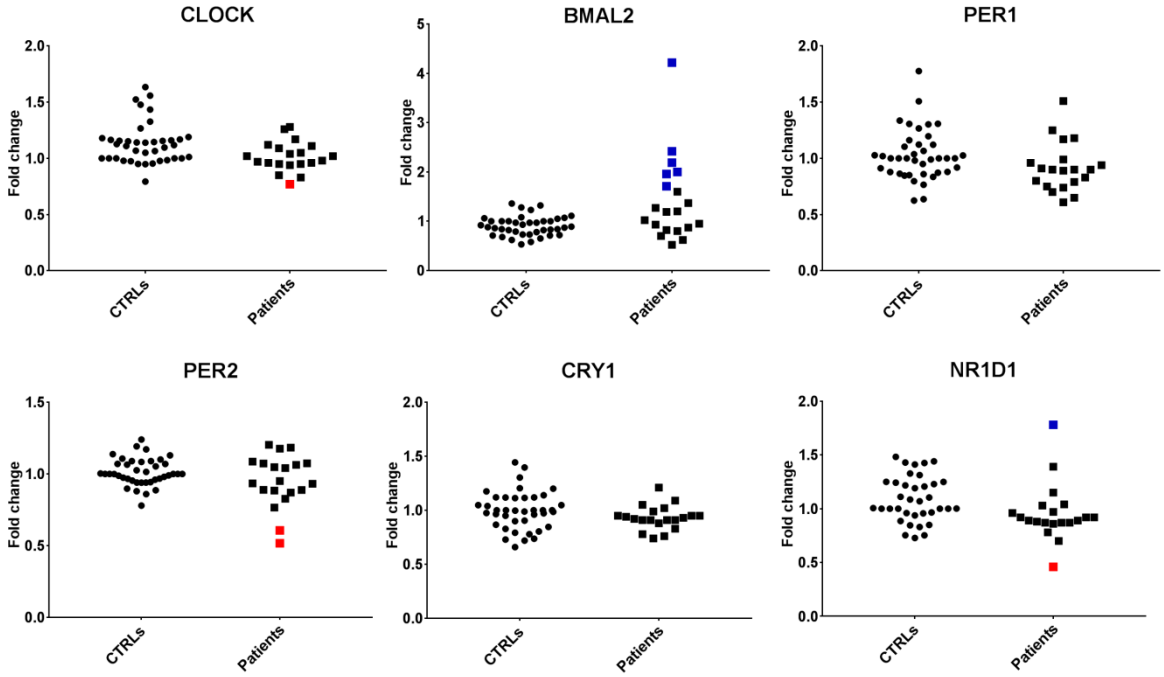

Fig. 23 Circadian rhythm genes expression analysis. Scatter plots of circadian rhythm genes relative expression are shown for both normal controls (circles) and 20 selected patients (squares). Patients with a decreased expression compared to control range are shown as red squares: SMS29 was slightly downregulated for *CLOCK*, SMS6 and SMS29 were downregulated for *PER2*, and SMS8 was decreased for *NR1D1*. Patients with an increased expression compared to control range are depicted in blue: *BMAL2* was upregulated in SMS8, SMS9, SMS15, SMS16, SMS20, SMS22, and SMS28; *NR1D1* was increased only in SMS27. Data were replicated at least twice and normalized against *TBP* (TATA box binding protein) and *ACTB* (actin-b) as housekeeping genes. Controls values of each replica are shown to highlight controls variability, whereas for patients an average value representative of all replicas was considered.

In detail, *BMAL2* was the most impaired gene since resulted significantly overexpressed in 6 patients out of 20 analyzed (SMS8-SMS9-SMS16-SMS20-SMS22-SMS28) ($p < 0.001$ **Fig.24**). *PER2* expression levels appeared decreased in patients SMS29 and SMS6, *NR1D1* was found upregulated in patient SMS27 and downregulated in SMS8, and *CLOCK* mRNA content resulted mildly downregulated in patient SMS29.

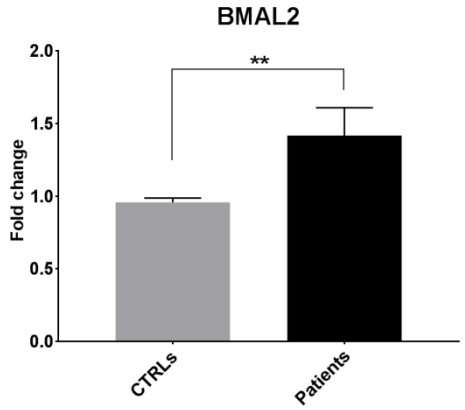

Fig.24 Ideogram view of *BMAL2* gene expression analysis. T-test study was applied to RT-qPCR data on *BMAL2* gene highlighting a significant difference between controls and patients that show on average a transcript level upregulation. Mean values ± SEM are shown. **p<0.001.

3.3 FUNCTIONAL APPROACH: HUMAN INDUCED PLURIPOTENT STEM CELLS (iPSCs)

3.3.1 Selection of patient for iPSCs reprogramming

Upon previous genomic scans in SMS/SMS-like cohort we selected patient SMS8, an 8 years old male who carries a 54 kb maternal deletion, disclosed through array-CGH, at Xq13.3, about 29 kb from 5' of *ZDHHC15* gene, which results in a reduced transcript level on peripheral blood cells of the patient. *ZDHHC15* encodes for a palmitoyl-transferase involved in neuronal differentiation and in synaptic plasticity, which has been already associated with X-linked mental retardation (MRX91) (OMIM#300577).

3.3.2 Generation and characterization of SMS-like patient iPSCs

Reprogramming to iPSCs was performed from patient's and parents' PBMCs using the integration-free Sendai virus. We generated three iPSC clones from patient and mother, and two clones from the father that were used as control iPSCs, taking into account the same family genetic background.

All iPSCs clones were checked by conventional karyotype and array-CGH analysis to evaluate the acquisition of any genomic alterations during the reprogramming process. In details, all clones maintained the normal 46,XY or 46,XX karyotype (**Fig.25 A**). The clones generated from patient's and his father's blood cells did not acquire any rearrangements compared to matched array-CGH blood profile; on the contrary in one of mother's iPSC clones a 160 kb rare deletion at 3q13.31 (**Fig.25 B**), not present in the blood, was identified. The identified rare deletion (chr3:114651290-114811608, hg19) involved the *ZBTB20* gene, which encodes for a transcriptional repressor that plays a role in many processes including neurogenesis, glucose homeostasis, and postnatal growth. Moreover, dysregulations of *ZBTB20* gene are responsible for the Primrose Syndrome (OMIM#259050) characterized by ID, recognizable facial appearance, brain abnormalities, hearing loss, hypotonia, and

macrocephaly [Cleaver et al., 2019]. Therefore, we ruled this clone out from further characterization (**Tab. 18**). By high resolution array-CGH we scored an overall frequency of 12.5% rearranged iPSC clones.

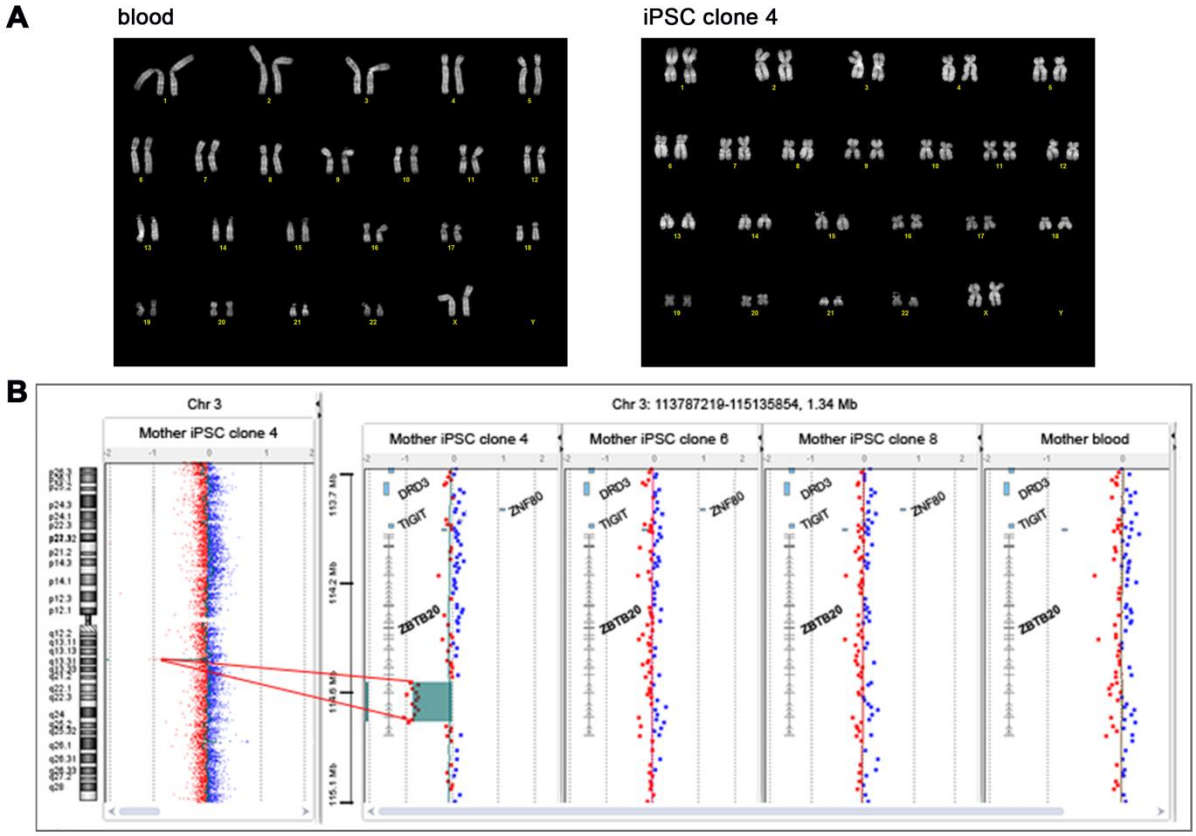

Fig.25 Control of iPSC clones for maintenance of the original karyotype. A) QFQ-banded karyotype of peripheral blood lymphocytes and of iPSC clone 4 of mother, showing no abnormalities. **B)** Array-CGH profile (180 K) showing the presence of a rare deletion at 3q13.31 (chr3:114651290-114811608, hg19) affecting *ZBTB20* gene in iPS clone 4 of the mother compared to clones 6, 8, and normal profiles of blood.

Moreover, the obtained iPSC clones showed the typical morphology, with a high nuclear to cytoplasmic ratio and formed compact multilayer colonies with defined edges (**Fig.26 A**).

The evaluation of pluripotency was performed by RT-PCR and by IF: total RNA of each iPSC clone was isolated and retro-transcribed to monitor by RT-PCR the expression of stem cell factors SOX2, OCT3/4 and NANOG (**Fig.26 B**); while Alkaline Phosphatase (AP), SSEA-4, and TRA-1-60 were controlled by immunofluorescence staining (**Fig.26 C**). In addition, pluripotency of generated iPSCs was examined *in vitro* through embryoid body (EB) formation and the following spontaneous differentiation into the three germ layers, which expression was evaluated by IF using specific markers (βIII tubulin for ectoderm, desmin for mesoderm and α-fetoprotein (AFP) for endoderm) (**Fig.27**).

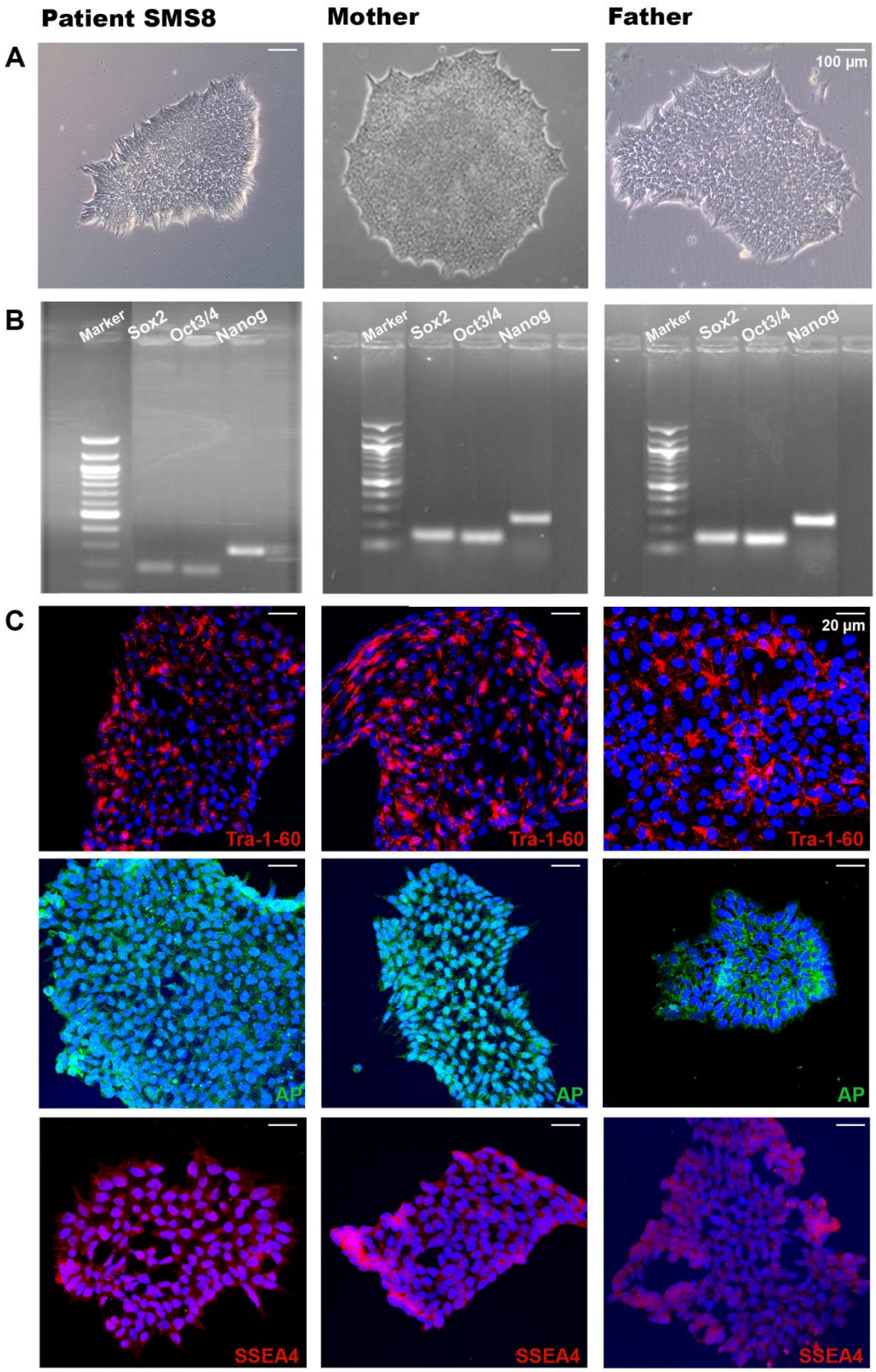

Fig.26 Characterization of human iPSCs derived from peripheral blood mononuclear cells of SMS8 patient and his parents. A) Above panels are representative pictures of iPSC colonies. Scale bar, 100 µm. **B)** RT-PCR showing the expression of pluripotency-associated genes Sox2, Oct3/4 and Nanog. **C)** Immunostaining showing positivity for the pluripotency markers TRA-1-60, AP, and SSEA-4. Nuclei are stained with DAPI. Scale bar, 20 µm. A single representative clone for each subject is shown.

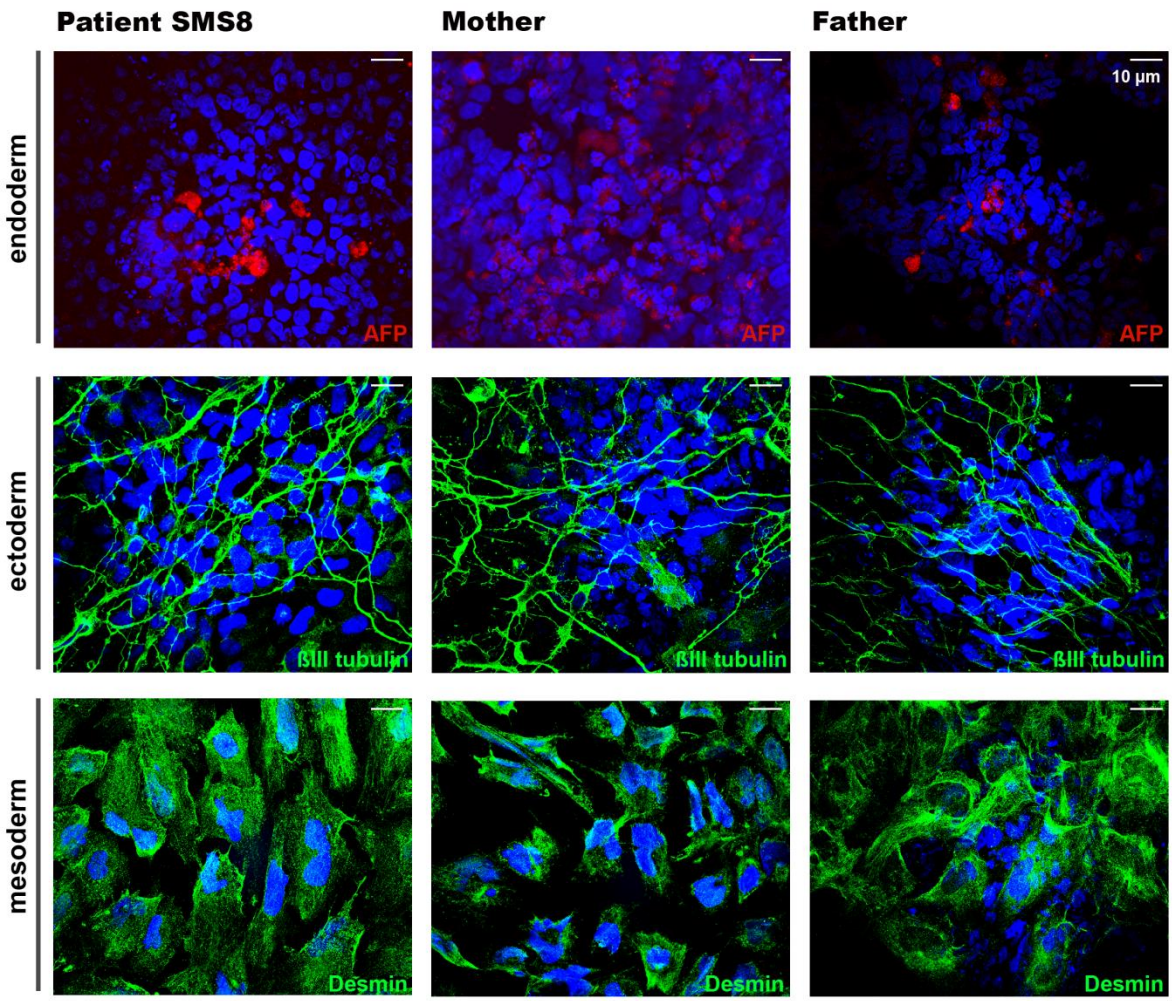

Fig.27 Evaluation of the potential to spontaneously differentiate into the three germ layers. Immunostaining showing positivity for endoderm (AFP), ectoderm (βIII tubulin) and mesoderm (Desmin). Nuclei are stained with DAPI. Scale bar, 10 µm. A single representative clone for each subject is shown.

The results of the overall iPSCs characterization are summarized in **Table 18**:

Tab.18 List of characterized iPSC clones

SAMPLE	iPSC CLONES	GENOMIC ALTERATIONS ACQUIRED	PLURIPOTENCY ASSESSMENT
SMS8	C1	NO	OK
	C2	NO	OK
	C7	NO	OK
SMS8 MOTHER	C4	YES	-
	C6	NO	OK
	C8	NO	OK
SMS8 FATHER	C8	NO	OK
	C11	NO	OK

Finally, selected iPSCs clones, found to have maintained full genomic stability and to express pluripotency markers, were analysed by RT-PCR to examine the *ZDHHC15* transcript level (**Fig.28**). Unexpectedly we did not identify any downregulation in *ZDHHC15* expression level in patient's iPSC clones compared to parents' and controls' iPSC clones, contrary to what observed on patient's peripheral blood cells.

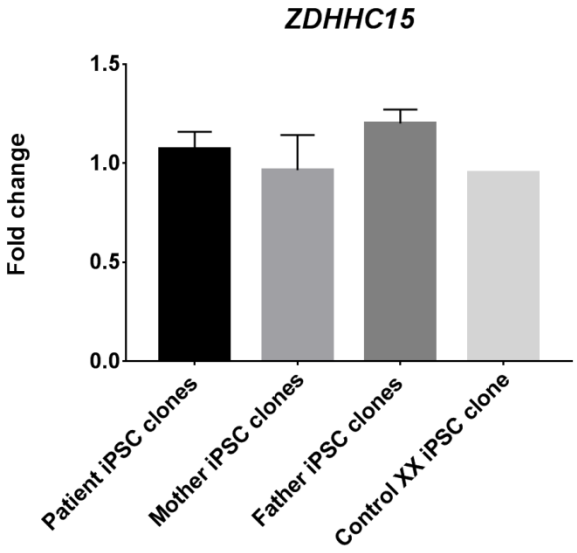

Fig.28 *ZDHCC15* RT-qPCR results on cDNA obtained from iPSC clones. Scatter plots, obtained using TaqMan probes, showing *ZDHHC15* gene relative expression in three clones of SMS8 patient, two clones of his mother, two of his father, and one iPSC clone of a XX control. In patient clones mRNA levels were comparable to those identified in mother's, father's, and control's iPSC clones. Data were normalized against *TBP* as housekeeping gene, and replicated with *GAPDH*.

3.3.3 Cortical neurons differentiation and characterization

We consequently proceeded with the differentiation of each iPSC clone into cortical neurons according to the monolayer protocol in N2B27 medium supplemented with Noggin (**Fig.29**) [Germain et al., 2014].

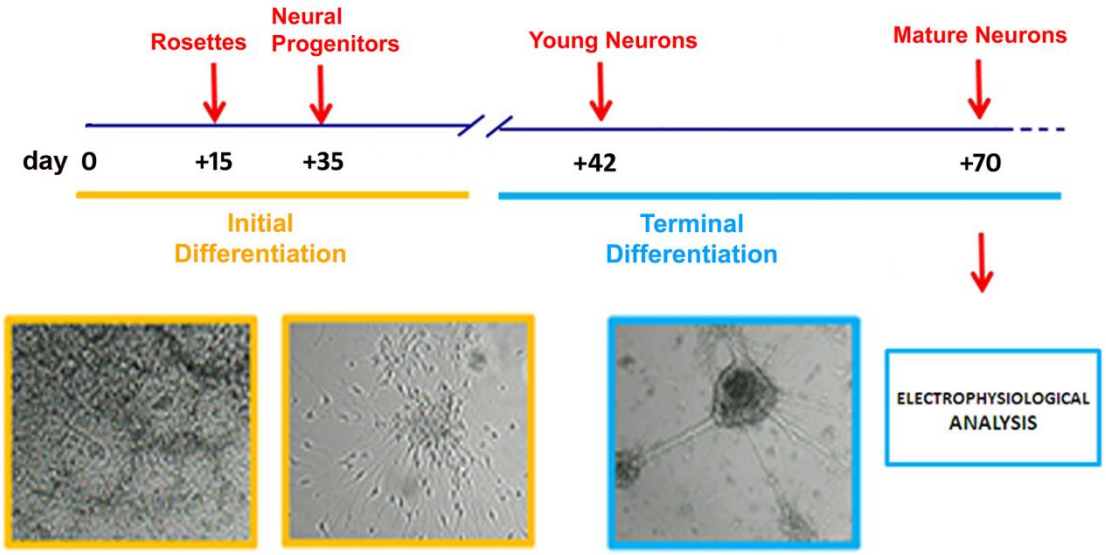

Fig.29 Workflow for cortical neurons differentiation. Modified from Alari et al., 2018.

The process was first marked by the appearance of the typical neural rosettes (14-16 days) (**Fig.30 A**), that showed positive immunofluorescence staining for the neuroectodermal stem cell markers Nestin and PAX6 (**Fig.30 B**). Then, the neural rosettes were manually cut and passaged on poly lysine-laminin coated dishes, and further induced to differentiate into neural progenitors (day 35) using a specific medium added with BDNF, GDNF, cAMP and Ascorbic Acid.

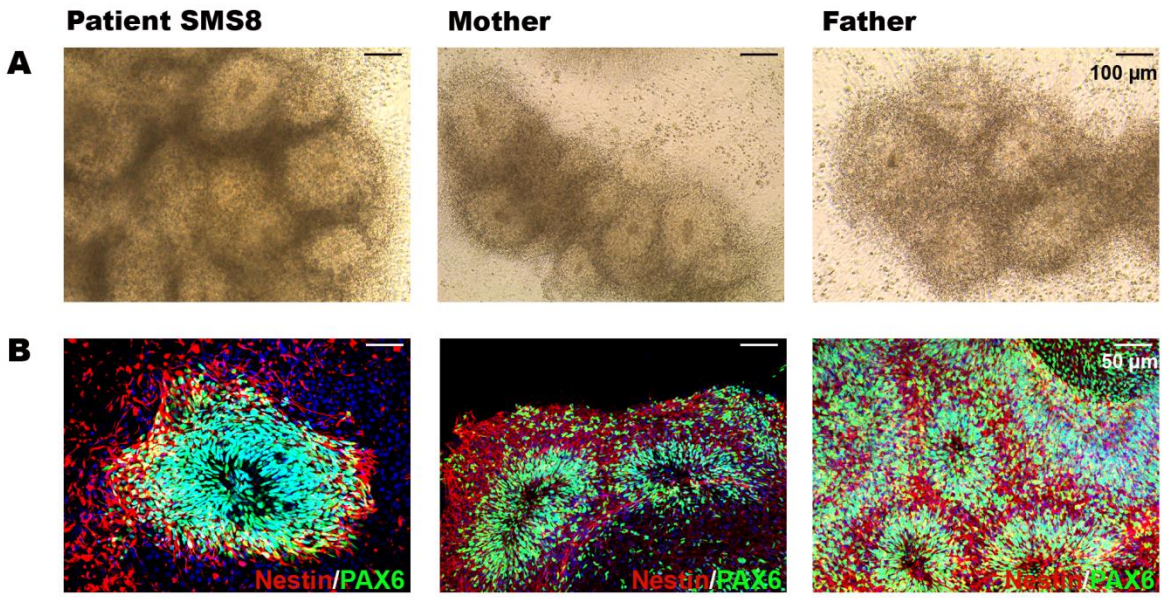

Fig.30 Morphological and immunofluorescence characterization of iPSC-derived neural rosettes. A) Images at bright-field microscope of neural rosettes (10×) Scale bar, 100 µm. **B)** IF positive staining of the neuroectodermal stem cell markers Nestin and PAX6. Nuclei are stained with DAPI. Scale bar, 50 µm. A single representative clone for each subject is shown.

Therefore, NPCs were further induced to differentiate into neurons. After prolonged maintenance in culture (at least 70 days), we obtained both patient and parents neurons. Most of the cells exhibited a typical neuronal morphology with long and abundant axons and dendrites as shown by βIII tubulin and SMI312 (Pan-Axonal Neurofilament Marker) staining (**Fig.31**). Characterization of the derived neurons was also deepened by the positive expression of different neuronal markers such as MAP2 (microtubule-associated protein 2) through RT-PCR and IF staining (**Fig.31-32**). Moreover, we confirmed that the highly intricate network of cells produced were enriched in cortical neurons by the positivity to TBR1 and CUX1, brain specific transcription factors involved in the regulation of cortical development and in the outgrowth of dendrite of cortical neurons, respectively (**Fig.31-32**). Most derived neurons both from patient and parents were also positive for VGLUT1, that encodes for the vesicular transporter of glutamate, one of the most common excitatory neurotransmitter produced by glutamatergic neurons (**Fig.31**), and for GAD1, also called GAD67, encoding for an enzyme responsible for catalyzing the production of inhibitory neurotransmitter γ-aminobutyric acid (GABA) (**Fig.32**). Representative images of ßII tubulin, CUX-1, MAP2, SMI312, and VGLUT1 IF staining from patient and parents are shown in **Fig.31**.

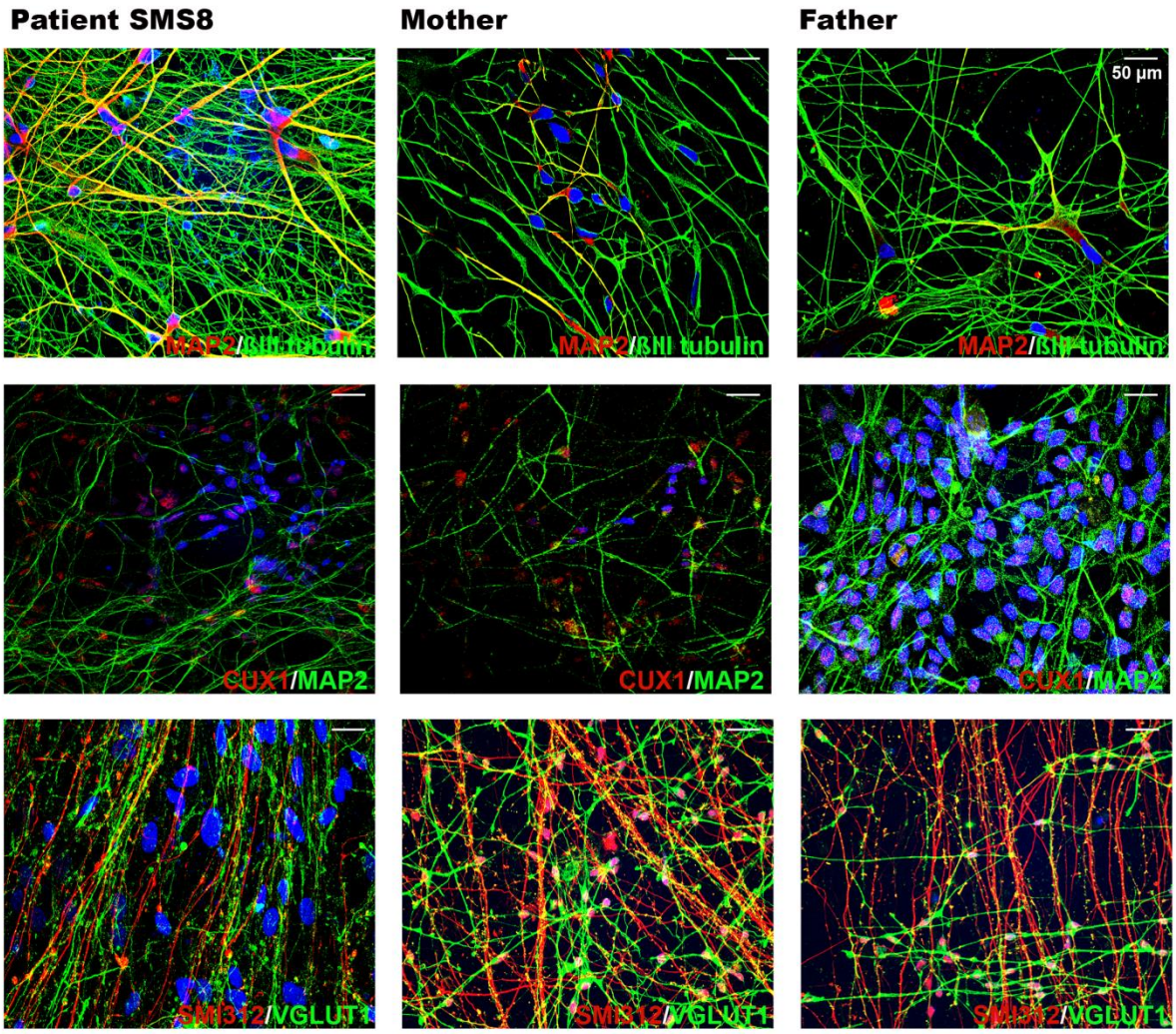

Fig.31 Immunofluorescence characterization of neuronal markers in patient's and parents' 70 days derived neurons. Immunostaining showing positivity for neuronal markers MAP2, ßII tubulin, CUX1, SMI312, and VGLUT1. Nuclei are stained with DAPI. Scale bar, 50 µm. A single representative clone for each subject is shown.

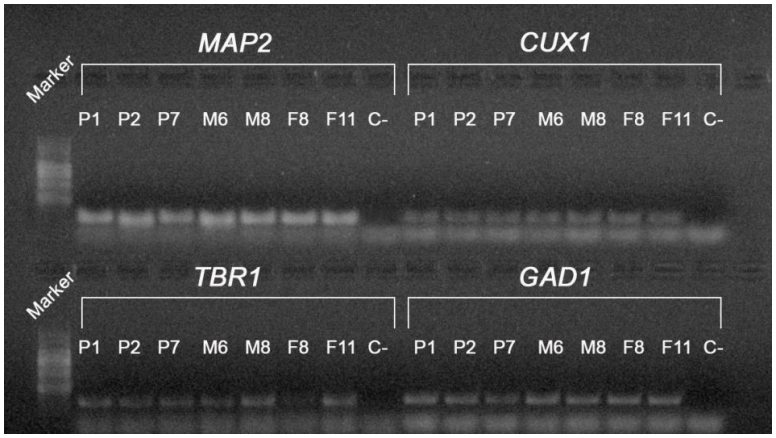

Fig.32 Expression evaluation of neuronal markers by means of RT-PCR. All genes tested are expressed in neurons differentiated from each iPSC clone obtained from patient and both parents (P1=neurons derived from patient's iPSC clone 1; P2=neurons derived from patient's iPSC clone 2; P7=neurons derived from patient's iPSC clone 7; M6=neurons derived from mother's iPSC clone 6; M8=neurons derived from mother's iPSC clone 8; P8=neurons derived from father's iPSC clone 8; P11=neurons derived from father's iPSC clone 11; C-=Negative control).

Subsequently, on mature cortical neurons *ZDHHC15* expression analyses were performed by means of RT-qPCR, to explore in a neuronal context the gene downregulation previously identified in peripheral blood cells. Although the experiments have been replicated more times, *ZDHHC15* neuronal mRNA levels showed an extreme variability, not letting us to determine the amount of transcript which should be expected and disclose an expression alteration in neurons derived from patient's iPSCs (data not shown).

3.3.4 Electrophysiology of mature cortical neurons

To investigate the synaptic properties of iPSC-derived differentiating neurons obtained from patient SMS8 and his parents, excitatory post synaptic currents in miniature (mEPSCs) were recorded. MEPSCs represent the basal neuronal transmission generated by the release of docked synaptic vesicles containing glutamate responsible for the activation of glutamatergic postsynaptic receptors. They were recorded by patch-clamp technique (whole-cell voltage clamp) clamping the voltage at -70 mV [Antonucci et al., 2013]. Recordings were performed over time, starting from 50 to approximately 75 days of differentiation (50, 55, 62, 72 days post differentiation).

Accordingly to physiology, recordings of neurons obtained from the healthy father showed a strong maturation trend over time as indicated by the constant increase of mEPSCs frequency and amplitude (**Fig.33 A,B**). These data were coherent with the pre- and postsynapse functional maturation. In fact, the mEPSCs frequency is a parameter usually associated with number of the presynaptic release sites and so, to a proper synaptogenesis process. Instead, the amplitude parameter reflects the expression of AMPA receptors on the postsynaptic compartment [Meyer et al., 2001; Kerchner and Nicoll, 2008]. Thus, an increase of these two measurements demonstrates an increased synaptic maturation and functionality.

Then, we recorded mEPSCs in differentiating neurons obtained from patient SMS8 and the transmitting mother. Surprisingly, we found opposite result from those previously described and obtained by the analysis of father-derived neurons. As indicated in **Figure 33 C-F**, no signs of increasing maturation were detected in terms of frequency or amplitude, suggesting that here the development of functional synapses is braked. Also, the comparison of frequency ad amplitude among the three groups (**Fig.33 G,H**) over time displayed a clear defected synaptic development.

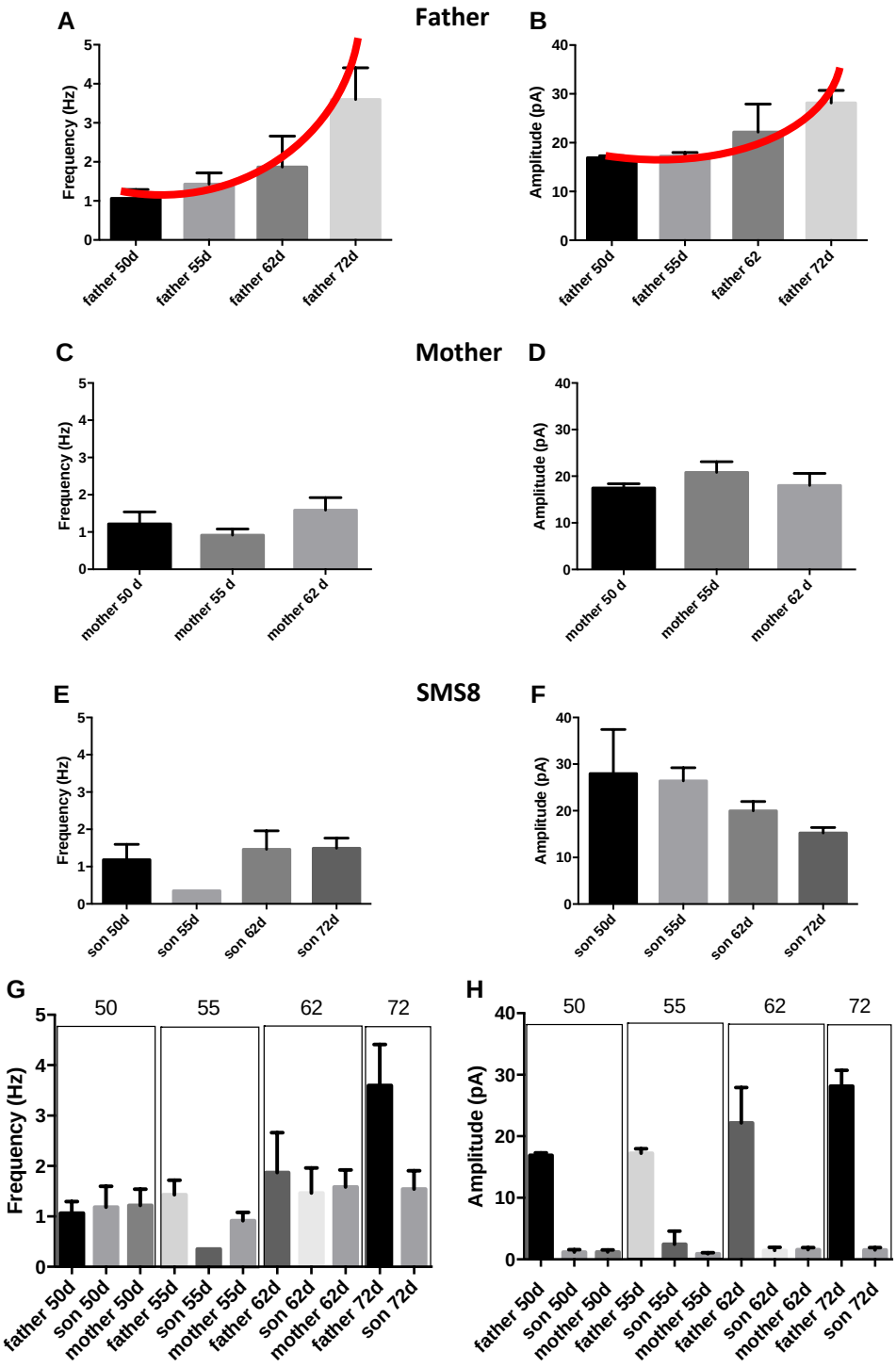

Fig.33 Electrophysiology of differentiating neurons derived from SMS8 and his parents. A-F) mEPSCs have been recorded at different time points from differentiating neurons derived from patient's father (**A** and **B**), patient's mother (**C** and **D**), and from the patient SMS8 (**E** and **F**). In the father-derived neurons mEPSCs frequency (**A**) and amplitude (**B**) increase over time indicating that during maturation excitatory synapses properly develop. **G-H)** Comparison of mEPSCs frequency and amplitude measurements over time among the three experimental groups (father – mother – patient SMS8).

DISCUSSION

4.1 Sample cohort selection and genomic investigation

Smith Magenis Syndrome is a complex dominant disorder mainly characterized by developmental delay, behavioural problems and circadian rhythm dysregulation, resulting from haploinsufficiency of *RAI1* gene due to either 17p11.2 deletion or mutations. The cohort assembled for this study includes 30 patients with SMS clinical suspicion, exhibiting several typical signs of the syndrome which is characterized by wide phenotypic heterogeneity. A careful clinical examination revealed that DD and ID are the most frequent clinical features with a frequency of 93% and 90%, respectively. Also cranio-facial dysmorphisms are common in the analyzed cohort, although highly variable; among them midface hypoplasia (21 out of 30) and brachycephaly (14 out of 29) are prevalent. Regarding sleep disturbance, 18 out of 30 patients (60%) show abnormalities in sleep-wake rhythmicity.

Little is known about the molecular mechanism underlying SMS, as *RAI1* interactors are yet poorly clarified. Moreover, up to date only 50% of patients clinically suspected SMS bear *RAI1* molecular defects highlighting that other unknown *loci* might be involved in SMS etiology and SMS-like phenotypes. In order to pinpoint rare pathogenic CNVs containing dosage sensitive genes that might be implicated in *RAI1* molecular pathways, high resolution array-CGH analysis was performed on 30 patients with SMS clinical suspicion, 28 without a molecular diagnosis, and 2 carrying 17p11.2 deletion previously disclosed by FISH, to finely define the deletion size and to exclude others pathogenic CNVs.

Overall, array-CGH analyses have enabled us to disclose 60 rare CNVs in 25 out of 30 patients, that based on gene content and inheritance were classified as likely benign (45/60), VOUS (13/60), or pathogenic (4/60). Regarding pathogenic CNVs, in SMS29 and SMS30 the recurrent 3.46 Mb 17p11.2 deletion was detected.

In SMS27 a 100 kb *de novo* deletion at 22q13.33 was identified including *SHANK3* gene, encoding a multidomain scaffold protein of the postsynaptic density involved in synapse function by modulating dendrite formation [Naisbitt et al., 1999; Monteiro and Feng, 2017]. *SHANK3* haploinsufficiency, resulting from both deletions and point mutations [Phelan and McDermid, 2012; Cochoy et al., 2015], is causative of Phelan-McDermid syndrome (PMS), also known as chromosome 22q13.3 deletion syndrome. PMS is a rare genetic disorder characterized by global DD, ID, ASD, and mild dysmorphisms, showing considerable clinical heterogeneity [Phelan and McDermid, 2012]. Up to now no clinical or molecular overlapping between SMS and PMS has been reported; however, the clinical re-evaluation of SMS27, in response to the identification of the rare CNV, reconfirmed the initial SMS clinical suspicion. Moreover, in the patient a missense *MBD5* variant (p.Thr1048Ile) has been disclosed through NGS analysis, inherited from the healthy mother. The p.T1048I variant has

been previously reported in an individual with intellectual disability but the parental testing was not performed [Wagenstaller et al., 2007]. This substitution maps in a region poorly conserved across species, and *in silico* analysis prediction showed that it likely does not alter the protein structure/function, nevertheless we cannot exclude its role as SMS phenotype modulator.

In patient SMS5 a 30 kb pathogenic deletion at 2q23.1, involving *MBD5* exons 1-2 and the promoter region, has been detected, reconfirming the phenotypic overlapping between 2q23.1 deletion syndrome and SMS. Interestingly, we disclosed the same rearrangement in the healthy father in a mosaic condition (~50% on blood). To date other two cases of parental blood mosaicism for a 2q23.1 microdeletion involving *MBD5* have been reported [Tadros et al., 2017]. These findings are relevant for sibling recurrence risk of individuals who have an apparent *de novo* 2q31.1 microdeletion. Moreover, in contrast with reduced expression reported by Mullegama and collaborators in lymphoblastoid cell lines of subjects affected by 2q23.1 deletion syndrome [Mullegama et al., 2015b], we observed in SMS5's blood *RAI1* normal mRNA levels.

Of note, among the 13 CNVs classified as VOUS, two similar deletions within 6p25.1 involving *FARS2* and *LYRM4* genes were identified in two unrelated patients (SMS16-SMS20), both inherited from their healthy mothers. A similar 6p25.1 deletion was reported in dizygotic twins characterized by dysmorphic features, borderline-mild ID, speech and language difficulties, and behavior abnormalities [Bozza et al., 2013]. Even in the reported twins the CNV was inherited from their mother, who however showed a borderline phenotype [Bozza et al., 2013]. No mutations were detected by sequencing and further studies will be performed in SMS16 and SMS20 to clarify the pathogenic role of the *FARS2* and *LYRM4* deletion, aimed to unveil a second "hit" contributing to the patients' phenotype.

In order to disclose the genetic defects responsible for the SMS-like phenotype of the molecularly unsolved patients of our cohort with a strong suggestive SMS phenotype, others genome-wide approaches, such as exome/genome sequencing are needed.

4.2 RAI1 intragenic deletion and concomitant overexpression in patient SMS25: Smith-Magenis or Potocki-Lupski syndrome?

Except for patient SMS25, a 17 years old girl with SMS clinical diagnosis (**Table 1**), no other *RAI1* alterations were detected by either MLPA and gene expression analyses. MLPA and sequencing analysis revealed in SMS25 a pathogenic 3.4 kb *de novo* heterozygous deletion encompassing entirely *RAI1* exon 5 and partially exon 6. The predicted protein encoded by the aberrant transcript is likely dysfunctional since lacks the PHD functional domain. To date in literature only other two SMS cases with *RAI1* intragenic deletions are reported, involving different exons: a patient harboring a 140 kb deletion involving exons 1 and 2 [Vieira et al., 2012], and a patient with a 29 bp deletion in exon 3

[Slager et al., 2003]. Unexpectedly, a significant increase in blood *RAI1* transcript levels of both patient SMS25 and her mother was found. *RAI1* overexpression, generally due to 17p11.2 duplication, is causative of PTLS. Consistently with the SMS clinical diagnosis, the upregulation involves only the maternal non-functional deleted allele. *RAI1* upregulation was also detected in the healthy mother, who does not present *RAI1* duplication nor any neurologic/behavioral clinical signs reflecting PTLS phenotype. The absence in the mother of PTLS neurologic/behavioral signs might be explained by the high phenotype variability and the penetrance defect already reported in other PTLS familiar cases [Yusupov et al., 2011; Magoulas et al., 2014; Alaimo et al., 2015], or by a normal *RAI1* expression in other tissues, such as the neuronal one, hypothesizing that the still unknown genetic variant causing *RAI1* overexpression is tissue specific. However, the mother's clinical re-evaluation pointed out that her facial features likely resemble the facial dysmorphism of the syndrome.

As the *RAI1* overexpression was found to be allele-specific, we hypothesize the involvement of a putative *cis* element, not yet identified. Genomic NGS panel targeted to the genomic region involving *RAI1* gene (both upstream and intronic sequences) on the SMS25 *trios*, could be useful to identify the supposed *cis* element allowing to better clarify the *RAI1* transcriptional regulation.

4.3 Correlation between the presence of sleep disturbance and an impaired expression of circadian rhythm genes

Sleep disturbance represents a hallmark of SMS and there is clinical and molecular evidence that the causative gene *RAI1* is involved in circadian rhythm. The circadian genes oscillatory expression, governed by a fine transcriptional modulation, is not restricted to central nervous system, but it can be observed in peripheral melatonin target tissues, such as blood and skin (fibroblasts). Therefore, we decided to evaluate the expression level of the main circadian rhythm genes in the blood of selected SMS/SMS-like patients, taking into account the facility and the high quality rate of RNA collection and extraction from this tissue.

Overall, the circadian rhythm genes analyzed were *CLOCK*, *BMAL2*, *CRY1*, *PER1*, *PER2*, and *NR1D1*, and 4 of them (*CLOCK*, *BMAL2*, *PER2*, and *NR1D1*) were found dysregulated. In detail, *BMAL2* was significantly overexpressed in 6 out of 20 analyzed patients, resulting the most impaired gene. Based on these results *BMAL2* appears as the circadian gene whose alterations are most detectable on blood. Moreover, statistical analysis (T-test study) applied to *BMAL2* RT-qPCR data highlighted a significant difference between controls and patients that showed on average a transcript level upregulation. Our results regarding *BMAL2* expression are in contrast with literature data, that reported a downregulation in *BMAL2* levels on fibroblasts collected from skin biopsies of three SMS patients carrying a common 17p11.2 deletion, a small unusual deletion, and a *RAI1* missense variant [Williams et al., 2012]. This discrepancy could be ascribed to the different tissues analyzed, where a

different regulation of many clock-controlled genes might be present. In the same article, Williams and collaborators reported that the "classical" SMS patients showed a decreased expression of *CLOCK* and *CRY1* genes, and an upregulation of *NR1D1* [Williams et al., 2012]. However, in our patient SMS29 carrying the typical deletion, as the reported patient, we observed only a mild donwregulation of *CLOCK* and *PER2* genes. Also in this case the different expression might be attributable to the different tissue samples analysed. Interestingly, we investigated the circadian rhythm genes expression even in patient SMS30, who carries the same classical 17p11.2 deletion but does not manifest any sleep alteration. This patient, referred to our laboratory during adulthood, displayed sleep-wake cycle anomalies during infancy, treated with Nopron only for a period, but resolved in adulthood the sleep problems, accordingly with the normal circadian rhythm genes expression subsequently found.

Among the SMS cohort, SMS27 presents a *de novo* deletion involving *SHANK3* gene responsible for Phelan-McDermid syndrome (PMS), a multisystem ID disorder [Soorya et al., 2013]. Of note 90% of individuals affected by PMS show marked sleep disturbance, namely difficulties with sleep initiation and sleep maintenance [Bro et al., 2017]. Recent RNA-seq studies in mutant mice with a deletion in Shank3 revealed a downregulated expression of some circadian transcription factors [Ingiosi et al., 2019], pinpointing the relevance of *SHANK3* as sleep modulator. Indeed, we observed a *NR1D1* upregulation in our patient SMS27.

Not in all cases studied we found a concordance between sleep disturbance and circadian genes expression dysregulation. Despite the presence of sleep disturbance, patient SMS25 did not show any altered expression for the tested genes. Given the peculiarity of the identified *RAI1* defect, it is not possible to exclude that in other tissues, in particular the neuronal one, the identified rearrangement might lead to a disruption of circadian gene expression. Moreover, since a deregulation of circadian rhythm genes expression in PTLS patients' lymphoblasts has been recently reported [Mullegama et al., 2017], we extended the RT-qPCR experiments also on blood cells of SMS25 mother. Accordingly with the absence of behavioral PTLS phenotype, as well as sleep problems, normal transcript levels of the circadian rhythm genes were found.

Of note, also patient SMS5 did not manifest any circadian rhythm genes expression alterations, despite she is affected by 2q23.1 deletion syndrome. Conversely, a previous study in lymphoblastoid cell lines of affected patients carrying *MBD5* deletion detected a dysregulation of circadian rhythm gene expression, with a mRNA levels decrease of *NR1D2*, *PER1*, *PER2*, and *PER3* as well as of *RAI1* [Mullegama et al., 2015b].

In conclusion, in some of the tested SMS/SMS-like patients (8/16), characterized by sleep disturbances and carrying different molecular defects, a quantitative dysregulation in the expression of one or more genes implicated in the circadian rhythm regulation emerged. Since we observed a

specific pattern of circadian rhythm genes expression for each patient, it will be important to evaluate more specifically, qualitatively and quantitatively, the manifestation of sleep disturbances, in order to better correlate phenotype with genotype and to understand how the genes inter-play in the circardian rhythm regulation. The assessment of circadian rhythm genes expression on blood turned out to be a useful preliminary approach to evaluate any circadian dysfunctions, prompting further studies in a more suitable cell model, for instance iPSCs- derived neurons.

4.4 ZDHHC15 as putative gene implicated in the onset of SMS-like phenotype, through iPSCs generation and cortical neurons differentiation

The SMS etiopathogenesis, like other NDDs, is incredibly difficult to explore, as a consequence of i) human brain complexity, ii) the impossibility of working with neurons from living subjects, and iii) the absence of a suitable animal model. To elucidate the role of new candidate genes of SMS-like disorders, we made use of iPSCs model. IPSCs similar to ESCs can evolve into fully differentiated tissues, including the neural one, recapitulating the progression of brain development and the neuronal dysfunctions responsible for NDDs. IPSCs retaining the genetic background of donor are patient-specific, and can be generated from any somatic cells, avoiding the ethical problems associated with scientific research based on ESCs.

To get this point, we studied the case SMS8 through iPSCs reprogramming and subsequent differentiation in cortical neurons. SMS8 is a male with SMS-like phenotype carrying a rare maternal deletion involving a highly conserved insulator sequence, mapping 29 kb from 5'UTR of *ZDHHC15* (Zinc Finger DHHC domain-containing protein 15) gene. Based on the evidence that we observed on blood a clear *ZDHHC15* transcript downregulation, we considered it as a strong candidate gene for the SMS-like phenotype. Interestingly, *ZDHHC15,* encoding for a palmitoyl-transferase highly expressed in the brain, has been previously associated to a nonsyndromic X-linked intellectual disability [Mansouri et al., 2005]. Notably, this post-translational modification seems to be extremely important in the nervous system, in particular for synapse development and plasticity [Fukata and Fukata, 2010; Globa and Bamji, 2017; Matt et al., 2019; Shah et al., 2019].

In this project we established for the first time the iPSC-derived neuronal model for SMS-like phenotype study. To date, indeed only one iPSCs line from a SMS *RAI1*-mutated patient has been generated and characterized [Altieri et al., 2018]. We successfully reprogrammed to iPSCs peripheral blood mononuclear cells from patient SMS8 and from his parents, using the integration-free Sendai virus, which is currently the most used for its efficiency, safety, and simple handling [Soares et al., 2016]. Each clone obtained was carefully characterized, checking for typical morphology, potential pluripotency, and maintenance of genomic stability. Of note we observed a frequency of rearranged

iPSC clones of 0% by conventional karyotyping and of 12.5% by high-resolution array-CGH. This data is consistent with the literature that show an increase in chromosomal aberrations after reprogramming. Schlaeger and collaborators, comparing non-integrating reprogramming methods for iPSCs generation, reported for Sendai virus approach an aneuploidy rate of 4.6% by karyotyping, whereas the frequency of CNVs detectable by array-CGH could be not determined since the low data uniformity [Schlaeger et al., 2015]. The detection rate of acquired CNVs depends on the array resolution, as CNVs detection increases with the increasing array-CGH resolution (180-400K). These data emphasize the importance of genomic monitoring to assure iPSCs phenotypic stability, clinical safety, and data robustness/reproducibility.

Patient's iPSCs were comparable to parents' iPSCs for morphology, expression of the pluripotency-related markers (Nanog, Oct3/4, Sox2, AP, SSEA4, and Tra-1-60), and capability of embryoid body formation and spontaneous differentiation into the three germ layers. Moreover, we did not identify any downregulation in *ZDHHC15* transcript level in patient's iPSC clones compared to parents' and control's iPSC clones, at difference of our previous observations on patient's peripheral blood. This finding can be explained by the fact that the *ZDHHC15* expression might be differentially regulated in different tissues, considering that the rare deletion upstream 5'UTR gene involves a predicted insulator element. This element might be not necessary for *ZDHHC15* expression in iPSCs context, though we cannot exclude *a priori* its effect on later differentiation stage.

Considering the patients' ID phenotype and high expression in the brain of palmitoyl-transferase ZDHHC15 and its function, we differentiated iPSCs into cortical neurons. Consistent with the protocol used, we obtained for each clone cortical neurons positive for pan neuronal (MAP2) and cortical-specific markers (TBR-1 and CUX1), for specific axons marker (SMI312 and βIII tubulin), and for glutamatergic and GABAergic neurons (VGLUT1 and GAD1, respectively). Although, by immunofluorescence analyses no differences in markers expression were observed between patient SMS8 and parent's iPSCs-derived neurons, and we were unable to determine the amount of *ZDHHC15* mRNA on mature cortical neurons (~ 70 days), since *ZDHHC15* neuronal transcript levels showed an extreme variability between all the samples analyzed, an altered neuronal functional activity of patient's cultered iPSCs-derived neurons was found by electrophysiology recordings. Indeed, evaluating electrophysiological mEPSCs profiles of differentiated neurons (detected at different days of maturation: 50-75), we observed defected excitatory synaptic development in patient's and mother's neuronal cultures compared to those derived from father's iPSCs. In cortical neurons obtained from SMS8 and his mother the absence of a progressive increase in mEPSCs frequency and amplitude, matching with pre- and postsynapse functional maturation, was detected. These preliminary results support our hypothesis that the presence of the rare Xq13.3 deletion

upstream *ZDHHC15* gene could be considered responsible for the patient's cognitive behavioral phenotype leading to a dysfunction in excitatory synapse maturation.

Our preliminary results are consistent with the recent literature data. Over 40% of synaptic proteins are palmitoylated, especially in response to changes in synaptic activity [Sanders et al., 2015]. For instance, palmitoylation of PSD95 (postsynaptic density protein 95), a scaffold protein of excitatory postsynaptic density (PSD) with a central role in synaptic plasticity, is necessary for its proper localization, clustering at PSD and its function [Fukata and Fukata, 2010]. The addition of palmitate at Cys3 and Cys5 of PSD95 is supposed to be the *core* mechanism by which PSD95 is attached at synaptic sites, where it determines the synaptic strength by modulating the availability of AMPA-type glutamate receptors (AMPAR) [Matt et al., 2019]. Moreover, the induced inhibition of palmitoylation in hippocampal neurons has been reported to cause a reduction of the amplitude and frequency of AMPAR, affecting excitatory transmission [el-Husseini and Bredt, 2002;]. Regarding *ZDHHC15* recent studies demonstrated its involvement in dendritic outgrowth and arborization, as well as in spine maturation and PSD95 trafficking [Shah et al., 2019]. Knockdown zDHHC15 rat hippocampal neurons showed, indeed, a significant reduction in the excitatory synapses density due to the decrease of palmitoylation [Shah et al., 2019]. These findings are very interesting since dendrite outgrowth alteration is one of the most common hallmark of ID [Casanova et al., 2012]. Moreover, *zdhhc15b*, the zebrafish horthologue of human ZDHHC15, was shown to be crucial for dopaminergic (DA) neurons development, namely permitting the maturation of DA progenitors [Wang et al., 2015].

The identical electrophysiological trend found in patient's and mother's derived cells could be addressed to a random X chromosome inactivation (XCI) observed in the maternal blood cells. Considering random XCI, the electrophysiological result obtained on the mother clone could be due to the inactivation of the X carrying the non deleted allele. To date, the mechanism of XCI in iPSCs is still under debate: some studies assumed that chrX is reactivated during reprogramming, leading to partial or full inactivation [Kim et al., 2014; Barakat et al., 2015], whereas others supposed that XCI remains stable during this process [Tchieu et al., 2010]. A recent study, conducted on over 700 samples by Bar and colleagues, has demonstrated that iPSCs maintain the XCI silencing status established in their parental cells [Bar et al., 2019]. By replicating the electrophysiological records, and by performing the XCI analysis on the two iPSC clones of the mother and the corresponding differentiated cortical neurons we might contribute to clarify if the XCI remains stable during the cells reprogramming. In addition, the hypothetical finding of different electrophysiological trends in neurons derived from these two clones eventually displaying an opposite XCI, would allow to strongly confirm the correlation between the presence of Xq13.3 deletion and a dysfunction in excitatory synapse maturation.

Supporting the role of *ZDHHC15* gene in SMS-like phenotype, mainly regarding sleep disturbances, we identified expression dysregulations in some of circadian rhythm genes (*BMAL2* and *NR1D1*) in peripheral blood sample. It would be interesting to replicate the same expression analyses also on mature cortical neurons derived from patient's iPSCs.

REFERENCES

Aasen T, Raya A, Barrero MJ, Garreta E, Consiglio A, Gonzalez F, Vassena R, Bilić J, Pekarik V, Tiscornia G, Edel M, Boué S, Izpisúa Belmonte JC. Efficient and rapid generation of induced pluripotent stem cells from human keratinocytes. Nat Biotechnol. 2008;26(11):1276-84.

Acquaviva F, Sana ME, Della Monica M, Pinelli M, Postorivo D, Fontana P, Malco MT, Nardone AM, Lonardo F, Iascone M and Scarano G. First evidence of Smith-Magenis syndrome in mother and daughter due to a novel RAI mutation. Am J Med Genet A. 2017;173(1):231–238.

Alaimo JT, Mullegama SV, Thomas MA, Elsea SH. Copy number loss upstream of RAI1 uncovers gene expression regulatory region that may impact Potocki-Lupski syndrome diagnosis. Mol Cytogenet. 2015;8:75.

Alari V, Russo S, Terragni B, Ajmone PF, Sironi A, Catusi I, Calzari L, Concolino D, Marotta R, Milani D, Giardino D, Mantegazza M, Gervasini C, Finelli P, Larizza L. iPSC-derived neurons of CREBBP- and EP300-mutated Rubinstein-Taybi syndrome patients show morphological alterations and hypoexcitability. Stem Cell Res. 2018;30:130-140.

Altieri F, Turco EM, Vinci E, Torres B, Ferrari D, De Jaco A, Mazzoccoli G, Lamorte G, Nardone A, Della Monica M, Bernardini L, Vescovi AL, Rosati J. Production and characterization of CSSI003 (2961) human induced pluripotent stem cells (iPSCs) carrying a novel puntiform mutation in RAI1 gene, Causative of Smith-Magenis syndrome. Stem Cell Res. 2018;28:153-156.

Antonucci F, Corradini I, Morini R, Fossati G, Menna E, Pozzi D, Pacioni S, Verderio C, Bacci A, Matteoli M. Reduced SNAP-25 alters short-term plasticity at developing glutamatergic synapses. EMBO Rep. 2013;14(7):645-51.

Ardhanareeswaran K, Mariani J, Coppola G, Abyzov A, Vaccarino FM. Human induced pluripotent stem cells for modelling neurodevelopmental disorders. Nat Rev Neurol. 2017;13(5):265-278.

Bar S, Seaton LR, Weissbein U, Eldar-Geva T, Benvenisty N. Global Characterization of X Chromosome Inactivation in Human Pluripotent Stem Cells. Cell Rep. 2019;27(1):20-29.e3.

Barakat TS, Ghazvini M, de Hoon B, Li T, Eussen B, Douben H, van der Linden R, van der Stap N, Boter M, Laven JS, Galjaard RJ, Grootegoed JA, de Klein A, Gribnau J. Stable X chromosome reactivation in female human induced pluripotent stem cells. Stem Cell Reports. 2015;4(2):199-208.

Benevento M, Iacono G, Selten M, Ba W, Oudakker A, Frega M, Keller J, Mancini R, Lewerissa E, Kleefstra T, Stunnenberg HG, Zhou H, van Bokhoven H, Nadif Kasri N. Histone Methylation by the Kleefstra Syndrome Protein EHMT1 Mediates Homeostatic Synaptic Scaling. Neuron. 2016;91(2):341-55.

Berger SI, Ciccone C, Simon KL, Malicdan MC, Vilboux T, Billington C, Fischer R, Introne WJ, Gropman A, Blancato JK, Mullikin JC; NISC Comparative Sequencing Program, Gahl WA, Huizing M, Smith ACM. Exome analysis of Smith-Magenis-like syndrome cohort identifies de novo likely pathogenic variants. Hum Genet. 2017;136(4):409-420.

Bi W, Sai GM, Shaw CJ, Walz K, Fonseca P, Wilson M, Potocki L, Lupski JR. Mutations of RAI1, a PHD-containing protein, in nondeletion patients with Smith-Magenis syndrome. Hum Genet. 2004;115(6):515–524.

Bi W, Saifi GM, Girirajan S, Shi X, Szomju B, Firth H, Magenis RE, Potocki L, Elsea SH, Lupski JR. RAI1 point mutations, CAG repeat variation, and SNP analysis in non-deletion Smith-Magenis syndrome. Am J Med Genet A. 2006;140(22):2454-63

Boone PM, Reiter RJ, Glaze DG, Tan DX, Lupski JR, Potocki L. Abnormal circadian rhythm of melatonin in Smith-Magenis syndrome patients with RAI1 point mutations. Am J Med Genet A. 2011;155A(8):2024–2027.

Bozza M, Bernardini L, Novelli A, Brovedani P, Moretti E, Canapicchi R, Doccini V, Filippi T, Battaglia A. 6p25 interstitial deletion in two dizygotic twins with gyral pattern anomaly and speech and language disorder. Eur J Paediatr Neurol. 2013;17(3):225-31.

Bro D, O'Hara R, Primeau M, Hanson-Kahn A, Hallmayer J, Bernstein J. Sleep Disturbances in Individuals With Phelan-McDermid Syndrome: Correlation With Caregivers' Sleep Quality and Daytime Functioning. Sleep. 2017;40(2).

Campbell IM, Yuan B, Robberecht C, Pfundt R, Szafranski P, McEntagart ME, Nagamani SC, Erez A, Bartnik M, Wiśniowiecka-Kowalnik B, Plunkett KS, Pursley AN, Kang SH, Bi W, Lalani SR, Bacino CA, Vast M, Marks K, Patton M, Olofsson P, Patel A, Veltman JA, Cheung SW, Shaw CA, Vissers LE, Vermeesch JR, Lupski JR, Stankiewicz P. Parental somatic mosaicism is underrecognized and influences recurrence risk of genomic disorders. Am J Hum Genet. 2014;95(2):173–182.

Carmona-Mora P and Walz K. Retinoic acid induced 1, RAI1: a dosage sensitive gene related to neurobehavioral alterations including autistic behavior. Curr Genomics. 2010;11(8):607–617.

Carmona-Mora P, Encina CA, Canales CP, Cao L, Molina J, Kairath P, Young LI, Walz K. Functional and cellular characterization of human retinoic acid induced 1 (RAI1) mutations associated with Smith-Magenis syndrome. BMC Molecular Biology. 2010;11:63.

Carpizo R, Martínez A, Mediavilla D, González M, Abad A, Sánchez-Barceló EJ. Smith-Magenis syndrome: a case report of improved sleep after treatment with beta1-adrenergic antagonists and melatonin. J Pediatr. 2006;149(3):409-11.

Carvill GL, Heavin SB, Yendle SC, McMahon JM, O'Roak BJ, Cook J, Khan A, Dorschner MO, Weaver M, Calvert S, Malone S, Wallace G, Stanley T, Bye AM, Bleasel A, Howell KB, Kivity S, Mackay MT, Rodriguez-Casero V, Webster R, Korczyn A, Afawi Z, Zelnick N, Lerman-Sagie T, Lev D, Møller RS, Gill D, Andrade DM, Freeman JL, Sadleir LG, Shendure J, Berkovic SF, Scheffer IE, Mefford HC. Targeted resequencing in epileptic encephalopathies identifies de novo mutations in CHD2 and SYNGAP1. Nat Genet. 2013;45(7):825-30.

Casanova JR, Nishimura M, Owens JW, Swann JW. Impact of seizures on developing dendrites: implications for intellectual developmental disabilities. Epilepsia. 2012;53 Suppl 1:116-24.

Chamberlain SJ, Chen PF, Ng KY, Bourgois-Rocha F, Lemtiri-Chlieh F, Levine ES, Lalande M. Induced pluripotent stem cell models of the genomic imprinting disorders Angelman and Prader-Willi syndromes. Proc Natl Acad Sci U S A. 2010;107(41):17668-73.

Chamberlain SJ. Disease modelling using human iPSCs. Hum Mol Genet. 2016;25(2):173–181.

Charrier A, Olliac B, Roubertoux P, Tordjman S. Clock Genes and Altered Sleep-Wake Rhythms: Their Role in the Development of Psychiatric Disorders. Int J Mol Sci. 2017;18(5).

Chen H, Qian K, Du Z, Cao J, Petersen A, Liu H, Blackbourn LW, Huang CL, Errigo A, Yin Y, Lu J, Ayala M, Zhang SC. Modeling ALS with iPSCs Reveals that Mutant SOD1 Misregulates Neurofilament Balance in Motor Neurons. Cell Stem Cell. 2014;14(6):796–809.

Cheung AY, Horvath LM, Grafodatskaya D, Pasceri P, Weksberg R, Hotta A, Carrel L, Ellis J. Isolation of MECP2-null Rett Syndrome patient hiPS cells and isogenic controls through X-chromosome inactivation.
Hum Mol Genet. 2011;20(11):2103-15.

Cho H, Zhao X, Hatori M, Yu RT, Barish GD, Lam MT, Chong LW, Ditacchio L, Atkins AR, Glass CK, Christopher Liddle C, Auwerx J, Downes M, Panda S and Evans RM. Regulation of circadian behaviour and metabolism by REV-ERB-a and REV-ERB-b. Nature. 2012;485(7396):123–127.

Cleaver R, Berg J, Craft E, Foster A, Gibbons RJ, Hobson E, Lachlan K, Naik S, Sampson JR, Sharif S, Smithson S; Deciphering Developmental Disorders Study, Parker MJ, Tatton-Brown K. Refining the Primrose syndrome phenotype: A study of five patients with ZBTB20 de novo variants and a review of the literature. Am J Med Genet A. 2019;179(3):344-349.

Cochoy DM, Kolevzon A, Kajiwara Y, Schoen M, Pascual-Lucas M, Lurie S, Buxbaum JD, Boeckers TM, Schmeisser MJ. Phenotypic and functional analysis of SHANK3 stop mutations identified in individuals with ASD and/or ID. Mol Autism. 2015;6:23.

Crumbley C and Burris TP. Direct regulation of CLOCK expression by REV-ERB. PLoS ONE. 2011;6(3);e17290.

Darvekar S, Johnsen SS, Eriksen AB, Johansen T, Sjøttem E. Identification of two independent nucleosome-binding domains in the transcriptional co-activator SPBP. Biochem J. 2012;442(1):65–75.

Darvekar S, Rekdal C, Johansen T, Sjøttem E. A phylogenetic study of SPBP and RAI1: evolutionary conservation of chromatin binding modules. PLoS ONE 2013;8(10):e78907.

De Leersnyder H. Smith-Magenis syndrome. Handb Clin Neurol. 2013;111:295-6.

Doers ME, Musser MT, Nichol R, Berndt ER, Baker M, Gomez TM, Zhang SC, Abbeduto L, Bhattacharyya A. iPSC-derived forebrain neurons from FXS individuals show defects in initial neurite outgrowth. Stem Cells Dev. 2014;23(15):1777-87.

Eberl HC, Spruijt CG, Kelstrup CD, Vermeulen M, Mann M. A map of general and specialized chromatin readers in mouse tissues generated by label-free interaction proteomics. Mol. Cell 2013;49(2),368–378.

Ebert DH and Greenberg ME. Activity-dependent neuronal signalling and autism spectrum disorder. Nature 2013;493(7432),327–337.

Edelman EA, Girirajan S, Finucane B, Patel PI, Lupski JR, Smith AC, Elsea SH. Gender, genotype, and phenotype differences in Smith-Magenis syndrome: a meta-analysis of 105 cases. Clin Genet. 2007;71(6):540–550.

el-Husseini Ael-D, Bredt DS. Protein palmitoylation: a regulator of neuronal development and function. Nat Rev Neurosci. 2002;3(10):791-802.

Elsea SH and Girirajan S. Smith-Magenis syndrome. Eur J Hum Genet. 2008;16(4):412–421.

Elsea, SH and Williams, SR. Smith-Magenis Syndrome: haploinsufficiency of RAI1 results in altered gene regulation in neurological and metabolic pathways. Expert Rev Mol Med. 2011;13:e14.

Falk RE and Casas KA. Chromosome 2q37 deletion: Clinical and molecular aspects. Am J Med Genet C Semin Med Genet. 2007;145C:357–371.

Farra N, Zhang WB, Pasceri P, Eubanks JH, Salter MW, Ellis J. Rett syndrome induced pluripotent stem cell-derived neurons reveal novel neurophysiological alterations. Mol Psychiatry. 2012;17(12):1261-71.

Fukata Y, Fukata M. Protein palmitoylation in neuronal development and synaptic plasticity. Nat Rev Neurosci. 2010;11(3):161-75.

Garay PM, Wallner MA, Iwase S. Yin-yang actions of histone methylation regulatory complex in the brain. Epigenomics 2016;8(12):1689-1708.

Gekakis N, Staknis D, Nguyen HB, Davis FC, Wilsbacher LD, King DP, Takahashi JS, Weitz CJ. Role of the CLOCK protein in the mammalian circadian mechanism. Science. 1998;280(5369):1564-9.

Germain ND, Banda EC, Becker S, Naegele JR, Grabel LB. Derivation and isolation of NKX2.1-positive basal forebrain progenitors from human embryonic stem cells. Stem Cells Dev. 2013;22(10):1477-89.

Germain ND, Chen PF, Plocik AM, Glatt-Deeley H, Brown J, Fink JJ, Bolduc KA, Robinson TM, Levine ES, Reiter LT, Graveley BR, Lalande M, Chamberlain SJ. Gene expression analysis of human induced pluripotent stem cell-derived neurons carrying copy number variants of chromosome 15q11-q13.1. Mol Autism. 2014;5:44.

Ghosh A, Michalon A, Lindemann L, Fontoura P, Santarelli L. Drug discovery for autism spectrum disorder: challenges and opportunities. Nat Rev Drug Discov. 2013;12(10):777-90.

Girirajan S, Elsas LJ, Devriendt K, Elsea SH. RA 1 variations in Smith-Magenis syndrome patients without 17p11.2 deletions. J Med Genet. 2005;42(11):820–828.

Girirajan S, Vlangos CN, Szomju BB, Edelman E, Trevors CD, Dupuis L, Nezarati M, Bunyan DJ, Elsea SH. Genotype-phenotype correlation in Smith-Magenis syndrome: evidence that multiple genes in 17p11.2 contribute to the clinical spectrum. Genet Med. 2006;8(7):417–427.

Globa AK, Bamji SX. Protein palmitoylation in the development and plasticity of neuronal connections. Curr Opin Neurobiol. 2017;45:210-220.

Goh ES, Banwell B, Stavropoulos DJ, Shago M, Yoon G. Mosaic microdeletion of 17p11.2-p12 and duplication of 17q22-q24 in a girl with Smith-Magenis phenotype and peripheral neuropathy. Am J Med Genet A. 2014;164A(3):748-52.

Greenberg F, Guzzetta V, Montes de Oca-Luna R, Magenis RE, Smith AC, Richter SF, Kondo I, Dobyns WB, Patel PI, Lupski JR. Molecular analysis of the Smith-Magenis syndrome: a possible contiguous-gene syndrome associated with del(17)(p11.2). Am J Hum Genet. 1991;49(6):1207–1218.

Greenberg F, Lewis RA, Potocki L, Glaze D, Parke J, Killian J, Murphy MA, Williamson D, Brown F, Dutton R, McCluggage C, Friedman E, Sulek M, Lupski JR. Multi-disciplinary clinical study of Smith-Magenis syndrome (deletion 17p11.2). Am J Med Genet. 1996;62(3):247–254.

Gropman AL, Duncan WC, Smith AC. Neurologic and developmental features of the Smith-Magenis syndrome (del 17p11.2). Pediatr Neurol. 2006;34(5):337-50.

Herculano-Houzel S. The human brain in numbers: a linearly scaled-up primate brain. Front Hum Neurosci. 2009;3:31.

Hodge JC, Mitchell E, Pillalamarri V, Toler TL, Bartel F, Kearney HM, Zou YS, Tan WH, Hanscom C, Kirmani S, Hanson RR, Skinner SA, Rogers RC, Everman DB, Boyd E, Tapp C, Mullegama SV, Keelean-Fuller D, Powell CM, Elsea SH, Morton CC, Gusella JF, DuPont B, Chaubey A, Lin AE, Talkowski ME. Disruption of MBD5 contributes to a spectrum of psychopathology and neurodevelopmental abnormalities. Mol Psychiatry. 2014;19(3):368-79.

Huang WH, Guenthner CJ, Xu J, Nguyen T, Schwarz LA, Wilkinson AW, Gozani O, Chang HY, Shamloo M and Luo L. Molecular and neural functions of RAI1, the causal gene for Smith-Magenis syndrome. Neuron. 2016; 92(2):392–406.

Iacono G, Dubos A, Méziane H, Benevento M, Habibi E, Mandoli A, Riet F, Selloum M, Feil R, Zhou H, Kleefstra T, Kasri NN, van Bokhoven H, Herault Y, Stunnenberg HG. Increased H3K9 methylation and impaired expression of Protocadherins are associated with the cognitive dysfunctions of the Kleefstra syndrome. Nucleic Acids Res. 2018;46(10):4950-4965.

Ingiosi AM, Schoch H, Wintler T, Singletary KG, Righelli D, Roser LG, Medina E, Risso D, Frank MG, Peixoto L. Shank3 modulates sleep and expression of circadian transcription factors. Elife. 2019;8. pii: e42819.

Israel MA, Yuan SH, Bardy C, Reyna SM, Mu Y, Herrera C, Hefferan MP, Van Gorp S, Nazor KL, Boscolo FS, Carson CT, Laurent LC, Marsala M, Gage FH, Remes AM, Koo EH, Goldstein LS. Probing sporadic and familial Alzheimer's disease using induced pluripotent stem cells. Nature. 2012;482(7384):216-20.

Jaillard S, Dubourg C, Gérard-Blanluet M, Delahaye A, Pasquier L, Dupont C, Henry C, Tabet AC, Lucas J, Aboura A, David V, Benzacken B, Odent S, Pipiras E. 2q23.1 microdeletion identified by array comparative genomic hybridisation: an emerging phenotype with Angelman-like features? J Med Genet. 2009;46(12):847–855.

Jean-Marçais N, Decamp M, Gérard M, Ribault V, Andrieux J, Kottler ML, Plessis G. The first familial case of inherited 2q37.3 interstitial deletion with isolated skeletal abnormalities including brachydactyly type E and short stature. Am J Med Genet A. 2015;167A(1):185-9.

Jiang H, Ren Y, Yuen EY, Zhong P, Ghaedi M, Hu Z, Azabdaftari G, Nakaso K, Yan Z, Feng J. Parkin controls dopamine utilization in human midbrain dopaminergic neurons derived from induced pluripotent stem cells. Nat Commun. 2012;3:668.

Johnson MA, Weick JP, Pearce RA, Zhang SC. Functional neural development from human embryonic stem cells: accelerated synaptic activity via astrocyte coculture. J Neurosci. 2007;27(12):3069-77.

Johnson MB, Kawasawa YI, Mason CE, Krsnik Z, Coppola G, Bogdanović D, Geschwind DH, Mane SM, State MW, Sestan N. Functional and evolutionary insights into human brain development through global transcriptome analysis. Neuron. 2009;62(4):494-509.

Juopperi TA, Kim WR, Chiang CH, Yu H, Margolis RL, Ross CA, Ming GL, Song H. Astrocytes generated from patient induced pluripotent stem cells recapitulate features of Huntington’s disease patient cells. Mol Brain. 2012;5:17.

Jones WD, Dafou D, McEntagart M, Woollard WJ, Elmslie FV, Holder-Espinasse M, Irving M, Saggar AK, Smithson S, Trembath RC, Deshpande C, Simpson MA. De novo mutations in MLL cause Wiedemann-Steiner syndrome. Am J Hum Genet. 2012;91(2):358-64.

Kearney HM, Thorland EC, Brown KK, Quintero-Rivera F, South ST; Working Group of the American College of Medical Genetics Laboratory Quality Assurance Committee. American College of Medical Genetics standards and guidelines for interpretation and reporting of postnatal constitutional copy number variants. Genet Med. 2011;13(7):680-5.

Kerchner GA, Nicoll RA. Silent synapses and the emergence of a postsynaptic mechanism for LTP. Nat Rev Neurosci. 2008;9(11):813-25.

Kim KY, Hysolli E, Tanaka Y, Wang B, Jung YW, Pan X, Weissman SM, Park IH. X Chromosome of female cells shows dynamic changes in status during human somatic cell reprogramming. Stem Cell Reports. 2014;2(6):896-909.

Kleefstra T, Brunner HG, Amiel J, Oudakker AR, Nillesen WM, Magee A, Geneviève D, Cormier-Daire V, van Esch H, Fryns JP, Hamel BCJ, Sistermans EA, de Vries BBA, van Bokhoven H. Loss-of-function mutations in euchromatin histone methyl transferase 1 (EHMT1) cause the 9q34 subtelomeric deletion syndrome. Am J Hum Genet. 2006;79:370–377.

Kleefstra T, Kramer JM, Neveling K, Willemsen MH, Koemans TS, Vissers LE, Wissink-Lindhout W, Fenckova M, van den Akker WM, Kasri NN, Nillesen WM, Prescott T, Clark RD, Devriendt K, van Reeuwijk J, de Brouwer AP, Gilissen C, Zhou H, Brunner HG, Veltman JA, Schenck A, van Bokhoven H. Disruption of an EHMT1-associated chromatin-modification module causes intellectual disability. Am J Hum Genet. 2012;91:73–82.

Koemans TS, Kleefstra T, Chubak MC, Stone MH, Reijnders MRF, de Munnik S, Willemsen MH, Fenckova M, Stumpel CTRM, Bok LA, Sifuentes Saenz M, Byerly KA, Baughn LB, Stegmann APA, Pfundt R, Zhou H, van Bokhoven H, Schenck A, Kramer JM. Functional convergence of histone methyltransferases EHMT1 and KMT2C involved in intellectual disability and autism spectrum disorder. PLoS Genet. 2017;13(10):e1006864.

Kondo T, Asai M, Tsukita K, Kutoku Y, Ohsawa Y, Sunada Y, Imamura K, Egawa N, Yahata N, Okita K, Takahashi K, Asaka I, Aoi T, Watanabe A, Watanabe K, Kadoya C, Nakano R, Watanabe D, Maruyama K, Hori O, Hibino S, Choshi T, Nakahata T, Hioki H, Kaneko T, Naitoh M, Yoshikawa K, Yamawaki S, Suzuki S, Hata R, Ueno S, Seki T, Kobayashi K, Toda T, Murakami K, Irie K, Klein WL, Mori H, Asada T, Takahashi R, Iwata N, Yamanaka S, Inoue H. Modeling Alzheimer's disease with iPSCs reveals stress phenotypes associated with intracellular Aβ and differential drug responsiveness. Cell Stem Cell. 2013;12(4):487-96.

Larizza L and Finelli P. Developmental disorders with intellectual disability driven by chromatin dysregulation: Clinical overlaps and molecular mechanisms. Clin Genet. 2019 Feb;95(2):231-240.

Le TN, Williams SR, Alaimo JT, Elsea SH. Genotype and phenotype correlation in 103 individuals with 2q37 deletion syndrome reveals incomplete penetrance and supports HDAC4 as the primary genetic contributor. Am J Med Genet A. 2019;179(5):782-79.

Leroy C, Landais E, Briault S, David A, Tassy O, Gruchy N, Delobel B, Grégoire MJ, Leheup B, Taine L, Lacombe D, Delrue MA, Toutain A, Paubel A, Mugneret F, Thauvin-Robinet C, Arpin S, Le Caignec C, Jonveaux P, Beri M, Leporrier N, Motte J, Fiquet C, Brichet O, Mozelle-Nivoix M, Sabouraud P, Golovkine N, Bednarek N, Gaillard D, Doco-Fenzy M. The 2q37-deletion syndrome: an update of the clinical spectrum including overweight, brachydactyly and behavioural features in 14 new patients. Eur J Hum Genet. 2013;21(6):602-12.

Lin DT, Conibear E. Enzymatic protein depalmitoylation by acyl protein thioesterases. Biochem Soc Trans. 2015;43(2):193-8.

Loebrich S and Nedivi E. The function of activity-regulated genes in the nervous system. Physiol. Rev. 2009; 89(4),1079-1103.

Loviglio MN, Beck CR, White JJ, Leleu M, Harel T, Guex N, Niknejad A, Bi W, Chen ES, Crespo I, Yan J, Charng WL, Gu S, Fang P, Coban-Akdemir Z, Shaw CA, Jhangiani SN, Muzny DM, Gibbs RA, Rougemont J, Xenarios I, Lupski JR, Reymond A. Identification of a RAI1-associated disease network through integration of exome sequencing, transcriptomics, and 3D genomics. Genome Med. 2016;8(1):105.

Magoulas PL, Liu P, Gelowani V, Soler-Alfonso C, Kivuva EC, Lupski JR, Potocki L. Inherited dup(17)(p11.2p11.2): expanding the phenotype of the Potocki-Lupski syndrome. Am J Med Genet A. 2014;164A(2):500-4.

Mansouri MR, Marklund L, Gustavsson P, Davey E, Carlsson B, Larsson C, White I, Gustavson KH, Dahl N. Loss of ZDHHC15 expression in a woman with a balanced translocation t(X;15)(q13.3;cen) and severe mental retardation. Eur J Hum Genet. 2005;13(8):970-7.

Marchetto MC, Carromeu C, Acab A, Yu D, Yeo GW, Mu Y, Chen G, Gage FH, Muotri AR. A model for neural development and treatment of Rett syndrome using human induced pluripotent stem cells. Cell. 2010;143(4):527-39.

Martins-Taylor K, Hsiao JS, Chen PF, Glatt-Deeley H, De Smith AJ, Blakemore AI, Lalande M, Chamberlain SJ. Imprinted expression of UBE3A in non-neuronal cells from a Prader-Willi syndrome patient with an atypical deletion. Hum Mol Genet. 2014;23(9):2364-73.

Matt L, Kim K, Chowdhury D, Hell JW. Role of Palmitoylation of Postsynaptic Proteins in Promoting Synaptic Plasticity. Front Mol Neurosci. 2019;12:8.

Meyer AC, Neher E, Schneggenburger R. Estimation of quantal size and number of functional active zones at the calyx of Held synapse by nonstationary EPSC variance analysis. J Neurosci. 2001;21(20):7889-900.

Miller DT, Adam MP, Aradhya S, Biesecker LG, Brothman AR, Carter NP, Church DM, Crolla JA, Eichler EE, Epstein CJ, Faucett WA, Feuk L, Friedman JM, Hamosh A, Jackson L, Kaminsky EB, Kok K, Krantz ID, Kuhn RM, Lee C, Ostell JM, Rosenberg C, Scherer SW, Spinner NB, Stavropoulos DJ, Tepperberg JH, Thorland EC, Vermeesch JR, Waggoner DJ, Watson MS, Martin CL, Ledbetter DH. Consensus statement: chromosomal microarray is a first-tier clinical diagnostic test for individuals with developmental disabilities or congenital anomalies. Am J Hum Genet. 2010;86(5):749-64.

Milne TA, Briggs SD, Brock HW, Martin ME, Gibbs D, Allis CD, Hess JL. MLL targets SET domain methyltransferase activity to Hox gene promoters. Mol Cell. 2002;10(5):1107-17.

Monteiro P, Feng G. SHANK proteins: roles at the synapse and in autism spectrum disorder. Nat Rev Neurosci. 2017;18(3):147-157.

Morris B, Etoubleau C, Bourthoumieu S, Reynaud-Perrine S, Laroche C, Lebbar A, Yardin C, Elsea SH. Dose dependent expression of HDAC4 causes variable expressivity in a novel inherited case of brachydactyly mental retardation syndrome. Am J Med Genet A. 2012;158A(8):2015–2020.

Mullegama SV, Alaimo JT, Chen L, Elsea SH. Phenotypic and Molecular Convergence of 2q23.1 Deletion Syndrome with Other Neurodevelopmental Syndromes Associated with Autism Spectrum Disorder. Int J Mol Sci 2015a;16(4):7627–7643.

Mullegama SV, Pugliesi L, Burns B, Shah Z, Tahir R, Gu Y, Nelson DL, Elsea SH. MBD5 haploinsufficiency is associated with sleep disturbance and disrupts circadian pathways common to Smith-Magenis and fragile X syndromes. Eur J Hum Genet. 2015b;23(6):781-9.

Mullegama SV and Elsea SH. Clinical and Molecular Aspects of MBD5-Associated Neurodevelopmental Disorder (MAND). Eur J Hum Genet. 2016;24(9):1376.

Mullegama SV, Alaimo JT, Fountain MD, Burns B, Balog AH, Chen L, Elsea SH. RAI1 overexpression promotes altered circadian gene expression and dyssomnia in Potocki-Lupski Syndrome. J Pediatr Genet 2017; 6(3):155–164.

Nakamura T, Mori T, Tada S, Krajewski W, Rozovskaia T, Wassell R, Dubois G, Mazo A, Croce CM, Canaani E. ALL-1 is a histone methyltransferase that assembles a supercomplex of proteins involved in transcriptional regulation. Mol Cell. 2002;10(5):1119-28.

Naisbitt S, Kim E, Tu JC, Xiao B, Sala C, Valtschanoff J, Weinberg RJ, Worley PF, Sheng M. Shank, a novel family of postsynaptic density proteins that binds to the NMDA receptor/PSD-95/GKAP complex and cortactin. Neuron. 1999;23(3):569-82.

Neira-Fresneda J and Potocki L. Neurodevelopmental disorders associated with abnormal gene dosage: Smith-Magenis and Potocki-Lupski syndromes. J Pediatr Genet 2015;4(3):159–67.

Nguyen HN, Byers B, Cord B, Shcheglovitov A, Byrne J, Gujar P, Kee K, Schule B, Dolmetsch RE, Langston W, Palmer T, Pera RR. LRRK2 Mutant iPSC-Derived DA Neurons Demonstrate Increased Susceptibility to Oxidative Stress. Cell Stem Cell. 2011;8(3):267–280.

Park IH, Arora N, Huo H, Maherali N, Ahfeldt T, Shimamura A, Lensch MW, Cowan C, Hochedlinger K, Daley GQ. Disease-specific induced pluripotent stem cells. Cell. 2008;134(5):877-86.

Park JP, Moeschler JB, Davies WS, Patel PI, Mohandas TK. Smith-Magenis syndrome resulting from a de novo direct insertion of proximal 17q into 17p11.2. Am J Med Genet. 1998;28;77(1):23-7.

Patil SR and Bartley JA. Interstitial deletion of the short arm of chromosome 17. Hum Genet. 1984;67:237-238.

Phelan K, McDermid HE. The 22q13.3 Deletion Syndrome (Phelan-McDermid Syndrome). Mol Syndromol. 2012;2(3-5):186-201.

Potocki L, Glaze D, Tan DX, Park SS, Kashork CD, Shaffer LG, Reiter RJ, Lupski JR. Circadian rhythm abnormalities of melatonin in Smith-Magenis syndrome. J Med Genet. 2000a;37(6):428–433.

Potocki L, Shaw CJ, Stankiewicz P, Lupski JR. Variability in clinical phenotype despite common chromosomal deletion in Smith-Magenis syndrome. Genet Med. 2003;5:430–4.

Praticò AD, Falsaperla R, Rizzo R, Ruggieri M, Verrotti A, Pavone P. A New Patient with Potocki-Lupski Syndrome: A Literature Review. J Pediatr Genet. 2018;7(1):29-34

Preitner N, Damiola F, Lopez-Molina L, Zakany J, Duboule D, Albrecht U, Schibler U. The orphan nuclear receptor REV-ERBalpha controls circadian transcription within the positive limb of the mammalian circadian oscillator. Cell. 2002;110(2):251-60.

Rakic P. A small step for the cell, a giant leap for mankind: a hypothesis of neocortical expansion during evolution. Trends Neurosci. 1995;18(9):383-8.

Ricard G, Molina J, Chrast J, Gu W, Gheldof N, Pradervand S, Schütz F, Young JI, Lupski JR, Reymond A, Walz K. Phenotypic consequences of copy number variation: insights from Smith-Magenis and Potocki-Lupski syndrome mouse models. PLoS Biol. 2010;8(11):e1000543.

Richards S, Aziz N, Bale S, Bick D, Das S, Gastier-Foster J, Grody WW, Hegde M, Lyon E, Spector E, Voelkerding K, Rehm HL; ACMG Laboratory Quality Assurance Committee. Standards and guidelines for the interpretation of sequence variants: a joint consensus recommendation of the American College of Medical Genetics and Genomics and the Association for Molecular Pathology. Genet Med. 2015;17(5):405-24.

Russo FB, Brito A, de Freitas AM, Castanha A, de Freitas BC, Beltrão-Braga PCB. The use of iPSC technology for modeling Autism Spectrum Disorders. Neurobiol Dis. 2019;130:104483.

Sances S, Bruijn LI, Chandran S, Eggan K, Ho R, Klim J, Livesey MR, Lowry E, Macklis JD, Rushton D, Sadegh C, Sareen D, Wichterle H, Zhang SC, Svendsen CN. Modeling ALS using motor neurons derived from human induced pluripotent stem cells. Nat Neurosci. 2016;19(4):542–553.

Sanchez-Danes A, Richaud-Patin Y, Carballo-Carbajal I, Jimenez-Delgado S, Caig C, Mora S, Di Guglielmo C, Ezquerra M, Patel B, Giralt A, Canals JM, Memo M, Alberch J, López-Barneo J, Vila M, Cuervo AM, Tolosa E, Consiglio A, Raya A. Disease-specific phenotypes in dopamine neurons from human iPS-based models of genetic and sporadic Parkinson's disease. EMBO Mol Med. 2012;4(5):380–395.

Sanders SS, Martin DD, Butland SL, Lavallée-Adam M, Calzolari D, Kay C, Yates JR 3rd, Hayden MR. Curation of the Mammalian Palmitoylome Indicates a Pivotal Role for Palmitoylation in Diseases and Disorders of the Nervous System and Cancers. PLoS Comput Biol. 2015;11(8):e1004405.

Sando R, N Gounko, S Pieraut, L Liao, J Yates III, Anton Maximov. HDAC4 governs a transcriptional program essential for Synaptic Plasticity and memory. Cell. 2012;151:821-834.

Sato TK, Panda S, Miraglia LJ, Reyes TM, Rudic RD, McNamara P, Naik KA, FitzGerald GA, Kay SA, Hogenesch JB. A functional genomics strategy reveals Rora as a component of the mammalian circadian clock. Neuron. 2004;43(4):527-37.

Shah BS, Shimell JJ, Bamji SX. Regulation of dendrite morphology and excitatory synapse formation by zDHHC15. J Cell Sci. 2019;132(13).

Shaw CJ, Bi W, Lupski JR. Genetic proof of unequal meiotic crossovers in reciprocal deletion and duplication of 17p11.2. Am J Hum Genet. 2002; 71(5):1072–1081.

Shaw CJ, Withers MA, Lupski JR. Uncommon deletions of the Smith-Magenis syndrome region can be recurrent when alternate low-copy repeats act as homologous recombination substrates. Am J Hum Genet. 2004;75(1):75–81.

Shaw CJ and Lupski JR. Non-recurrent 17p11.2 deletions are generated by homologous and non-homologous mechanisms. Hum Genet. 2005; 116(1–2):1–7.

Shcheglovitov A, Shcheglovitova O, Yazawa M, Portmann T, Shu R, Sebastiano V, Krawisz A, Froehlich W, Bernstein JA, Hallmayer JF, Dolmetsch RE. SHANK3 and IGF1 restore synaptic deficits in neurons from 22q13 deletion syndrome patients. Nature. 2013;503(7475):267-71.

Schlaeger TM, Daheron L, Brickler TR, Entwisle S, Chan K, Cianci A, DeVine A, Ettenger A, Fitzgerald K, Godfrey M, Gupta D, McPherson J, Malwadkar P, Gupta M, Bell B, Doi A, Jung N, Li X, Lynes MS, Brookes E, Cherry AB, Demirbas D, Tsankov AM, Zon LI, Rubin LL, Feinberg AP, Meissner A, Cowan CA, Daley GQ. A comparison of non-integrating reprogramming methods. Nat Biotechnol. 2015;33(1):58-63.

Sheridan SD, Theriault KM, Reis SA, Zhou F, Madison JM, Daheron L, Loring JF, Haggarty SJ. Epigenetic characterization of the FMR1 gene and aberrant neurodevelopment in human induced pluripotent stem cell models of fragile X syndrome. PLoS One. 2011;6(10):e26203.

Shuib S, Saaid NN, Zakaria Z, Ismail J, Abdul Latiff Z. Duplication 17p11.2 (Potocki-Lupski Syndrome) in a child with developmental delay. Malays J Pathol. 2017;39(1):77–81.

Slager RE, Newton TL, Vlangos CN, Finucane B, Elsea SH. Mutations in RAI1 associated with Smith-Magenis syndrome. Nature Genetics. 2003;33(4):466–468.

Smith AC, McGavran L, Robinson J, Waldstein G, Macfarlane J, Zonona J, Reiss J, Lahr M, Allen L, Magenis E. Interstitial deletion of (17)(p11.2p11.2) in nine patients. Am J Med Genet 1986;24(3):393–414.

Smith AC, Magenis RE, Elsea SH. Overview of Smith-Magenis syndrome. J Assoc Genet Technol. 2005;31:163–7.

Smith AC and Gropman AL. Smith-Magenis syndrome. In: Cassidy S & Allanson J, eds. Management of Genetic Syndromes. 3 ed. New York, NY: Wiley-Blackwell; 2010:739-67.

Smith AC, Boyd KE, Brennan C, Charles J, Elsea SH, Finucane BM, Foster R, Gropman A, Girirajan S, Haas-Givler B. Smith-Magenis Syndrome. In: Adam MP, Ardinger HH, Pagon RA, Wallace SE, Bean LJH, Stephens K, Amemiya A, editors. GeneReviews®[Internet]. Seattle (WA): University of Washington, Seattle; 1993-2019. 2001 Oct 22 [updated 2019 Jun 20].

Soares FA, Pedersen RA, Vallier L. Generation of Human Induced Pluripotent Stem Cells from Peripheral Blood Mononuclear Cells Using Sendai Virus. Methods Mol Biol. 2016;1357:23-31.

Soorya L, Kolevzon A, Zweifach J, Lim T, Dobry Y, Schwartz L, Frank Y, Wang AT, Cai G, Parkhomenko E, Halpern D, Grodberg D, Angarita B, Willner JP, Yang A, Canitano R, Chaplin W, Betancur C, Buxbaum JD. Prospective investigation of autism and genotype-phenotype correlations in 22q13 deletion syndrome and SHANK3 deficiency. Mol Autism. 2013;4(1):18.

Staerk J, Dawlaty MM, Gao Q, Maetzel D, Hanna J, Sommer CA, Mostoslavsky G, Jaenisch R. Reprogramming of human peripheral blood cells to induced pluripotent stem cells. Cell Stem Cell. 2010;7(1):20-4

Tadros S, Wang R, Waters JJ, Waterman C, Collins AL, Collinson MN, Ahn JW, Josifova D, Chetan R, Kumar A. Inherited 2q23.1 microdeletions involving the MBD5 locus. Mol Genet Genomic Med. 2017;5(5):608-613.

Takahashi K, Tanabe K, Ohnuki M, Narita M, Ichisaka T, Tomoda K, Yamanaka S. Induction of pluripotent stem cells from adult human fibroblasts by defined factors. Cell. 2007;131(5):861-72.

Talkowski ME, Mullegama SV, Rosenfeld JA, van Bon BW, Shen Y, Repnikova EA, Gastier-Foster J, Thrush DL, Kathiresan S, Ruderfer DM, Chiang C, Hanscom C, Ernst C, Lindgren AM, Morton CC, An Y, Astbury C, Brueton LA, Lichtenbelt KD, Ades LC, Fichera M, Romano C, Innis JW, Williams CA, Bartholomew D, Van Allen MI, Parikh A, Zhang L, Wu BL, Pyatt RE, Schwartz S, Shaffer LG, de Vries BB, Gusella JF, Elsea SH. Assessment of 2q23.1 microdeletion syndrome implicates MBD5 as a single causal locus of intellectual disability, epilepsy, and autism spectrum disorder. Am J Hum Genet. 2011;89(4): 551–563.

Tchieu J, Kuoy E, Chin MH, Trinh H, Patterson M, Sherman SP, Aimiuwu O, Lindgren A, Hakimian S, Zack JA, Clark AT, Pyle AD, Lowry WE, Plath K. Female human iPSCs retain an inactive X chromosome. Cell Stem Cell. 2010;7(3):329-42.

Toulouse A, Rochefort D, Roussel J, Joober R, Rouleau GA. Molecular cloning and characterization of human RAI1, a gene associated with schizophrenia. Genomics. 2003;82(2):162–171.

Truong HT, Dudding T, Blanchard CL, Elsea SH. Frameshift mutation hotspot identified in Smith-Magenis syndrome: case report and review of literature. BMC Med Genet. 2010;11:142.

Urbach A, Bar-Nur O, Daley GQ, Benvenisty N. Differential modeling of fragile X syndrome by human embryonic stem cells and induced pluripotent stem cells. Cell Stem Cell. 2010;6(5):407-11.

van Bon BW, Koolen DA, Brueton L, McMullan D, Lichtenbelt KD, Adès LC, Peters G, Gibson K, Moloney S, Novara F, Pramparo T, Dalla Bernardina B, Zoccante L, Balottin U, Piazza F, Pecile V, Gasparini P, Guerci V, Kets M, Pfundt R, de Brouwer AP, Veltman JA, de Leeuw N, Wilson M, Antony J, Reitano S, Luciano D, Fichera M, Romano C, Brunner HG, Zuffardi O, de Vries BB. The 2q23.1 microdeletion syndrome: clinical and behavioural phenotype. Eur J Hum Genet. 2010;18(2):163-70.

Vetrini F, McKee S, Rosenfeld JA, Suri M, Lewis AM, Nugent KM, Roeder E, Littlejohn RO, Holder S, Zhu W, Alaimo JT, Graham B, Harris JM, Gibson JB, Pastore M, McBride KL, Komara M, Al-Gazali L, Al Shamsi A, Fanning EA, Wierenga KJ, Scott DA, Ben-Neriah Z, Meiner V, Cassuto H, Elpeleg O, Holder JL Jr, Burrage LC, Seaver LH, Van Maldergem L, Mahida S, Soul JS, Marlatt M, Matyakhina L, Vogt J, Gold JA, Park SM, Varghese V, Lampe AK, Kumar A, Lees M, Holder-Espinasse M, McConnell V, Bernhard B, Blair E, Harrison V; DDD study, Muzny DM, Gibbs RA, Elsea SH, Posey JE, Bi W, Lalani S, Xia F, Yang Y, Eng CM, Lupski JR, Liu P. De novo and inherited TCF20 pathogenic variants are associated with intellectual disability, dysmorphic features, hypotonia, and neurological impairments with similarities to Smith-Magenis syndrome. Genome Med. 2019 Feb 28;11(1):12

Vieira GH, Rodriguez JD, Carmona-Mora P, Cao L, Gamba BF, Carvalho DR, de Rezende Duarte A, Santos SR, de Souza DH, DuPont BR, Walz K, Moretti-Ferreira D, Srivastava AK. Detection of classical 17p11.2 deletions, an atypical deletion and RAI1 alterations in patients with features suggestive of Smith-Magenis syndrome. Eur J Hum Genet. 2012;20(2):148-54.

Vilboux T, Ciccone C, Blancato JK, Cox GF, Deshpande C, Introne WJ, Gahl WA, Smith AC, Huizing M. Molecular analysis of the Retinoic Acid Induced 1 gene (RAI1) in patients with suspected Smith-Magenis syndrome without the 17p11.2 deletion. PLoS One. 2011;6(8):622861.

Vlangos CN, Yim DK, Elsea SH. Refinement of the Smith-Magenis syndrome critical region to approximately 950kb and assessment of 17p11.2 deletions. Are all deletions created equally? Mol Genet Metab. 2003;79:134–41.

Walz K, Paylor R, Yan J, Bi W, Lupski JR. Rai1 duplication causes physical and behavioral phenotypes in a mouse model of dup(17)(p11.2p11.2). J Clin Invest. 2006;116:3035-41.

Walz K and Young JI. The methyl binding domain containing protein MBD5 is a transcriptional regulator responsible for 2q23.1 deletion syndrome. Rare Dis. 2014 Nov 3;2(1):e967151.

Wagenstaller J, Spranger S, Lorenz-Depiereux B, Kazmierczak B, Nathrath M, Wahl D, Heye B, Glaser D, Liebscher V, Meitinger T, Strom TM. Copy-number variations measured by single-nucleotide-polymorphism oligonucleotide arrays in patients with mental retardation. Am J Hum Genet. 2007;81(4):768-79.

Wang F, Chen X, Shi W, Yao L, Gao M, Yang Y, Hao A. Zdhhc15b Regulates Differentiation of Diencephalic Dopaminergic Neurons in zebrafish. J Cell Biochem. 2015;116(12):2980-91.

Wheeler PG, Huang D, Dai Z. Haploinsufficiency of HDAC4 does not cause intellectual disability in all affected individuals. Am J Med Genet A. 2014;164A(7):1826-9.

Williams SR, Mullegama SV, Rosenfeld JA, Dagli AI, Hatchwell E, Allen WP, Williams CA, Elsea SH. Haploinsufficiency of MBD5 associated with a syndrome involving microcephaly, intellectual disabilities, severe speech impairment, and seizures. European Journal of Human Genetics. 2010a;18: 436–441.

Williams SR, Aldred MA, Der Kaloustian VM, Halal F, Gowans G, McLeod DR, Zondag S, Toriello HV, Magenis RE, Elsea SH. Haploinsufficiency of HDAC4 causes brachydactyly mental retardation syndrome, with brachydactyly type E, developmental delays, and behavioral problems. Am J Hum Genet. 2010b;87:219–228.

Williams SR, Zies D, Mullegama SV, Grotewiel MS, Elsea SH. Smith-Magenis syndrome results in disruption of CLOCK gene transcription and reveals an integral role for RAI1 in the maintenance of circadian rhythmicity. Am J Hum Genet. 2012;90(6):941–949.

Woodbury-Smith M, Nicolson R, Zarrei M, Yuen RKC, Walker S, Howe J, Uddin M, Hoang N, Buchanan JA, Chrysler C, Thompson A, Szatmari P, Scherer SW. Variable phenotype expression in a family segregating microdeletions of the NRXN1 and MBD5 autism spectrum disorder susceptibility genes. NPJ Genom Med. 2017;3;2.

Xue Y, Cai X, Wang L, Liao B, Zhang H, Shan Y, Chen Q, Zhou T, Li X, Hou J, Chen S, Luo R, Qin D, Pei D, Pan G. Generating a non-integrating human induced pluripotent stem cell bank from urine-derived cells. PLoS One. 2013;8(8):e70573.

Yagi T, Ito D, Okada Y, Akamatsu W, Nihei Y, Yoshizaki T, Yamanaka S, Okano H, Suzuki N. Modeling familial Alzheimer's disease with induced pluripotent stem cells. Hum Mol Genet. 2011;20(23):4530-9.

Yan J, Bi W, Lupski JR. Penetrance of craniofacial anomalies in mouse models of Smith-Magenis syndrome is modified by genomic sequence surrounding Rai1: not all null alleles are alike. Am J Hum Genet. 2007;80(3):518–525.

Yan X, Qin H, Qu C, Tuan RS, Shi S, Huang GT. iPS cells reprogrammed from human mesenchymal-like stem/progenitor cells of dental tissue origin. Stem Cells Dev. 2010;19(4):469-80.

Yang J, Cai J, Zhang Y, Wang X, Li W, Xu J, Li F, Guo X, Deng K, Zhong M, Chen Y, Lai L, Pei D, Esteban MA. Induced pluripotent stem cells can be used to model the genomic imprinting disorder Prader-Willi syndrome. J Biol Chem. 2010;285(51):40303-11.

Yang SP, Bidichandani SI, Figuera LE, Juyal RC, Saxon PJ, Baldini A, Patel PI. Molecular analysis of deletion (17)(p11.2p11.2) in a family segregating a 17p paracentric inversion: implications for carriers of paracentric inversions. Am J Hum Genet. 1997;60(5):1184–1193.

Yu J, Vodyanik MA, Smuga-Otto K, Antosiewicz-Bourget J, Frane JL, Tian S, Nie J, Jonsdottir GA, Ruotti V, Stewart R, Slukvin II, Thomson JA. Induced pluripotent stem cell lines derived from human somatic cells. Science. 2007;318(5858):1917-20.

Yusupov R, Roberts AE, Lacro RV, Sandstrom M, Ligon AH. Potocki-Lupski syndrome: an inherited dup(17)(p11.2p11.2) with hypoplastic left heart. Am J Med Genet A. 2011;155A(2):367-71.

Zaręba-Kozioł M, Figiel I, Bartkowiak-Kaczmarek A, Włodarczyk J. Insights Into Protein S-Palmitoylation in Synaptic Plasticity and Neurological Disorders: Potential and Limitations of Methods for Detection and Analysis. Front Mol Neurosci. 2018;11:175.

Zhang F, Potocki L, Sampson JB, Liu P, Sanchez-Valle A, Robbins-Furman P, Navarro AD, Wheeler PG, Spence JE, Brasington CK, Withers MA, Lupski JR. Identification of uncommon recurrent Potocki-Lupski syndrome-associated duplications and the distribution of rearrangement types and mechanisms in PTLS. American Journal of Human Genetics. 2010; 86(3):462–470.

Zhang N, An MC, Montoro D, Ellerby LM. Characterization of Human Huntington's Disease Cell Model from Induced Pluripotent Stem Cells. PLoS Curr. 2010;2:RRN1193.

Zori RT, Lupski JR, Heju Z, Greenberg F, Killian JM, Gray BA, Driscoll DJ, Patel PI, Zackowski JL. Clinical, cytogenetic, and molecular evidence for an infant with Smith-Magenis syndrome born from a mother having a mosaic 17p11.2p12 deletion. Am J Med Genet. 1993;47(4):504–511.